

**Langhans-type Multinucleated Giant Cells in
Giant Cell Arteritis**

Daniel Joseph Maunder

**Submitted to Newcastle University for the degree of Doctor
of Philosophy in the Faculty of Medical Sciences**

September 2021

Abstract

Langhans-type multinucleated giant cells (LMGCs) are observed in a selection of seemingly disparate idiopathic pathologies including sarcoidosis, Crohn's disease, granulomatosis with polyangiitis, and giant cell arteritis (GCA). The origin of LMGCS is unclear, though two different formation mechanisms have been proposed; cell-to-cell fusion and modified cell division with failed cytokinesis involving DNA damage signalling. Present across species, they may possess as yet undiscovered functional adaptations, and evidence suggests that they may play a destructive role in GCA. The tissue microenvironment of GCA-affected arteries is also poorly understood, in particular, the molecular pathways involved in driving intimal hyperplasia remain elusive.

To facilitate the characterisation of LMGCS in the context of GCA, an *in vitro* LMGC culture system was developed using GM-CSF and IFN γ to differentiate primary monocytes, and subsequently interrogated using single cell RNA sequencing. Cultured LMGCS were shown to be morphologically representative of those in disease, and *transcriptional* analysis revealed upregulation of gene modules relating to leukocyte activation, smooth muscle cell proliferation, cell-extracellular matrix interactions and chemokine activity.

With fluorescent imaging techniques and electron microscopy it was shown that cultured LMGCS and those from GCA-affected temporal artery tissue contain large chromatin bridges, indicative of cytokinesis failure. Staining for the marker 53BP1 indicated that IFN γ induced DNA damage in these cells, though multinucleation rate was unaffected by additional ROS scavengers. Live confocal imaging revealed the fusion of cultured monocytes to form LMGCS and abnormal cell division. Investigations into the functional adaptations of cultured LMGCS showed that they may enter a state of premature senescence with increased capacity for ROS production.

Together these data indicate that LMGCS form by a combination of cell fusion and DNA-damage induced cytokinesis failure, and persist in a senescent state with enhanced capacity for the production of damaging ROS.

Acknowledgements

This thesis was funded and supported by the National Institute for Health Research (NIHR) Newcastle Biomedical Research Centre (Newcastle BRC), to whom I would like to express enormous gratitude for their support throughout the project. I would also like to thank the generous patients who agreed to donate excised temporal artery tissue, and the healthy blood donors without whom this research would not have been possible.

I carried out this research as a member of the Haniffa Lab, within the Immunity and Inflammation theme of the Translational and Clinical Research Institute at Newcastle University. I consider myself incredibly lucky to have worked alongside a team of excellent scientists and kind, thoughtful people. I owe particular thanks to my supervisors, Professor Muzlifah Haniffa and Dr Gary Reynolds, who provided constant support and showed belief in my abilities, continually challenging me to improve myself. I am especially grateful for the patience shown by Dr Reynolds throughout the project, allowing me to grow both my research skills and my confidence. I am also keen to acknowledge the technical and personal support of current and former members of the group, namely Emily Stephenson, Justin Engelbert, Dr Rachel Botting, Dr David Dixon, Dr James Fletcher, Dr Kile Green and Simone Webb.

I also thank Professor Jonathan Higgins, and Dr Mark Levasseur for help with live cell imaging and understanding cytokinesis; Dr Rolando Berlinguer Palmi and Dr Alex Laude for bioimaging support; Dr Kathryn White, Tracey Davey and Ross Laws for performing and supporting the analysis of electron microscopy images; Dr Andrew Filby, Dr David McDonald, Dr Gill Hulme, Andrew Fuller, Carly Knill and Loredana Trevi for help and support with flow cytometry and FACS; Dr David Jamieson for help with ImageStream; and finally all of the technical support staff within the Immunity and Inflammation theme.

Table of contents

ABSTRACT	I
ACKNOWLEDGEMENTS	II
TABLE OF CONTENTS	III
LIST OF FIGURES AND TABLES	VI
ABBREVIATIONS.....	VIII
CHAPTER 1. GENERAL INTRODUCTION.....	1
1.1. GIANT CELL ARTERITIS.....	1
1.1.1. Introduction to GCA.....	1
1.1.2. The diagnosis and treatment of GCA.....	2
1.1.3. The aetiology of GCA.....	3
1.1.4. The pathogenesis of GCA.....	5
1.1.5. T cells in GCA.....	6
1.1.6. Monocytes and macrophages in GCA.....	7
1.2. POLYPOIDY.....	8
1.2.1. The structure of the cell nucleus.....	8
1.2.2. The cellular effects of polyploidy.....	10
1.2.3. Polyploidy via incomplete cell division with failed cytokinesis.....	12
1.2.4. Polyploidy via endoreduplication.....	16
1.2.5. Polyploidy via cell fusion.....	16
1.2.5.1. Macrophage fusion.....	17
1.3. MULTINUCLEATED GIANT CELLS	20
1.3.1. Osteoclasts.....	21
1.3.2. Foreign body-type multinucleated giant cells.....	22
1.3.3. Langhans-type multinucleated giant cells.....	22
1.4. AIMS OF THIS STUDY	24
CHAPTER 2. GENERATING LANGHANS-TYPE MULTINUCLEATED GIANT CELLS <i>IN VITRO</i>.....	26
2.1. INTRODUCTION.....	26
2.2. USING FLOW CYTOMETRY TO ASSESS MULTINUCLEATION	29
2.2.1. Validation of multinucleated cell gating strategy using ImageStream.....	29
2.2.2. Validation of LMGC sorting strategy with FACS.....	31
2.3. COMPARING LMGC CULTURE METHODS FROM THE LITERATURE	34
2.4. OPTIMISATION OF MY CHOSEN <i>IN VITRO</i> LMGC CULTURE SYSTEM.....	36
2.4.1. Titrating GM-CSF and IFN γ	36
2.4.2. Optimising culture time, monocyte seeding density and culture medium.....	38
2.5. MORPHOLOGICAL EVALUATION OF <i>IN VITRO</i> LMGCs	40
2.6. DISCUSSION	42
CHAPTER 3. SINGLE CELL RNA SEQUENCING OF <i>IN VITRO</i> LMGCs AND GCA AFFECTED TEMPORAL ARTERY TISSUE.....	44
3.1. INTRODUCTION.....	44
3.1.1. RNA sequencing of <i>in vitro</i> LMGCs.....	44
3.1.2. RNA sequencing of GCA-affected temporal artery tissue.....	45

3.1.3. Chapter aims.....	45
3.2. SINGLE CELL RNA SEQUENCING OF <i>IN VITRO</i> LMGCs	46
3.2.1. Single cell sorting strategy.....	46
3.2.2. Dataset pre-processing.....	48
3.2.2.1. Applying quality control metrics.....	48
3.2.2.2. Identification of highly variable genes and principal component analysis	50
3.2.3. Unbiased cell clustering.....	52
3.2.4. Identification of cluster markers	54
3.2.5. Pathway analysis.....	55
3.3. SEQUENCING OF TEMPORAL ARTERY	57
3.3.1. Temporal artery dissociation procedure.....	57
3.3.2. Unbiased clustering and manual annotation of subsequent populations.....	59
3.3.3. Cell population analysis	61
3.3.4. Identification of a LMGC gene signature.....	63
3.4. DISCUSSION	66
CHAPTER 4. THE MECHANISM OF LMGC FORMATION; THE ROLE OF DNA DAMAGE IN FAILED CYTOKINESIS	68
4.1. INTRODUCTION.....	68
4.1.1. The mechanism of LMGC formation.....	68
4.1.2. The role of DNA damage signalling in macrophage polyploidy.....	69
4.1.3. Chapter aims.....	71
4.2. LIVE CELL IMAGING: <i>IN VITRO</i> LMGCs APPEAR TO FORM BY A COMBINATION OF CELL FUSION AND INCOMPLETE CELL DIVISION	72
4.3. THE PRESENCE OF CHROMATIN BRIDGES SUPPORTS INCOMPLETE CELL DIVISION.....	75
4.3.1. <i>In vitro</i> LMGCs exhibit large chromatin bridges between pairs of nuclei.....	75
4.3.2. Electron microscopy reveals chromatin bridges between pairs of nuclei in LMGCs from GCA affected temporal artery tissue.....	78
4.4. IFNγ DRIVEN DNA DAMAGE AND REPLICATIVE STRESS IN LMGCs.....	83
4.4.1. LMGCs express 'DNA damage response' gene signature.....	83
4.4.2. IFN γ induces DNA double strand breaks.....	84
4.4.3. Culture with a reactive oxygen species scavenger has no effect on LMGC formation.....	86
4.5. DISCUSSION	87
CHAPTER 5. INVESTIGATING THE FUNCTIONAL PHENOTYPE OF LMGCs	89
5.1. INTRODUCTION.....	89
5.1.1. The role of LMGCs in GCA pathogenesis.....	89
5.1.2. Premature senescence and the senescence associated secretory phenotype.....	89
5.1.3. Chapter aims.....	91
5.2. LMGCs EXHIBIT INCREASED P21 EXPRESSION	91
5.3. INVESTIGATING THE EXHIBITION OF SENESCENCE ASSOCIATED SECRETORY PHENOTYPE BY LMGCs ...	93
5.3.1. Secretion gene module upregulation by LMGCs.....	93
5.3.2. Measuring cytokine production by LMGCs.....	95
5.3.3. LMGCs exhibit high capacity for ROS production	97
5.4. INVESTIGATING THE PHAGOCYtic PROPERTIES OF <i>IN VITRO</i> LMGCs	103
5.5. DISCUSSION	108
CHAPTER 6. GENERAL DISCUSSION AND FUTURE WORK.....	110
6.1. GENERAL DISCUSSION.....	110
6.1.1. <i>In vitro</i> model generation and validation.....	111
6.1.2. The mechanism of LMGC formation.....	113

6.1.3. <i>The functional adaptations of LMGCs</i>	115
6.2. FUTURE WORK	117
CHAPTER 7. MATERIALS AND METHODOLOGY	120
7.1. MATERIALS	120
7.1.1. <i>Antibodies</i>	120
7.1.2. <i>Tissue culture materials</i>	121
7.1.3. <i>Other materials</i>	122
7.2. METHODOLOGY	125
7.2.1. <i>Tissue culture</i>	125
7.2.1.1. <i>Primary monocyte acquisition</i>	125
7.2.1.2. <i>PBMC isolation from healthy donor blood</i>	126
7.2.1.3. <i>Cell counting</i>	126
7.2.1.4. <i>Monocyte isolation from PBMCs</i>	126
7.2.1.5. <i>Generation of macrophages and multinucleated giant cells</i>	127
7.2.1.6. <i>Cell culture maintenance</i>	127
7.2.2. <i>Flow cytometry</i>	128
7.2.2.1. <i>Using flow cytometry and FACS to assess ploidy</i>	128
7.2.2.2. <i>ImageStream</i>	128
7.2.2.3. <i>Intracellular cytokine staining</i>	129
7.2.3. <i>Generation of cytopins and giemsa staining</i>	129
7.2.4. <i>Electron microscopy</i>	130
7.2.5. <i>Immunocytochemistry</i>	131
7.2.6. <i>Live cell confocal imaging</i>	132
7.2.7. <i>Measuring capacity for the production of reactive oxygen species</i>	133
7.2.7.1. <i>MitoSOX staining</i>	133
7.2.7.2. <i>CellROX staining</i>	133
7.2.8. <i>FITC DEXTRAN uptake microscopy</i>	133
7.2.9. <i>Single cell RNA sequencing</i>	134
7.2.9.1. <i>In vitro LMGC culture preparation for scRNAseq</i>	134
7.2.9.2. <i>cDNA Library generation for smart-seq2</i>	134
7.2.9.3. <i>Temporal artery processing</i>	136
7.2.9.4. <i>10x library generation</i>	137
7.2.9.5. <i>Computational analysis</i>	138
7.2.10. <i>General methodology</i>	138
REFERENCES	139

List of figures and tables

TABLE 1. THE CLINICAL FEATURES OF GCA AND THEIR FREQUENCY OF INCIDENCE.....	2
TABLE 2. GENE POLYMORPHISMS IMPLICATED IN GIANT CELL ARTERITIS.....	4
FIGURE 1. THE STRUCTURE OF CHROMOSOMES.	10
FIGURE 2. THE PHASES AND REGULATORY CHECKPOINTS OF THE CELL CYCLE.	13
TABLE 3. MACROPHAGE/MONOCYTE DERIVED MULTINUCLEATED GIANT CELL SUBSETS.	20
TABLE 4. A SELECTION OF NOTABLE PUBLICATIONS IN WHICH LMGCS ARE GENERATED.	26
FIGURE 3. IMAGING FLOW CYTOMETRY OF <i>IN VITRO</i> LMGCS.	30
FIGURE 4. USING FACS TO VALIDATE MULTINUCLEATED CELL SORTING STRATEGY.	32
FIGURE 5. COMPARISON OF <i>IN VITRO</i> LMGC CULTURE PROTOCOLS FROM THE LITERATURE.....	35
FIGURE 6. OPTIMISING CYTOKINE CONCENTRATIONS.	37
FIGURE 7. OPTIMISATION OF CULTURE CONDITIONS.	39
FIGURE 8. MORPHOLOGICAL ASSESSMENT OF CULTURED MACROPHAGES, LMGCS AND OSTEOCLASTS.	41
FIGURE 9. LMGC SORTING STRATEGY AND PLATE LAYOUT FOR SS2.	47
FIGURE 10. QUALITY CONTROL PLOTS.....	49
FIGURE 11. VARIABLE GENE IDENTIFICATION AND PCA.	51
FIGURE 12. UNBIASED POPULATION CLUSTERING BY UMAP.	53
FIGURE 13. IDENTIFICATION OF DIFFERENTIALLY EXPRESSED GENES.....	54
FIGURE 14. UPREGULATED GENE MODULES IN LMGCS.	56
FIGURE 15. TEMPORAL ARTERY DIGESTION WORKFLOW.	58
FIGURE 16. UNBIASED CLUSTERING OF TAB AND MATCHED BLOOD.	60
FIGURE 17. POPULATION ANALYSIS OF TAB AND MATCHED BLOOD.....	62
FIGURE 18a. UNBIASED RE-CLUSTERING OF TAB MACROPHAGES, AND SHARED DEGS WITH <i>IN VITRO</i> LMGCS.....	64
FIGURE 18b. LACK OF AN <i>IN VITRO</i> LMGC GENE SIGNATURE IN GCA NEGATIVE PATIENTS.....	66
FIGURE 19. CAPTURING LMGC FORMATION BY LIVE CONFOCAL IMAGING.....	73
FIGURE 20. LIVE CELL IMAGING QUANTIFICATION OF MITOSES AND FUSION EVENTS.....	74
FIGURE 21. CONFOCAL IMAGING OF <i>IN VITRO</i> LMGCS, OSTEOCLASTS AND FBGCS.....	76
FIGURE 22. CHROMATIN BRIDGES WITHIN <i>IN VITRO</i> LMGCS BY CONFOCAL IMAGING.....	77
FIGURE 23. NUCLEUS SEGMENTATION FROM SCANNING ELECTRON MICROSCOPY IMAGES OF <i>IN</i> <i>VITRO</i> , AND TAB LMGCS.	79
FIGURE 24. RECONSTRUCTING CHROMATIN BRIDGES FROM SCANNING ELECTRON MICROSCOPY IMAGES IN 3D.....	81

FIGURE 25. DIFFERENTIALLY EXPRESSED GENES OF LMGCs RELATING TO THE DNA DAMAGE RESPONSE.....	83
FIGURE 26. MEASURING IFN γ INDUCED DNA DAMAGE BY 53BP1 IMMUNOFLUORESCENCE.....	85
FIGURE 27. THE EFFECT OF MITOTEMPO IN CULTURE ON LMGC FORMATION.....	87
FIGURE 28. P21 IMMUNOFLUORESCENCE.....	92
FIGURE 29. SECRETORY GENE MODULE UPREGULATION BY <i>IN VITRO</i> LMGCs.	94
FIGURE 30. MEASURING THE PRODUCTION CAPACITY OF TNFA, IL-6 AND IL-1 β BY <i>IN VITRO</i> LMGCs.	96
FIGURE 31. MEASURING CAPACITY FOR ROS PRODUCTION BY LMGCs USING MITOSOX.	98
FIGURE 32. MEASURING THE CAPACITY FOR ROS PRODUCTION BY LMGCs USING CELLROX.....	100
FIGURE 33. ANALYSING CELLROX-STAINED LMGCs BY IMAGESTREAM.	102
FIGURE 34. SCANNING ELECTRON MICROSCOPY SECTIONS OF A SINGLE LMGC AT A RANGE OF HEIGHTS.	104
FIGURE 35. FITC DEXTRAN UPTAKE ASSAY OF <i>IN VITRO</i> LMGC CULTURES.....	106
FIGURE 36. REPRESENTATIVE FLUORESCENCE MICROSCOPY IMAGES TAKEN OF FITC DEXTRAN INCUBATED LMGC CULTURES.	107
TABLE 5. ANTIBODIES USED FOR THIS RESEARCH.	120
TABLE 6. TISSUE CULTURE MATERIALS USED FOR THIS RESEARCH.....	122
TABLE 7. ALL OTHER MATERIALS USED FOR THIS RESEARCH.....	125
TABLE 8. CLINICAL METADATA FOR TEMPORAL ARTERY BIOPSIES USED.	132

Abbreviations

53BP1	p53 binding protein 1
AAV	ANCA associated vasculitis
AB	Antibody
ADAM	A disintegrin and metalloproteinase domain
AF	Alexa fluorophore
ALIX	Programmed cell death 6-interacting protein
α MEM	Minimum essential medium alpha
ANCHR	Zinc finger FYVE-type containing protein
ANOVA	Analysis of variance
APC	Adenomatous polyposis coli
APC/C	Anaphase-promoting complex/cyclosome
ATM	Ataxia-telangiectasia mutated
ATP	Adenosine triphosphate
ATR	Ataxia-telangiectasia RAD3-related
BCG	Bovis bacillus Calmette-Guérin
BFA	Brefeldin A
BLP	Bacterial lipoproteins
BSA	Bovine serum albumin
Bub3	Budding uninhibited by benzimidazole 3
BubR1	Budding uninhibited by benzimidazole receptor 1
c-FOS	Cellular oncogene Fos
CCL	C-C motif chemokine ligand
CCR	C-C chemokine receptor
CD	Cluster of differentiation
Cdc2	Cell division control protein 2
Cdc20	Cell division control protein 20
Cdc25A	M-phase inducer phosphatase 1

cDNA	Complementary deoxyribonucleic acid
Cep55	Centrosome protein 55
cGAS	cyclic GMP-AMP synthase
Chk1	Checkpoint kinase 1
Chk2	Checkpoint kinase 2
CHMP3	Charged multivesicular body protein 3
ConA	Concanavalin A
CPC	Chromosomal passenger complex
CRH	Corticotropin-releasing hormone
CRP	C-reactive protein
CX3CR	C-X3-C motif chemokine receptor
CXCL	C-X-C motif chemokine ligand
DAP12	DNAX activating protein 12
DAPI	4',6-diamidino-2-phenylindole
DC	Dendritic cell
DC-STAMP	Dendritic cell-specific transmembrane protein
DDR	DNA damage response
DEG	Differentially expressed gene
DMEM	Dulbecco's modified eagle medium
DMSO	Dimethyl sulfoxide
DNA	Deoxyribonucleic acid
DNMT	DNA methyltransferase
DRAQ5	1,5-bis[2-(di-methylamino) ethyl]amino-4, 8-dihydroxyanthracene-9, 10-dione
ECM	Extracellular matrix
ECT2	Epithelial cell transforming 2
EDTA	Ethylenediaminetetraacetic acid
eNOS	Endothelial nitric oxide synthase / nitric oxide synthase 3
ESR	Erythrocyte sedimentation rate
FACS	Fluorescence associated cell sorting
FBGC	Foreign body-type multinucleated giant cell
FCCF	Flow Cytometry Core Facility

FCS	Fetal calf serum
FITC	Fluorescein isothiocyanate
FSC A/H	Forward scatter area/height
FSL-1	Pam2CGDPKHPKSF
GCA	Giant cell arteritis
GEF	Guanine nucleotide exchange factor
GM-CSF	Granulocyte-macrophage colony-stimulating factor
GO	Gene ontology
GPC4	Glypican 4
GTP	Guanine triphosphate
HBSS	Hank's balanced salt solution
HLA	Human leukocyte antigen
ICAM1	Intercellular adhesion molecule 1
IFN	Interferon
IFN	Interferon
IGFBP	Insulin-like growth factor binding protein
IKK	I κ B kinase
IL	Interleukin
iNOS	Inducible nitric oxide synthase
IRF3	Interferon-regulatory factor 3
LFA-1	Lymphocyte function-associated antigen 1
LMGC	Langhans-type multinucleated giant cell
LPS	Lipopolysaccharide
LTA	Lymphotoxin alpha
LTB	Lymphotoxin beta
M-CSF	Macrophage colony-stimulating factor
MACS	Magnetic-activated cell sorting
Mad2	Mitotic arrest-deficient protein 2
MCC	Mitotic checkpoint complex
mDia1	Diaphanous-related formin-1
MgcRacGAP	Rac GTPase-activating protein 1
MHC	Major histocompatibility complex

MI	Myocardial infarction
MIB	Microscopy image browser
Mklp1	Mitotic kinesin-like protein 1
MMP	Matrix metalloproteinase
MN	Micronuclei
MoAB	Monoclonal antibody
NF-1	Neurofibromatosis type 1
NFATc1	Nuclear factor of activated T cells 1
NFkB	Nuclear factor kappa B
NHSBT	NHS Blood and Transplant Service
NK	Natural killer
NLRP1	Nucleotide-binding oligomerization domain, leucine rich repeat and pyrin domain containing 1
NOS2	Nitric oxide synthase 2
OC	Osteoclast
p16	Cyclin-dependent kinase inhibitor 2A
p21	Cyclin-dependent kinase inhibitor 1
p38	Mitogen-activated protein kinase 14
p53	tumour protein P53
Pam3CSK4	Pam3CysSerLys4
PBMC	Peripheral blood mononuclear cell
PBS	Phosphate-buffered saline
PC	Principal component
PCA	Principal component analysis
PDGF	Platelet derived growth factor
PE	Phycoerythrin
PMA	Phorbol myristate acetate
PML	Promyelocytic leukaemia
PMR	Polymyalgia rheumatica
PRC1	Protein regulator of cytokinesis 1
PtdSer	Phosphatidylserine
PTP-PEST	Protein tyrosine phosphatase non-receptor type 12

Rac1	Ras-related C3 botulinum toxin substrate 1
RANK	Receptor activator of nuclear factor kappa B
RANKL	Receptor activator of nuclear factor kappa B ligand
RhoA	Ras homolog family member A
RNA	Ribonucleic acid
ROCK	Rho Kinase
RONS	Reactive oxygen and nitrogen species
ROS	Reactive oxygen species
RPMI	Royal Park Memorial Institute culture medium
SASP	Senescence-associated secretory phenotype
SEM	Scanning electron microscopy
SEM	Standard error of the mean
SFC	Splicing factor compartments
SLAMF7	Signalling lymphocytic activation molecule family member 7
SNARE	Soluble N-ethylmaleimide sensitive factor attachment protein receptor
snRNP	Small nuclear ribonucleoproteins
SO	Superoxide
SS2	Smart-Seq2
SSC A/H	Side scatter area/height
STAT6	Signal transducer and activator of transcription 6
STING	Stimulator of interferon genes
t-SNE	T-distributed stochastic neighbour embedding
TAB	Temporal artery biopsy
TAB2	TGF-beta activated kinase 1 binding protein 2
TAK1	TGF-beta activated kinase 1
TBHP	Tert-butyl hydroperoxide
TCR	T-cell receptor
Th	T helper
TLR	Toll-like receptor
TNF	Tumour necrosis factor
TRAF6	TNF receptor-associated factor 6

TRAP	Tartrate-resistant acid phosphatase
Treg	Regulatory T cell
TREM-2	Triggering receptor expressed on myeloid cells 2
TREX	Three prime repair exonuclease
Tsg101	Tumour-susceptibility gene 101
ULK	Unc-51 like autophagy activating kinase
UMAP	Uniform manifold approximation and projection
VEG-F	Vascular endothelial growth factor
VSMC	Vascular smooth muscle cell

Chapter 1. General Introduction

1.1. Giant cell arteritis

1.1.1. Introduction to GCA

Giant cell arteritis (GCA), also known as temporal arteritis and historically as granulomatous arteritis or Horton arteritis, is an age-related systemic inflammatory vasculitis affecting medium and large blood vessels with a predilection for those of the neck and head. It is the most common form of vasculitis in North America and Western Europe, affecting approximately 204 in every 100,000 people over the age of 50 as of 2015¹. There are epidemiological factors which provide some insight into the aetiology of the pathology, the foremost of these being age. GCA almost exclusively affects individuals over the age of 50, with an average age of onset of 74-76 years². In addition, GCA is more prevalent in white people than people of any other ethnicity, and also more common in people of Scandinavian descent. Women are more susceptible than men, and there is evidence of familial aggregation suggesting a genetic element. Despite these factors, we still have a poor understanding of the aetiology.

When a patient presents with suspected GCA, it is treated by clinicians as a medical emergency due to the serious and potentially irreversible nature of the sequelae, which are outlined in table 1. The most common symptoms involve the intracranial arteries; headaches with scalp tenderness and jaw claudication, which are observed in 80% and 40% of cases respectively. Headaches can be either unilateral or bilateral, and are usually severe³. Approximately 30% of cases result in visual loss and this is irreversible in 10-15% of cases⁴. Ocular symptoms, often a harbinger of visual loss, can follow scalp tenderness and headaches. Constitutional symptoms, including malaise, anorexia, weight loss, polymyalgia rheumatica and fatigue are also common and are associated with extracranial large vessel disease. Whilst less common, GCA can lead to increased risk of myocardial infarction (MI) and stroke, which are potentially life threatening. A population-based study showed that approximately 10% of GCA cases lead to MI and 7.5% result in stroke. Individuals with GCA were 4 times more likely to experience MI in later life than age-matched controls⁵. GCA patients are also 2.5 times more likely to develop cerebrovascular complications such as stroke⁶; and other vascular complications such as aneurysms and stenosis are also 2.5 times more likely⁷.

Frequency	Clinical features
Typical	Headaches, scalp tenderness, jaw claudication, anaemia
Common	Ocular symptoms (including visual loss), malaise, anorexia, weight loss
Uncommon	Myocardial infarction, stroke, limb claudication, high fever

Table 1. The clinical features of GCA and their frequency of incidence.

1.1.2. The diagnosis and treatment of GCA

GCA can be difficult to diagnose due its non-specific symptoms such as headache and malaise and a lack of specific biomarkers. No single test is diagnostic and clinicians rely on a combination of clinical examination, pathology (temporal artery biopsy), laboratory findings and imaging techniques. Abnormal laboratory findings in GCA include markers of inflammation including the erythrocyte sedimentation rate (ESR) and the C-reactive protein (CRP) test. A non-invasive diagnostic tool commonly used is duplex sonography. With this technique, information regarding the extent of inflammation within an artery and luminal narrowing can be gathered without the need for surgery. It is most commonly applied to the temporal arteries but other commonly affected vessels such as the axillary and facial artery can be assessed. Signs suggestive of GCA include vessel obstruction or thickening of the artery wall due to inflammation (termed a 'halo'). While these signs can persist, often they resolve with treatment⁸.

Despite these advances, the current gold standard for diagnosis remains a temporal artery biopsy (TAB). Tissue is analysed by pathologists to assess for features suggestive of GCA such as disruption of the internal elastic lamina and the presence of lymphocytic or granulomatous inflammation. Although it has high specificity, TAB is less sensitive with meta-analyses estimating 77%⁹. Explanations for this include the presence of skip lesions due to patchy discrete sections of inflammation rather than in a continuous manner. Importantly, although the condition is named for the presence of multinucleated giant cells they are not seen on histology in around 50% of positive cases¹⁰.

The mainstay of treatment in GCA is the use of high dose corticosteroids such as Prednisolone or Methylprednisolone. Due to the potentially catastrophic complications of untreated

disease, glucocorticoid treatment is administered as soon as possible and typically alleviates systemic inflammation within 24-48 hours. This is achieved by the inhibition of inflammatory mediators such as cytokines, chemokines and adhesion molecules, and by upregulating the expression of anti-inflammatory molecules¹¹. While this treatment is effective in the alleviation of systemic inflammation, it comes with a plethora of co-toxicities, which can be particularly problematic in older people, a demographic comprising the vast majority of GCA patients.

1.1.3. The aetiology of GCA

The onset of GCA is undoubtedly age-related, as it presents almost exclusively in individuals over the age of 50, yet the mechanism by which age becomes a risk factor is unknown. One possibility is that there is a reduction in DNA methylation with age. This reduction may lead to the overexpression of certain genes. A MARK-AGE study published in 2016 shows that levels of DNA methyltransferase DNMT1 and DNMT3B, proteins responsible for DNA methylation are reduced with age; a phenomenon which was significantly more pronounced in females than males, correlating with the higher rates of GCA in females over males¹².

Evidence suggests that infectious agents play a role in GCA onset, and that age is a strong risk factor due to increased susceptibility to infection with age. Epidemiological studies note that GCA occurs in a cyclic seasonal pattern, indicating a possible role for infectious agents in the onset of GCA¹³. However, findings of other studies do not support this hypothesis, with no indication of a seasonal component^{14,15}. Simplex virus, human parainfluenza 1 and chlamydia pneumonia have been identified in temporal artery biopsies from GCA patients, but these findings have not been reproduced by independent groups¹⁶⁻¹⁸.

Associations between a number of genetic factors and GCA have been identified. There is a strong link between GCA and the human leukocyte antigen (HLA) region¹⁹⁻²¹. The HLA region, also known more globally as the major histocompatibility complex (MHC), is crucial for the adaptive immune response to infection. Genes within the HLA region are highly polymorphic, and a number of alleles have been shown to be associated with GCA, including those in HLA-DRB1*0401, HLA-DRB1*0404 and HLA-DRB1*0408 haplotypes²²⁻²⁴. Other polymorphic genes which have been associated with GCA are outlined in table 2.

Gene	Implicated polymorphism(s)	Known protein function(s)	Patient cohort size (GCA/Controls)	Replicated?	P-value (allele test)
IL10	-592 C/A promoter ²⁵	Anti-inflammatory	140/220	NO	0.0002
TNF	TNFA2 allele ²⁸	Pro-inflammatory, angiogenesis	62/147	NO	0.003
IL6	SNP rs7805828 ²⁶	Pro-inflammatory, B cell differentiation, T cell differentiation	82/166	NO	0.06
	SNP rs1546766 ²⁶		82/166	NO	0.0119
MMP9	Rs2250889 ²⁹	Breakdown of ECM, cell migration	30/23	NO	0.009
CCL2	SNP rs1860190 ²⁶	Pro-inflammatory, chemokine involved in monocyte and basophil recruitment	30/65	NO	NS
IFNg	Allele*3 intron 1 ³⁰	Pro-inflammatory, cell adhesion	59/129	NO	0.01
TLR4	Rs4986790 ³¹	Toll-like receptor, pro-inflammatory	210/678	NO	0.01
ICAM1	G/R 241 ³²	Pro-inflammatory, cell adhesion	56/228	NO	0.00005
VEGF	SNP rs1885657 ²⁶	Pro-inflammatory, angiogenesis	92/200	YES	0.019
	SNP rs2010963 ²⁶		103/226	YES	0.021
	SNP rs699946 ²⁶		82/166	YES	0.0097
	SNP rs699947 ²⁶		82/166	NO	0.0137
	C634 ³³		82/166	NO	0.0364
NOS2	SNP rs2779251 ²⁶	Pro-inflammatory, mediates IL-6, IL-8 synthesis	82/166	NO	<0.0001

Table 2. Gene polymorphisms implicated in giant cell arteritis.

Protein functions of genes implicated in giant cell arteritis development from the literature. The pro-inflammatory mediators and receptors IFN γ , IL-21, IL-23R, IL-17RA, TNF, IL-6, IL-1 β , IL-2, IL-18, LTA, LTB, CCR7, CD6 and NLRP1 have all been shown to be hypomethylated in temporal artery biopsies from patients with confirmed GCA³⁴. This supports the concept of age-induced hypomethylation as a risk factor in the onset of the condition.

1.1.4. The pathogenesis of GCA

The pathogenesis of GCA is not well understood. Current ideas and theories are represented by the immunopathological model of GCA pathogenesis, which can be separated into four main stages (Reviewed in³⁵):

Stage 1 – Resident immature dendritic cells (DCs) are activated in the adventitia of affected arteries, potentially via the activation of toll like receptors (TLRs) by danger signals such as infectious agents. Activated DCs then take on antigen presenting capabilities as part of the innate immune response to infection, expressing MHC-II receptors, co-stimulatory receptors such as CD80 and CD86, and chemokines such as CCL19, CCL20 and CCL21^{36, 37}.

Stage 2 – Activated DCs with this antigen presenting capacity interact with T cells via MHC-II/TCR interactions and this, coupled with the presence of inflammatory cytokines in the adventitia leads to the differentiation and proliferation of T cell subsets which drive inflammation. Two specific helper T cell populations have been heavily implicated; Th1 cells which amongst other products secrete IFN γ , and Th17 cells which secrete IL-17. Polarised T cells begin to infiltrate the media and adventitia of the artery wall through smaller vessels penetrating the artery wall called vasa vasorum³⁸⁻⁴⁰.

Stage 3 – The inflammatory state of the artery wall is amplified due to a persistent secretion of pro-inflammatory mediators by the ever-growing local population of T cells. IFN γ produced by Th1 cells acts on vascular smooth muscle cells, causing them to secrete a number of chemokines including CCL2, CXCL9, CXCL10 and CXCL11. At this stage peripheral blood monocytes are starting to be recruited to the site of inflammation through the vasa vasorum by chemokine attraction. These monocytes differentiate into mature macrophages and some form multinucleated giant cells via a mechanism which is debated in the literature and will be discussed at length in this thesis. These same chemokines are also responsible for the recruitment of cytotoxic CD8+ T cells to the area, which also secrete IFN γ amongst other pro-inflammatory mediators, effectively causing an inflammatory positive feedback loop. CD8+ T cells are also thought to play a role in the pathways involved in vascular remodelling.

Stage 4 – After some time, constant inflammatory signals result in a mass of immune cells recruited to the initial site called a granuloma. The ischemic consequences of GCA occur as a result of VSMC hyperproliferation and the formation of a ‘neo-intima’, which is believed to be driven by mediators secreted by cells within the granuloma, but the details of these interactions remain unclear.

1.1.5. T cells in GCA

CD8+ T cells are implicated in the pathogenesis of a number of autoimmune diseases such as immune thrombocytopenia and rheumatoid arthritis^{41, 42}, and types of vasculitis, including ANCA-associated vasculitis and granulomatosis with polyangiitis^{43, 44}. Our understanding of CD8+ T cells in the context of GCA was advanced with a recent study in which CD8+ immune responses, potentially driven by CXCR3, are shown to be increased in patients with GCA, and that higher proportions of CD8+ T cells in temporal artery tissue (>6% total cells) directly correlates with disease severity⁴⁵.

Once migrated to the lesions of the artery wall, CD4+ T cells are thought to play a role in large by producing the cytokines interferon gamma (IFN γ) and interleukin 17 (IL-17) amongst a host of other cytokines and growth factors^{37, 46-48}. In particular IL-17 is thought to be important, with monoclonal antibodies targeting it and its receptor currently undergoing phase II and III trials. While IL-17 production is sensitive to corticosteroid treatment, in contrast, IFN γ -producing T cells are relatively unaffected by corticosteroid treatment. No consistent auto-antigen has been identified in GCA but there is some evidence for clonality as a fraction of CD4+ T cells from distinct sites of granulomatous inflammation in temporal arteries share identical T cell receptor specificities⁴⁹.

Studies in to changes in circulating T cell fractions in GCA have shown variable and sometimes conflicting results. One study examining 61 patients with GCA or PMR, prior to/following treatment in comparison with healthy controls showed a reduction in circulating blood Treg and Th1 cells of those with GCA, and an increase in Th17 cells⁵⁰. Other studies have demonstrated a reduction in the number of circulating CD8+ T cells⁵¹⁻⁵³; However, a later study, albeit lacking some statistical power, showed no difference in CD8+ T cells or circulating central memory CD4+ T cells and naïve T cells, but a reduction in the number of effector CD4+

T cells⁵⁴. Of these effector CD4+ T cells a greater proportion were CD161+ in GCA compared with healthy controls, a phenotype shown to infiltrate GCA affected arteries and produce IL-17⁵⁰.

1.1.6. Monocytes and macrophages in GCA

Resident macrophages are abundant in artery walls, as they are in most tissues, where they have important roles in innate immunity and tissue homeostasis. They arise prenatally, differentiating from yolk sac-derived progenitor cells, or fetal liver precursors. Postnatally, the macrophage populations are bolstered by the immigration of cells of bone marrow origin. These resident macrophages are then maintained over time due to proliferation of local populations, and in a small part due to adult bone marrow haematopoiesis²⁹⁴. During arterial inflammation, peripheral monocytes may enter the artery wall through vasa vasorum, differentiating and increasing the size of the local macrophage population.

Different macrophage subsets, defined by their surface marker expression and/or their secretome, have been shown to have distinct roles in the pathogenesis of GCA. In the adventitia of GCA affected arteries, TGF-β1⁺iNOS⁻ macrophages have been shown to contribute to the production of cytokines such as IL-6 and IL-1β. In the intimal layer, macrophages expressing MMP-2 are thought to play a role in the breakdown of extracellular matrix^{292,293}.

Peripheral blood monocytes can be categorised by flow cytometry as classical (CD14^{bright}CD16^{neg}), non-classical (CD14^{dim}CD16^{bright}), or as an intermediate subset (CD14^{bright}CD16^{bright}). A study which examined 42 patients with newly diagnosed GCA or PMR showed elevated overall peripheral blood monocyte counts compared with healthy controls, with an increased proportion of classical monocytes, and decreased non-classical, suggesting the recruitment of non-classical monocytes to the sites of inflammation. The majority of monocytes recruited to the affected temporal arteries of GCA patients expressed typical non-classical monocyte surface proteins CD16 and CX3CR1. Few co-expressed CD16 and CCR2, a classical monocyte marker⁵⁵. The CD16 expressing monocyte/macrophage lineages are thought to possess a pro-inflammatory phenotype in vasculature with patrolling and surveillance functionality⁵⁶. However, as arterial macrophages are considered to be self-renewing in the steady state the role of peripheral monocytes is unclear⁵⁷.

Infiltrating monocytes differentiate into macrophages upon activation by the various inflammatory factors released by other immune cells in the arteries of GCA patients. Macrophages are thought to be involved in the necrosis of vascular smooth muscle and breakdown of the elastic membrane mediated by ROS and MMP2, which lead to some of the major sequelae of GCA, including aneurysms⁵⁸. Although the mechanism underlying this arterial damage is poorly understood, gene expression analysis revealed the expression of mitochondrial products by CD68+ macrophages at the junction of the media and intima of affected arteries, and an indication that lipid peroxidation occurs to the vascular smooth muscle cells in the vicinity of these macrophages⁵⁸. The expression of mitochondrial products indicates that these macrophages may alter their metabolism to promote the generation and secretion of ROS.

1.2. Polyploidy

1.2.1. The structure of the cell nucleus

Understanding of intracellular structure of cells began with the foundational discovery of the cell nucleus. The first study to definitively identify this vital and complex organelle was carried out in 1802, in which orchid cells were illustrated by the botanical artist Francis Bauer⁵⁹. The nucleus was observed in a similar fashion in subsequent studies and designated various names before being termed the 'nucleus' by R. Brown, although at this time its significance was not yet understood⁶⁰. Later, during work on cell theory, the importance of the nucleus was beginning to become clear. Advancements in imaging methodology allowed visualisation of structures within the nucleus itself, including the nucleolus and strands of chromatin⁶¹.

Intranuclear structures were not well studied until the 1980s, at which time their study was propagated by the emergence of fluorescence microscopy techniques. Different compartments of the nucleus are not separated by membranes, as is the case with other intracellular organelles. However, despite this, they are thought to be distinct due to differences in protein expression between compartments and visual differences as observed with fluorescence and electron microscopy. The major compartments identified include the nucleolus, the splicing factor compartments (SFCs), the promyelocytic leukaemia (PML) oncoprotein bodies, and the Cajal bodies, which are broadly responsible for ribosome

biogenesis, splicing factor recruitment, control of transcription and viral infection, and the assembly of small nuclear ribonucleoproteins (snRNPs) respectively⁶²⁻⁶⁷.

The nucleus contains strands of genetic material, located with differing densities in the different nuclear compartments⁶⁸. This is observed in the form of chromosomes, which comprise strands of DNA, RNA, and structural proteins called histones. Vast quantities of DNA are packaged into chromosomes by the nature of their interactions with histones. DNA strands are wound around these proteins, eight of which are typically packed together to form a nucleosome. Many nucleosomes are then connected into a fibre-like structure, chromatin, which makes up the eventual structure of the chromosome⁶⁹⁻⁷¹. A whole chromosome is made up of two halves, chromatids, which are joined at a central point called the centromere. This structure is crucial for mitosis, during which chromatids separate following spindle fibre attachment. At the ends of each chromosome are regions of DNA sequences composed of tandem repeats of the sequence TTAGGG. This region of DNA forms a tertiary structure called a 'T-loop', a process involving the protein shelterin^{72, 73}. These structures, now known as telomeres, serve as a protective shield at the chromosome ends otherwise vulnerable to DNA damage and, of particular pertinence to work later described in this thesis, chromosome fusion events⁷⁴.

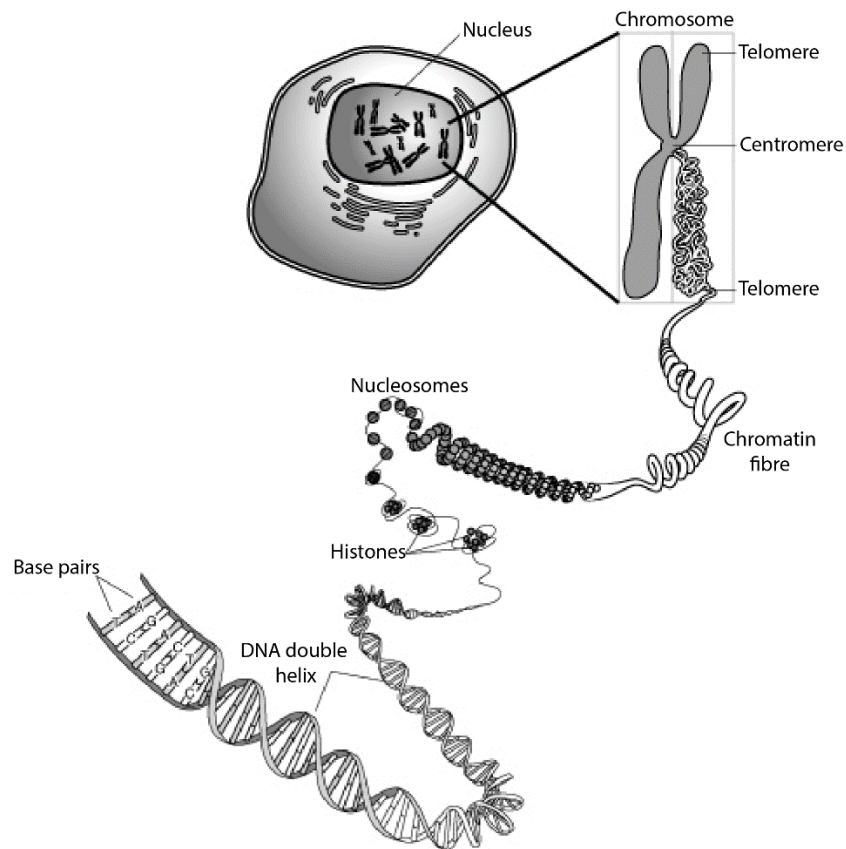


Figure 1. The structure of chromosomes.

DNA packaging within the nucleus

1.2.2. The cellular effects of polyploidy

The term 'ploidy' refers to the number of complete chromosomes within a given cell. The nomenclature used in the study of chromosomes includes the letter 'C' which is used to convey the quantity of DNA content within a cell, and 'N' which is used to convey the number of sets of chromosomes. A haploid cell contains a single set of chromosomes, and is labelled 1N, and 1C. A diploid cell is therefore 2N, 2C. Following the S phase of the cell cycle, but before

cytokinesis, the cellular DNA content doubles up to 4C, but the number of chromosomes remains 2N, as sister chromatids are considered a single chromosome.

Not all of our cells contain the same quantity of chromosomes. In the human body only sex cells, egg and sperm cells, are haploid (1N, 1C); Whilst the majority of human cells are diploid (2N, 2C). There are a number of polyploid cell types containing more than 2 sets of chromosomes, these may also be referred to as multinucleate/multinucleated. For a cell to be considered polyploid it must contain a minimum of three copies of the haploid genome (3C+). Polyploidization may offer an evolutionary advantage potentially granting cells beneficial functional adaptations, a concept which is supported by the fact that it is a highly conserved and widespread phenomenon across animal and plant species.

Extensive polyploidy was first identified in plants, and later studies revealed it to a lesser extent amongst numerous animal species, including fish, reptiles, insects, and mammals⁷⁵⁻⁷⁷. The evolutionary advantages of polyploidy are not well understood, though a number of benefits to cell survival and growth have been proposed in the literature.

There is evidence that polyploidy plays a role in tissue repair. In mammals, hepatocyte polyploidy may support the regeneration of liver tissue following injury, or chemotoxic stress and ageing by undergoing reductive mitoses to rapidly increase the rate of regeneration⁷⁸⁻⁸⁰. Similarly, in *Drosophila* polyploidy has been shown to not only be involved, but required for wound-healing^{81, 82}. The regenerative properties of these cells are thought to be a result of their higher capacity for growth than mononucleated cells, which may be due to the ability to synthesis proteins in greater quantities^{83, 84}.

Polyploidy may also serve as a protective measure for the cells themselves, increasing survival signals to strengthen apoptotic resistance⁸⁵. One possibility is that multinucleated cells form in order to pool their mitochondrial resources in response to mitochondrial damage or dysfunction, allowing intracellular mitochondrial fusion events to take place and rescue ATP production by increasing oxidative phosphorylation⁸⁶. Previously it has been shown that mitochondria are indeed elongated in multinucleated giant cells of epithelioid granulomas, though further studies are required to explore this in humans⁸⁷. *In vitro* macrophage-derived multinucleated cells have also been shown to have greater concentrations of mitochondria

than mononucleated macrophages suggesting that their functional adaptations may require increased energy, such as active transport⁸⁸.

The physical size of polyploid cells may be beneficial for the creation of tissue-protective barriers or other functions, and there are examples of this across animal and plant species. In *Drosophila*, subperineurial glia are observed with up to thirty nuclei per cell, and are linked to the maintenance of the blood-brain barrier⁸⁹. In murine models, multinucleated trophoblast giant cells and keratinocytes are proposed to play roles in formation of the placental barrier and protection of the skin respectively⁹⁰⁻⁹².

1.2.3. Polyploidy via incomplete cell division with failed cytokinesis

Polyplody arises through a number of distinct mechanisms, one of which is incomplete rounds of the cell cycle in which cytokinesis is not completed. The cell cycle is subject to a series of checkpoints, at which protein machinery ensures the process can safely proceed. A broad outline of the phases of the cell cycle and the regulatory checkpoints within is shown in figure 2. Twice during interphase, regulatory checks of chromosome viability are carried out. Known as the G1/S and G2/M cell cycle checkpoints, they prevent progression into subsequent stages of the cell cycle in instances where DNA damage is identified, as a preventative measure against the proliferation of damaged and potentially dangerous cells. When these regulatory mechanisms are dysfunctional, cells carrying mutated, damaged or dysfunctional chromosomes can be reproduced causing genomic instability⁹³. In the absence of DNA damage signalling, cyclin complexes instruct the progression from interphase to mitosis, in which two further regulatory checkpoints have been proposed; The mitotic checkpoint and the abscission checkpoint.

The mitotic checkpoint, also known as the spindle assembly checkpoint, occurs during mitosis and ensures correct spindle attachment to chromosomes so that duplicated chromatids are separated correctly during karyokinesis. This checkpoint is triggered by unattached

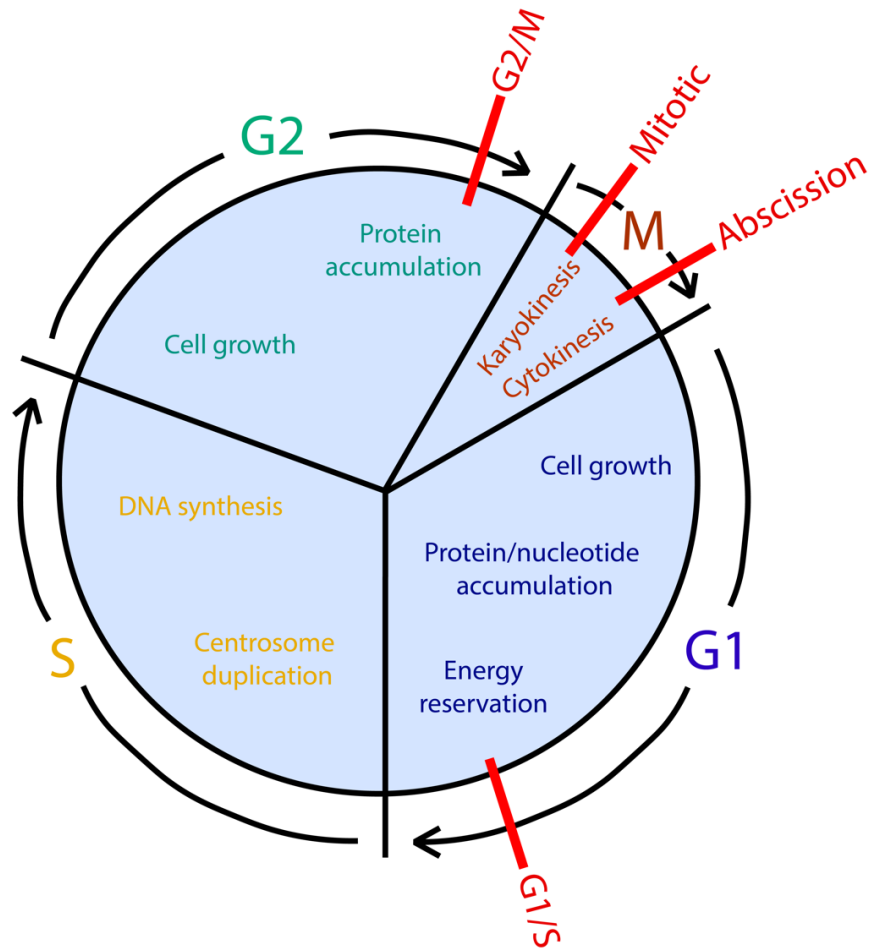


Figure 2. The phases and regulatory checkpoints of the cell cycle.

Interphase (G1, S and G2), and mitosis (M). Red lines represent cell cycle checkpoints.

kinetochores, and targets the protein complex APC/C-Cdc20 which acts to degrade cyclin B1 and securin, inactivating cdk1 and liberating separase from its complex respectively. Separase then acts to induce chromosome separation and preparation for mitotic exit occurs. APC/C is inhibited by the mitotic checkpoint complex (MCC), ultimately blocking the release of separase and the inactivation of cdk1, arresting the separation process until chromosomes are properly aligned on the spindle. The MCC comprises mitotic arrest-deficient protein 2 (mad2), cdc20, budding uninhibited by benzimidazole receptor 1 (bubR1) and budding uninhibited by benzimidazole 3 (Bub3)⁹⁴. This checkpoint is robust; The signals generated by a single unattached kinetochore are sufficient to induce total arrest in mitosis⁹⁵.

The abscission checkpoint occurs at cytokinesis, ensuring proper separation of daughter cells following mitosis, but is less well characterised than the other checkpoints discussed here due

to the relative recency of its identification. Reasons for the activation of this checkpoint and cell cycle arrest at this stage include the presence of chromatin bridges between daughter nuclei and defective assembly of nuclear pores. The presence of chromatin in the midbody during cytokinesis is detected by Aurora B kinase, the sole enzymatically active component of the chromosomal passenger complex (CPC) which governs cytokinesis timing as well as numerous functions throughout cell division^{96, 97}. Aurora B inactivation at the midbody typically triggers abscission, but following the detection of chromatin bridges it is activated for a prolonged period. This sustained activation is sufficient to stabilize the kinesin-like protein mklp1, inhibiting the ingression of the cleavage furrow⁹⁷. Binucleation is a common result of abscission checkpoint activation, when chromatin bridges are unable to be resolved, which will be discussed later in this thesis.

A number of multinucleated cell types arise as a result of incomplete mitosis with failed cytokinesis⁹⁸⁻¹⁰⁰. Cytokinesis itself is a complex process with multiple stages and failure can occur at any stage for different reasons. In many instances this results in cell death as a defence mechanism against unmitigated malignancy, however, cells can avoid apoptosis and survive in a polyploid state. The process of cytokinesis can be separated into four major stages, induction of the cleavage plane, ingression of the cleavage furrow, formation of the midbody, and abscission; This section will outline our current understanding of the mechanisms involved in failure at each stage.

The induction of the cleavage plane is thought to be initiated by microtubules, with equatorial astral microtubules, polar astral microtubules and central spindle microtubules implicated in contraction of the cleavage furrow, inhibition of cortical contractility and delivery of signals to ensure an appropriate division plane is achieved respectively¹⁰¹⁻¹⁰³. Of the signals delivered by microtubules to perform these functions, activation of the small GTPase RhoA which localises to a specific stretch of the cleavage furrow is crucial¹⁰⁴⁻¹⁰⁶. The guanine nucleotide exchange factor ECT2, which exists in an auto-inhibited form, is stabilised by the GTPase activating protein MgcRacGAP^{104, 107, 108}. ECT2, now in an active conformation, is able to activate RhoA within a narrow zone of the cleavage furrow determined by tethering of MgcRacGAP to the central spindle¹⁰⁹. Failure at this stage can occur as a result of aberrant microtubule elongation or spindle positioning, which perturbs the delivery of RhoA activation signals¹⁰⁰. This has been demonstrated as the mechanism involved in the polyploidization of

hepatocytes^{100, 110}. Failure may also occur in cells in which the tumour suppressor Adenomatous Polyposis Coli (APC) is mutated, which is thought to be critical for complete cytokinesis playing roles in the formation of the mitotic spindle^{111, 112}.

Following the induction of the cleavage plane, the cleavage furrow is arranged and its ingression is instigated by proteins which are recruited by activated RhoA¹¹³. This stage involves the polymerization of actin filaments and the motor activity of myosin, mediated by Rho Kinase (ROCK)¹¹⁴. Effector proteins called formins, in particular mDia1 which is stabilised by Rho signalling, are important for actin filament nucleation and cytokinesis can be blocked by injection of inhibitory antibodies^{115, 116}. Dysfunctional signalling leading to inhibition of formins may result in failure of cytokinesis at this stage. The motor activity of Myosin is necessary for cleavage furrow ingression although the mechanism is poorly understood¹¹⁷. Cytokinesis failure may arise due to ineffective localisation to the cleavage furrow, by perturbations the key scaffolding proteins involved in the organisation of actin and myosin such as anillin and septins¹¹⁸⁻¹²².

The third stage of cytokinesis is the formation of the midbody/midzone/central spindle, which is necessary to keep daughter nuclei separated and ultimately ensure equal distribution of chromosomes between daughter cells. The midbody comprises microtubules with associated gamma-tubulin ends, and is maintained by the microtubule bundling protein PRC1^{123, 124}. Cleavage furrow ingression can occur in the absence of PRC1 demonstrating that this stage can be completed without the central spindle, but cytokinesis cannot be completed¹²⁵. A number of proteins including MKLP1, MgcRacGAP, citron kinase and ECT2 have been implicated in the formation and maintenance of the midbody by their proximity to it, though their functions are unclear and further studies are required to investigate any associations with cytokinesis failure at this stage¹²⁶.

The final stage of cytokinesis, abscission, is a complex process involving many intracellular trafficking and membrane fusion proteins which results in complete separation of daughter cells. SNARE proteins are a family of fusion proteins which are strongly implicated in this end-stage¹²⁷⁻¹²⁹. As with PRC1, an absence of SNARE proteins due to depletions or mutations results in incomplete cytokinesis following successful cleavage furrow ingression¹³⁰. Trafficking proteins such as charged multivesicular body protein 3 (CHMP3), tumor-susceptibility gene 101 (Tsg101), Alix, and centrosome protein 55 (cep55) are localised to the

midbody during this stage and are also thought to play a key role in abscission¹³¹⁻¹³⁴. Perturbation of the signalling of any of these factors may lead to failure to abscise and polyploidy, though this has only been demonstrated to be true of cep55 and CHMP3^{131, 132}.

1.2.4. Polyploidy via endoreduplication

Endoreduplication is a modified cell division program during which DNA replication occurs in the absence of chromatin condensation, chromatin segregation or cytokinesis¹³⁵. Like cell fusion and failed cytokinesis this only occurs in the formation of a limited number of polyploid cell types, but is highly conserved across species having been demonstrated in protists, plants, arthropods, molluscs, and mammals¹³⁶⁻¹³⁸. This suggests that the process is not simply a dysfunction, but a functionally beneficial mechanism for an as yet unclear purpose.

While evidence is lacking, there is some speculation in the literature as to what the functional adaptations offered by endoreduplication are. Some believe it may be a mechanism to maintain an appropriate nucleus-volume to cell-volume ratio. A greater than average sized cell would require higher transcriptional capability due to the increased need to generate proteins to maintain an increased number of organelles. The process of endoreduplication may, therefore, fulfil that need by providing more DNA content for gene expression. Similarly, increased nuclear content could also allow for rapid expansion of cell size, which would be beneficial for certain plant cells, such as seeds which need to grow quickly¹³⁹. Endoreduplication cycles identified in plant tissues specialised for the storage of seeds, cotyledons and endosperms, led to the idea that it was a mechanism for storing either free nucleotides or nitrogen which would be needed for the development of any fertilised seed embryo^{140, 141}. The most widely accepted of these theories is that endoreduplication offers increased gene expression in situations where it is necessary to rapidly elevate transcriptional capacity¹³⁶.

1.2.5. Polyploidy via cell fusion

Exoplasmic membrane fusion is a fundamental, essential process in both human development and in mature individuals. The fusion of two or more of the same cell type results in the formation of a syncytium, which are found in muscle, bone, and cartilage as well as placenta. Many multinucleated giant cells are examples of syncytia, arising from the fusion of stem cell precursors of the same phenotype. The fusion of different cell types results in the formation of a heterokaryon. Some multinucleated giant cells are examples of heterokaryons, for

example those which form by the fusion of bone marrow derived stem cells with hepatocytes, cardiomyocytes or neurons^{142, 143}. Whilst the important functions of the cell fusion process are well studied, the molecular mechanisms which drive it are less clear. Membrane fusion is a critical step in viral infection, as cellular infection requires fusion of the viral membrane and the membrane of the host cell; Viruses are also known to form pathological syncytia. As a result, many molecular studies have focussed on viral fusion, providing valuable insight into the proteins involved. Six classes of cell fusion proteins, called fusogens, have been identified and categorised based on their tertiary structure: Class I, II, III and IV virus-cell fusogens, and class I and II cell-cell fusogens. Fusogens act by changing their conformation upon activation, or 'triggering', from metastable pre-fusion structures to structures conducive to membrane fusion; Different classes of fusogens undergo different conformational changes. Possible triggers for this activation include receptor binding, changes in pH and proteolytic cleavage.

1.2.5.1. Macrophage fusion

Macrophages are thought to possess an increased potential for cell fusion when compared with other myeloid cell types, and a number of multinucleated cell types arise from macrophage fusion. Though the specific mechanisms involved in macrophage fusion are still being studied, our current understanding of the process can be described in four functional steps (Reviewed in¹⁴⁴):

1. Cellular reprogramming to a fusion-ready state

As macrophages are exposed to certain exogenous or endogenous factors, signalling cascades are triggered resulting in upregulation of genes necessary for cell fusion. Some of the exogenous factors known to drive this process are produced by immune cells. The Th2 cytokines IL-4 and IL-13 have been shown to induce macrophage fusion, as well as IL-3, IFN γ , GM-CSF, M-CSF and RANKL¹⁴⁴⁻¹⁴⁷. Activation of macrophages by these factors leads to transcriptional changes resulting in the upregulation of cell fusion proteins like dendritic cell-specific transmembrane protein (DC-STAMP) and E-Cadherin^{148, 149}. Factors produced by macrophages themselves may also appear to be necessary for these transcriptional adjustments. An example of this is DNAX activating protein 12 (DAP12), a protein produced by macrophages. DAP12 associates with a number of cell surface receptors including triggering receptor expressed on myeloid cells 2 (TREM-2), which has been implicated in multinucleated giant cell formation¹⁵⁰.

2. Chemotaxis

Chemotaxis is the movement of cells following changing concentration gradients of chemoattractants such as chemokines. This is a critical step in any cell fusion event to ensure cells are sufficiently proximal. The chemokine CCL2 is thought to play a key role in macrophage fusion, as demonstrated by a murine CCL2 knockout study in which multinucleation was measured¹⁵¹. A number of studies have also shown that CCL2 is required for osteoclastogenesis, though this may be in part due to the importance of the CCL2/CCR2 axis in monocyte recruitment to sites of bone resorption¹⁵²⁻¹⁵⁵. The cytosolic protein tyrosine phosphatase PTP-PEST may also play a role in macrophage migration leading to fusion, having been shown to be required for osteoclastogenesis¹⁵⁶.

3. Membrane attachment

With macrophages in close proximity following chemotaxis, the next stage of the process is the contact and subsequent attachment of cell membranes. A number of cell surface proteins have been implicated in this process. One such molecule which is thought to be a key player is the cell surface trafficking and fusion protein E-cadherin which, when blocked, prevents *in vitro* macrophage membrane attachment and fusion¹⁴⁹. Furthermore, IL-4 treatment of macrophages has been shown to promote a transcriptional upregulation of E-cadherin in a STAT6-dependent manner, as well as DC-STAMP¹⁴⁹. E-cadherin is also implicated in membrane attachment during osteoclastogenesis¹⁵⁷.

Integrins may also play a key role in macrophage membrane attachment. The integrin family of proteins are crucial cell surface proteins most well studied in their capacity to attach cell membranes with extracellular matrix to propagate cell migration¹⁵⁸. Their role in cell to cell fusion is less well studied, though $\beta 1$ and $\beta 2$ integrins have been shown to mediate mycobacterial lipid-induced and IL-4 induced macrophage fusion *in vitro*^{159, 160}.

4. Rearrangement of the cytoskeleton

Cytoskeletal rearrangements are critical for successful cell fusion. This has been demonstrated in the context of syncytia formation by the fusion of myoblasts, but is less

well characterised during macrophage fusion¹⁶¹⁻¹⁶³. As cells merge, reorganisation of the resultant multinucleated cell is necessary to maintain or adapt cellular functionality and escape programmed cell death. This reorganisation is dependent on cytoskeletal rearrangements by guanine nucleotide exchange factors (GEFs). Ras-related C3 botulinum toxin substrate 1 (Rac1), a downstream protein activated by GEFs is involved in FBGC formation, suggesting a similar mechanism in IL-4 induced macrophage multinucleation to that shown in myoblasts¹⁶⁴. A recent study has also demonstrated the importance of ubiquitin in the remodelling of the cytoskeleton during mammalian cell fusion¹⁶⁵.

The area of the membrane at which contact is made and adhesion occurs with the membrane of a second cell, undergoes conformational changes. Interestingly, the phospholipid phosphatidylserine (PtdSer) is thought to be involved. PtdSer is typically localised to the plasma membranes inner leaflet and upon the activation of certain signalling cascades, particularly those relating to apoptosis, ptdser is redistributed to the outer surface of the cell membrane by proteins called flippases. This allows its recognition by phagocytic cells as an indication that the cell is undergoing programmed cell death and is a target for phagocytosis. Studies of the composition of the outer membrane during cell fusion reveal that ptdser is exposed on the outer membrane during both myoblast and macrophage fusion^{166, 167}.

A number of other factors have identified which may mediate the macrophage fusion process, but the mechanisms by which they achieve this are less well understood than those discussed in the four stages discussed. The intracellular adhesion molecule ICAM1 and lymphocyte function-associated antigen 1 (LFA-1) are upregulated during in human macrophages programmed for fusion, and ICAM1 has also been shown to localise to sites of membrane attachment^{168, 169}. The tetraspanins CD9 and CD81 are involved in numerous cell fusion events such as the fusion of sperm and egg cells, and myoblast syncytia formation¹⁷⁰⁻¹⁷². Despite this, some evidence suggests they have an inhibitory effect on both viral syncytia formation and in the fusion of mononuclear phagocytes^{173, 174}. There are, however, conflicting reports as CD9 has been shown to be positively involved in HIV-1-induced fusion events and osteoclastogenesis, and both CD9 and CD81 implicated in the formation of multinucleated giant cells from macrophages¹⁷⁵⁻¹⁷⁷. Additionally, CD9 and CD81, along with further

tetraspanins CD53 and CD63 are differentially expressed by different monocyte subsets, which may be linked with the different capacities for cell fusion between them¹⁷⁸. Other factors implicated in macrophage fusion through poorly characterised mechanisms include metalloproteinase 9 (MMP9), CD47 and the intracellular domain of CD44¹⁷⁹⁻¹⁸¹.

1.3. Multinucleated giant cells

In the above section, the broad mechanisms by which multinucleated cells arise were discussed. As the focus of this thesis is a specific macrophage/monocyte derived multinucleated cell type, Langhans-type multinucleated giant cells (LMGCs), here multinucleated cells of similar lineage will be compared. The most well characterised of these are outlined in table 3:

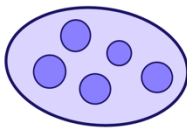
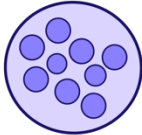
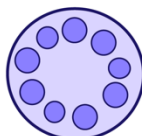
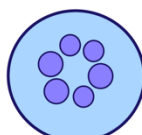
Cell type	Proposed formation mechanism(s)	Associated pathologies	Known markers	Morphology
Osteoclast	Cell fusion	<ul style="list-style-type: none"> - Osteoporosis - Renal osteodystrophy - Osteopetrosis - Paget's disease - Rickets 	<ul style="list-style-type: none"> - TRAP - Cathepsin K - c-FOS - NFATc1 	
Foreign body giant cell	Cell fusion	<ul style="list-style-type: none"> - Foreign body granuloma responses - Leprosy 	<ul style="list-style-type: none"> - CD68 - DCSTAMP - E-Cadherin 	
Langhans multinucleated giant cell	Cell fusion Modified cell division	<ul style="list-style-type: none"> - Giant cell arteritis - Granulomatosis with polyangiitis - Sarcoidosis - Crohn's disease - Tuberculosis 	<ul style="list-style-type: none"> - CD68 - iNOS - Langhans-type S100+ 	
Touton (Xanthelasmatic) giant cell	Cell fusion Lipid uptake	<ul style="list-style-type: none"> - Fat necrosis - Xanthoma - Xanthogranulomas 	<ul style="list-style-type: none"> - CD68 	

Table 3. Macrophage/monocyte derived multinucleated giant cell subsets.

Proposed formation mechanisms, related pathologies, known phenotypic markers, and morphological representations.

Cell fusion is widely accepted as the common mechanism for the formation of these phenotypically distinct multinucleated giant cells, though the differences in the stimuli required and the circumstances leading to their formation suggest that the specific signal transduction pathways involved may be different. The marked differences in both morphology and functional adaptations between cell types also indicates differences in the pathways involved in their respective formations. The specific mechanism of LMGC formation is discussed in greater detail in chapter 4 of this thesis.

1.3.1. Osteoclasts

The formation mechanism and functional adaptations of osteoclasts are relatively well understood. They secrete collagenase, an enzyme which degrades the hydroxyapatite mineral component of bone, and are the only multinucleated giant cells known to carry out this function¹⁸². Bone resorption is an essential process for the maintenance of bone, and deficiency in the formation of osteoclasts leads to the development of conditions such as osteopetrosis, in which bone-matrix fills the cavity of the bone marrow as it cannot be resorbed¹⁸³. Osteopetrosis can lead to death due to increased risk of infection and immune deficiency^{184, 185}. Hyperactive osteoclasts are also problematic, leading to excessive bone resorption and osteosclerosis¹⁸⁶.

A number of culture systems for the generation of osteoclasts *in vitro* have been developed. There are two key cytokines used to induce osteoclastogenesis, macrophage-colony stimulating factor (M-CSF) and receptor activator of NFκB ligand (RANKL)¹⁸⁷⁻¹⁸⁹. Early studies involved the isolation of osteoclasts or osteoclast precursors from the extracted bones of euthanised animals, and subsequent tissue culture¹⁹⁰⁻¹⁹². They have more recently been derived from macrophage cell lines, primary pluripotent stem cells or peripheral blood mononuclear phagocytes (PBMCs), including those from humans by M-CSF and RANKL stimulation in culture¹⁹³⁻¹⁹⁵. The molecular pathways through which RANK-RANKL signalling drives osteoclastogenesis are well studied. The RANK transmembrane protein interacts with TNF receptor-associated factor 6 (TRAF6), which has shown to be necessary for osteoclastogenesis¹⁹⁶. The downstream signalling cascade of TRAF6 involves p62, TGF-beta activated kinase 1 binding protein 2 (TAB2), TGF-beta activated kinase 1 (TAK1), IκB kinase 1/2 (IKK1/2), and p38, ultimately leading to the induction of transcription factors such as nuclear factor of activated T cells c1 (NFATc1) which regulate osteoclastogenesis¹⁹⁷⁻¹⁹⁹.

1.3.2. Foreign body-type multinucleated giant cells

Like osteoclasts, foreign body-type multinucleated giant cells (FBGCs) are thought to form by the fusion of myeloid precursors. They are observed as part of the 'foreign body response' in which immune cells respond to invasion by large foreign objects, making them particularly common with the insertion of catheters or biomaterials, or invasion by parasites. They are also observed in infectious pathologies such as leprosy²⁰⁰. FBGCs have been demonstrated to have enhanced complement-mediated phagocytosis, suggesting a role in particle clearance²⁰¹. There are, however, conflicting reports showing their reduced phagocytic capacity, which may be due to the difficulty in the identification of macrophage polykaryon subsets, and differences in the method used to measure endocytosed particles^{202, 203}.

Studies of the foreign body reaction have largely been performed in murine models; Implantation of plastic or glass coverslips is used to induce FBGC formation *in vivo*. Tissue-resident macrophages cluster around the implanted material and undergo cell fusion events to form FBGCs on its surface, covering up to 25% of it²⁰⁴⁻²⁰⁶. *In vitro* FBGC culture systems have been developed which use primary monocyte/macrophages stimulated by either interleukin 4 (IL-4) or 13 (IL-13)^{207, 208}. The signalling pathways which act downstream of these cytokines to induce macrophage fusion are not as well studied as those involved in osteoclastogenesis, though β 1 and β 2 integrins have been implicated¹⁶⁰.

1.3.3. Langhans-type multinucleated giant cells

LMGCs are defined by their distinctive morphology with a horseshoe-shaped arrangement of nuclei, and are observed in a number of seemingly disparate pathologies such as Crohn's disease, granulomatosis with polyangiitis and giant cell arteritis (GCA). They also co-exist with FBGCs in a number of pathologies, for example in the cutaneous lesions of sarcoidosis²⁰⁹, suggesting that they may be induced by shared factors, though this has been disproven experimentally, with *in vitro* LMGCs instead forming in response to GM-CSF, IFN γ , IL-13 and TLR2 agonists^{99, 210}. The *in vitro* culture systems used to generate LMGCs in the literature will be discussed in greater detail in chapter 2 of this thesis. In brief, early efforts relied on the implantation of glass coverslips into mice to illicit the foreign body response and cause the generation of multinucleated giant cells, some of which morphologically resembled LMGCs. Later studies used the *in vitro* differentiation of peripheral monocytes into LMGCs using a

variety of factors; GM-CSF, M-CSF, IL-15, IFN γ , TLR2 agonists, 30% AB+ human serum, IL-3, ConA and ConA conditioned media have all been used^{99, 207, 210-214}. The detection and measurement of LMGCs has improved with technological advances, from basic staining and light microscopy to high resolution confocal microscopy, and even more recently flow cytometry^{99, 211, 214}.

The differences in the factors inducing the formation of different myeloid derived polyploid cells suggest the involvement of distinct signalling pathways. It is unclear to what extent these pathways differ though the formation of LMGCs, whilst still poorly understood, is seemingly more compounded than the cell fusion mechanisms of osteoclasts and FBGCs. Historically, evidence in the literature indicated cell fusion as the sole formation mechanism for LMGCs, however, more recent evidence also implicates modified cell division with failed cytokinesis^{99, 215-217}. Cell-cycle dependent polyploidy is responsible for the formation of a number of well characterised multinucleated cell types in humans, including megakaryocytes, trophoblasts and hepatocytes^{100, 218, 219}. However, for these cell types polyploidy has a beneficial effect by granting enhanced functionality. It is unclear whether this is the case for LMGCs. The mechanism of LMGC formation will be discussed in greater detail in chapter 4 of this thesis.

Polyplody typically offers beneficial functional adaptations, for example, osteoclasts are able to secrete collagenase and resorb bone following multinucleation. The functional adaptations of LMGCs are not well understood, though we have some clues from studies into the pathologies in which they're described. During this project LMGCs were studied in the context of GCA, where they have previously been implicated in ROS mediated damage to arterial walls⁵⁸, production of pro-inflammatory mediators driving intimal hyperplasia via the breakdown of the elastic lamina and vascular smooth muscle cell hyperproliferation²²⁰⁻²²², and the formation of intimal vasa vasorum further driving inflammation⁴⁰. The functional adaptations of LMGCs are explored further in chapter 5 of this thesis.

1.4. Aims of this study

The overall aim of this research was to build on current knowledge of LMGCs in the context of GCA, characterising them in terms of their origin and functional adaptations to ultimately better understand their role in GCA. Existing evidence in the literature is nebulous, with divergent studies suggesting either cell fusion or modified cell division as the sole mechanism of LMGC formation. This variance may not be helped by the number of different *in vitro* culture systems used to study LMGCs, with numerous factors shown to induce their differentiation from primary monocytes. Speculative evidence links LMGCs to ROS mediated arterial damage in GCA, as well as indicating their potential involvement in driving intimal hyperplasia.

The overarching hypothesis of this research is that LMGCs in GCA form by DNA-damage induced cytokinesis failure and exert a pro-inflammatory phenotype. By generating and validating an *in vitro* LMGC culture system which recapitulates to some degree, the *in vivo* process, I aimed to identify constituents of the LMGC secretome which may play a role in the pathogenesis of GCA; I hypothesised that LMGCs express, to a higher degree than mononucleated macrophages, cytokines known to drive the inflammatory granulomatous reaction in GCA such as IL-6 and TNF α , and damaging reactive oxygen species which cause lipid peroxidation of vascular smooth muscle cells in affected arteries. By uncovering the role that LMGCs play in GCA it may highlight the importance of targeting them therapeutically, and by better understanding the mechanism by which they form we may, with much further investigation, identify novel therapeutic targets in the future.

The objectives of this study were:

- To test different *in vitro* LMGC culture systems from the literature to identify the protocol with highest LMGC yield, and to validate this morphologically
- To interrogate *in vitro* LMGCs transcriptionally using single cell RNA sequencing, as well as temporal artery biopsies to identify LMGC transcripts in GCA-affected tissue
- To investigate the mechanism of *in vitro* LMGC formation with high resolution imaging techniques
- To investigate the functional adaptations of *in vitro* LMGCs, with support from single cell RNA sequencing data

Chapter 2. Generating Langhans-type multinucleated giant cells *in vitro*

2.1. Introduction

Due to the relative rarity of pathologies in which LMGCs are present, and the difficult nature of tissue acquisition from patients, obtaining *in situ* LMGCs for research can be strenuous and time-consuming. It is therefore critical to develop a robust *in vitro* culture system, which effectively recapitulates the *in vivo* process, to study the characteristics of LMGCs. The aims of this chapter were to compare LMGC culture protocols from the literature, and then to adopt, optimise and validate the most effective of these to generate a robust culture system with high LMGC yield, facilitating *in vitro* functional assays. A selection of publications in which LMGCs have been generated *in vitro* are outlined in table 4:

DATE	AUTHOR(S)	LMGC GENERATION METHOD	LMGC DETECTION METHOD
1974	M. Mariano & W. G. Spector	IN VIVO - Mice implanted with glass coverslips	Light microscopy
1977	A. H. Warfel	IN VITRO - BCG added to rabbit alveolar cells	Light microscopy / SEM
1978	H. J. van der Rhee et al.	IN VIVO - Mice implanted with Melinex plastic	Light microscopy
1982	A. E. Postlewaite et al.	IN VITRO - Human monocytes + 30% AB+ human serum	Light microscopy
1982	A. R. Murch et al.	IN VIVO - Mice implanted with Melinex plastic	Light microscopy
1991	R. I. Enelow et al.	IN VITRO - IL-3 and IFN-gamma	Light microscopy
1994	Fais S et al.	IN SITU - IFN-gamma	Immunohistochemistry
1995	A. K. McNally et al.	IN VITRO - GM-CSF and IFN-gamma added to macrophages	Light microscopy
1997	J. Möst et al.	IN VITRO - ConA conditioned media / PMA + anti HLA-DR MoAB	Light microscopy
1999	A. Gasser & J. Möst	IN VITRO - BCG + cytokine-containing supernatants	Light microscopy
2007	G. Lay et al.	IN VITRO - M. tuberculosis added to macrophages	Immunofluorescence
2011	H. Sakai et al.	IN VITRO - ConA stimulated T cell co-culture	Light microscopy
2016	L. Herrtwich et al.	IN VITRO - M-CSF + TLR2 agonists added to macrophages	Immunofluorescence / Flow cytometry
2018	T. C. Champion et al.	IN VITRO - ConA added directly to primary monocytes	Immunofluorescence / SEM
2019	S. Mezouar et al.	IN VITRO - ConA added directly to primary monocytes	Immunofluorescence
2020	H. Wang et al.	IN VITRO - IL-15 added to primary monocytes	Immunofluorescence

Table 4. A selection of notable publications in which LMGCs are generated.

in vivo/situ with animal models or excised human tissue (red ), or *in vitro* with monocyte/macrophage culture systems (blue ).

Early studies investigating the factors involved in the formation of LMGCs were largely performed in animal models. The most common technique was to use plastic or glass implantation in live animals to illicit a 'foreign body' immune response, including the formation of inflammatory multinucleated giant cells, morphologically representative of what are now referred to as LMGCs / Langhans giant cells / inflammatory giant cells²²³⁻²²⁵. At this time, *in vitro* studies were few in number, but some early *in vitro* culture systems using animal cells were developed. A. H. Warfel, in 1977, demonstrated that rabbit alveolar cells became multinucleated in response to culture with BCG²²⁶. Five years later Postlewaite et al. generated human LMGCs using monocytes isolated from peripheral blood, a methodology which became more common in various adaptations after 1990, and is still used^{99, 207, 211-214, 227-230}.

Studies before 1990 almost exclusively used light microscopy in combination with various staining techniques, such as May-Grunwalk-Giemsa stain, Wright's stain, and standard Giemsa to detect and measure the formation of multinucleated giant cells. As experimental techniques and technologies advanced over time there was a shift away from standard light microscopy towards immunofluorescence and fluorescence microscopy. Staining cells with DNA-binding dyes such as DAPI allows accurate visualisation of nuclei, and co-staining for structural proteins such as actin or tubulin allows for visualisation of the cell cytoskeleton. DNA staining could now also be combined with standard light microscopy to give a clearer image detailing the gross morphology of the cell and the number of nuclei within. This combination improved the ability of scientists to detect and quantify multinucleated giant cell formation, reducing some of the ambiguity observed with less advanced staining methods.

Multinucleation is most commonly measured using imaging techniques, however, a recent paper by Herrtwich et al. demonstrated that it was feasible to use flow cytometry to assess ploidy⁹⁹. Whilst lacking some validation, they were able to show that cell suspensions comprising both mononucleated and multinucleated cells could be separated and sorted by ploidy using flow cytometry, by staining cells with a DNA-binding dye. Cells with higher DNA content were seemingly brighter in the appropriate detection channel for the dye used. The use of flow cytometry as a tool for the measurement of ploidy offers a number of advantages compared with microscopy techniques. Microscopy, if not performed in a blinded fashion, may introduce bias during selection of imaging fields, when deciding on which cells

to count or exclude, or when manually determining areas to in which to calculate mean pixel intensity. Flow cytometry is a high throughput method; The speed at which multinucleated cells can be counted is higher and it can be performed easily for an entire culture, rather than measuring a selection of representative cells as is practical for microscopy. Additionally, the staining procedure is often quicker and cheaper, without as much need for secondary antibody incubations.

Producing *in vitro* LMGCs in high quantities will be beneficial for further experimentation, therefore I aimed to use light microscopy, fluorescence microscopy, flow cytometry and FACS to optimise an *in vitro* LMGC culture system for maximal LMGC yield. First, I aimed to validate flow cytometry as a suitable technique for the measurement of polyploidy using a combination of FACS, cytopins, and giema staining. Initially, a combination of GM-CSF and IFN γ was used to induce *in vitro* LMGC formation from primary monocyte cultures. This was chosen due to the immediate availability of cytokines, and as multiple sources in the literature strongly implicate IFN γ in the multinucleation process^{147, 168, 210, 231}.

2.1.1. Chapter aims

The aim for this chapter given the eclectic, non-uniform nature of LMGC culture protocols in the literature was to select, optimise, and morphologically validate a single protocol for use in the subsequent chapters of this thesis. I hypothesised that flow cytometry would be more suitable than microscopy techniques for the measurement of LMGC yield due to its high-throughput, unbiased nature.

The objectives of this chapter were as follows:

1. To assess the viability of flow cytometry for the detection and measurement of multinucleated giant cells from mixed cultures.
2. To compare published *in vitro* LMGC culture methods and optimise a chosen method for maximal yield.
3. To validate *in vitro* LMGCs in terms of their recapitulation of tissue LMGCs morphologically.

2.2. Using flow cytometry to assess multinucleation

2.2.1. Validation of multinucleated cell gating strategy using ImageStream

To assess the suitability of flow cytometry to discriminate populations of multinucleated cells and mononucleated cells within mixed cell suspensions, imaging flow cytometry was used, 'ImageStream'. This technology bridges the gap between flow cytometry and fluorescence microscopy by providing microscopy images, both brightfield and fluorescent, for each event that passes the detector. This allows the user to gather additional morphological information, which we hoped would allow the visual confirmation of multinucleated cells.

Once grown, adherent LMGC cultures were incubated with trypsin to create single cell suspensions and stained with DRAQ5, a far-red fluorescent DNA-binding dye suitable for detection by flow cytometry. Cells were run on the imaging flow cytometer (ImageStream X Mark II) and DRAQ5 intensity was used as a gating metric to discriminate cells based on their ploidy. Within the DRAQ5^{low} population, exclusively mononucleated cells were observed, whereas the DRAQ5^{hi} population contained both single LMGCs, and aggregated clumps of mononucleated cells.

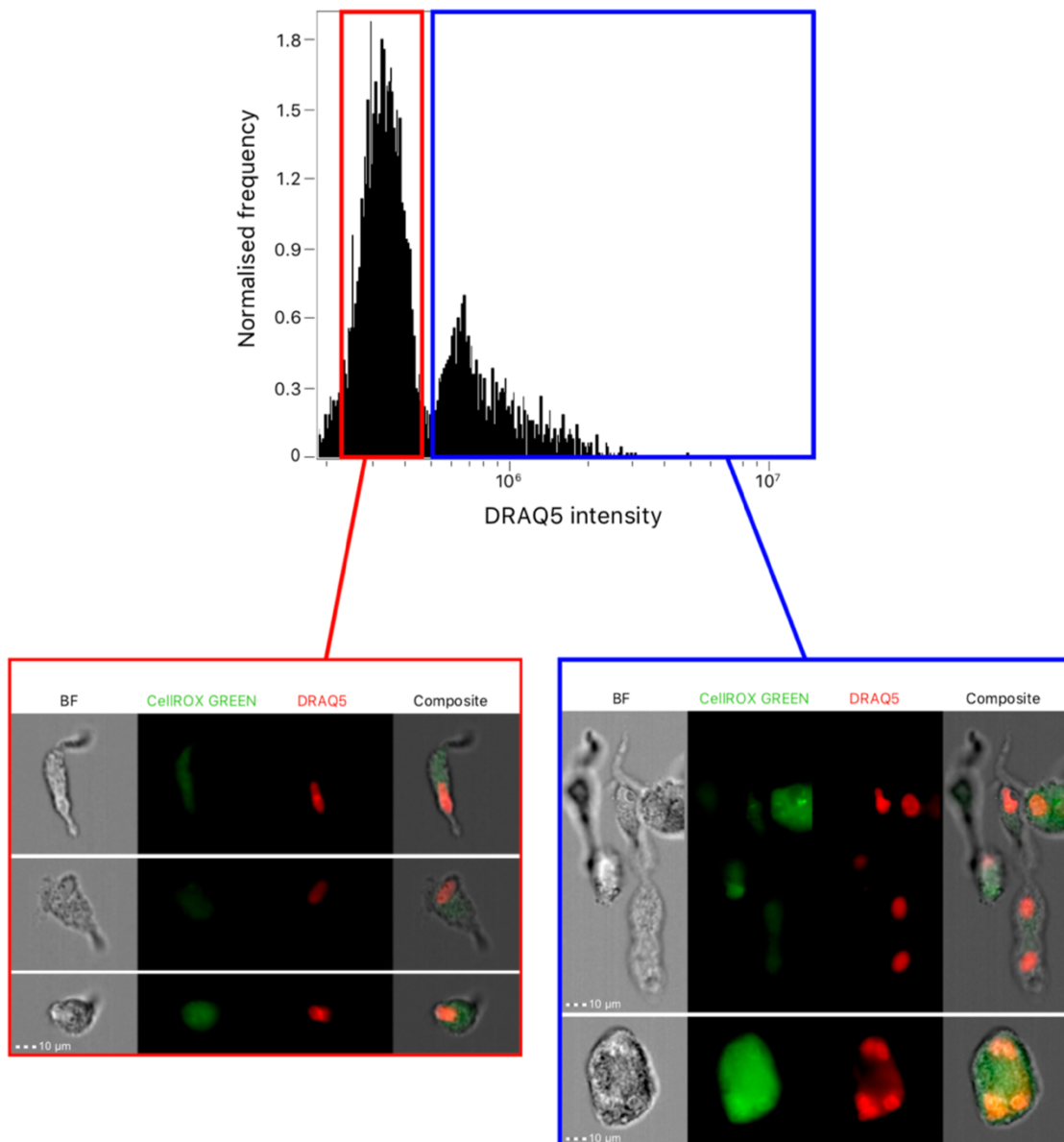


Figure 3. Imaging flow cytometry of *in vitro* LMGCs.

Imaging flow cytometry of mononucleated, aggregated and multinucleated cells. Gating strategy used to distinguish suspected mononucleated (red, DRAQ5^{low}) and multinucleated (blue, DRAQ5^{hi}) populations shown. Representative brightfield (BF) and fluorescence (CellIROX GREEN, DRAQ5) images shown below. Scale bars = 10µm. N=1.

This data demonstrates that mononucleated cells can be partially separated from multinucleated cells by flow cytometry using DNA-binding dyes, however, populations of multinucleated cells were impure; Clusters of mononucleated and binucleated cells were often observed in addition to multinucleated cells. In flow cytometry cell aggregates, often two conjoined cells termed 'doublets', are eliminated using an FSC-H (forward scatter height) vs FSC-A (forward scatter area) gate, but we later found that this would also eliminate multinucleated cells and so could not be used. To address this technical limitation, I next aimed to quantify the impurity of DRAQ5^{hi} populations following fluorescence-activated cell sorting (FACS).

2.2.2. Validation of LMGC sorting strategy with FACS

To further investigate and quantify the extent to which multinucleated cells can be isolated from mixed cell suspensions by flow cytometry, FACS was performed which was followed by cytopins and then giemsa staining. Cultures were prepared as before, and once sufficiently developed to the point at which large cells could be observed, all cells were harvested again with trypsin-EDTA, and stained with DRAQ5. Stained cells were run on the FACSFusion cell sorter, and distinct populations were clear based on the brightness of the DNA dye. Three populations were sorted, labelled as DRAQ5^{low}, DRAQ5^{med}, and DRAQ5^{hi}. These were proposed to represent populations of mononucleated cells (1N), cells with 2 or 3 nuclei (2-3N), and cells containing more than 3 nuclei (4N+) respectively. Once these populations were sorted, a cytopin was used to adhere cells to microscopy slides. Standard giemsa staining was performed according the Sigma 'Standard giemsa' protocol, stained for 20 minutes at room temperature, washed with dH₂O three times and air dried. Once dry, slides were mounted with a coverslip, using DPX mountant, and air dried again before being imaged on the Zeiss AxioImager upright fluorescence microscope. Using a 20x objective lens, a 5x5 field of view grid was imaged. Complete images were then analysed manually to determine the number of nuclei per cell, for a minimum of 100 cells per population.

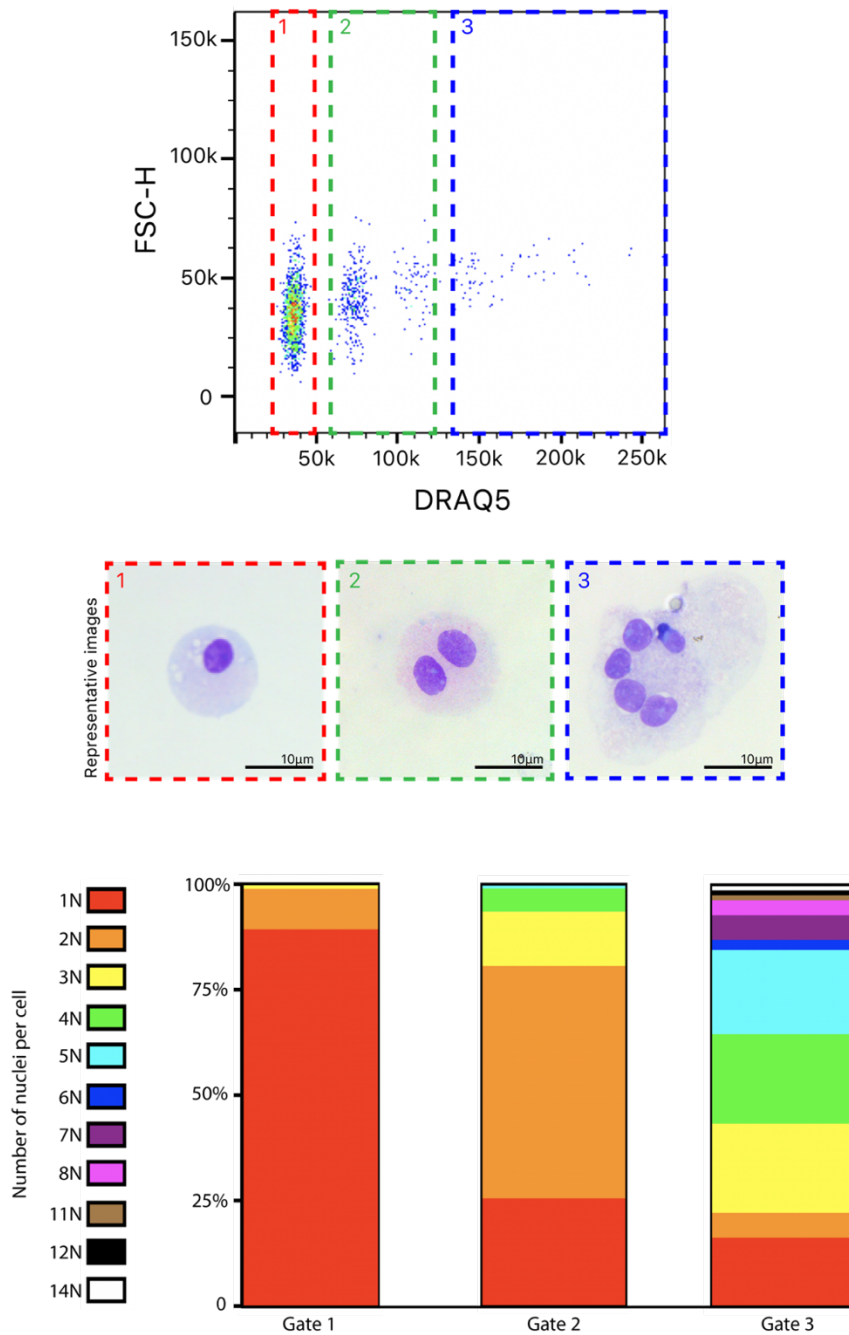


Figure 4. Using FACS to validate multinucleated cell sorting strategy.

Top – Gating strategy. DRAQ5^{low}, DRAQ5^{med}, and DRAQ5^{hi} gates (1, 2, and 3 respectively) shown. Middle – Giemsa-stained representative images. Scale bars = 10µm. Multinucleated cells displayed typical LMGC nuclei arrangement. Bottom – Number of nuclei per cell of 100 cells for each gate, corresponding to the above gating strategy. N=1.

This data shows the relative purities of the three FACS gates used. Reassuringly, the majority of cells from gate 1 were mononucleated, with a small number of binucleated cells also observed. This could possibly have been resolved by using a stricter gate, or it may be a result of variation in the size of nuclei. When analysing the giemsa stained images of cells, it became apparent that nuclei varied greatly in size, so it follows that a small selection of binucleated cells may have had smaller nuclei, and a DRAQ5 brightness comparable to mononucleated cells. The majority of DRAQ5^{med} cells of the second gate contained either two or three nuclei. Purity was lower than gate one, with roughly a quarter of cells being mononucleated. The most likely reason for this is the lack of ability to remove doublets, as discussed in 2.2.1. Gate 3 was the least pure, with approximately forty percent of cells containing either one, two or three nuclei. Again, this is likely due to the inclusion of doublets, or larger cell aggregates. Pleasingly, this was the only gate containing large multinucleated cells with 5 or more nuclei. With more donors to provide statistical power, this data could be used to apply an adjustment factor to subsequent flow cytometry data to account for the impurities of the gating strategy and give a more accurate measure of multinucleation.

2.3. Comparing LMGC culture methods from the literature

As discussed there are numerous protocols for the generation of LMGCs *in vitro* outlined in the literature, a selection of which are outlined in table 4. It is therefore difficult for researchers to determine the most effective and appropriate method for their own research. The low quantity of LMGCs produced by many protocols is an obstacle which may impede some experimental techniques. Using flow cytometry to assess the extent of multinucleation, the following primary monocyte culture conditions were used to assess LMGC yield:

- Granulocyte-macrophage colony-stimulating factor (**GM-CSF**) (5ng/mL) and Interferon gamma (**IFN γ**) (50ng/mL). Protocol taken from 1995 study by A. McNally and J. Anderson²⁰⁷. The authors used concentrations of 5ng/mL GM-CSF and 50ng/mL IFN γ . Later in this chapter, these concentrations were titrated to optimise for maximum LMGC yield.
- Interleukin 3 (**IL-3**) (56ng/mL) and **IFN γ** (50ng/mL). Protocol taken from 1998 study by T. Byrd¹⁴⁷. This combination of factors also used in 1992 study by R. Enelow et al²¹⁰.
- **GM-CSF** (50ng/mL) alone. This was used to determine whether multinucleation could be achieved in the absence of a pro-inflammatory mediator. Using IFN γ alone was also tried and found to be insufficient for cell survival in culture.
- Macrophage colony-stimulating factor (**M-CSF**) (20ng/mL) and the toll-like receptor 2 agonist **Pam3CSK4** (300ng/mL). Protocol taken from 2016 study by L. Herrtwich et al⁹⁹.
- **M-CSF** (50ng/mL) and **IFN γ** (200ng/mL). This was used to determine whether multinucleation in the presence of inflammatory stimulation was also dependent on GM-CSF.
- **M-CSF** (20ng/mL) alone. This was used to determine whether multinucleation is dependent on stimulation by pro-inflammatory mediators.

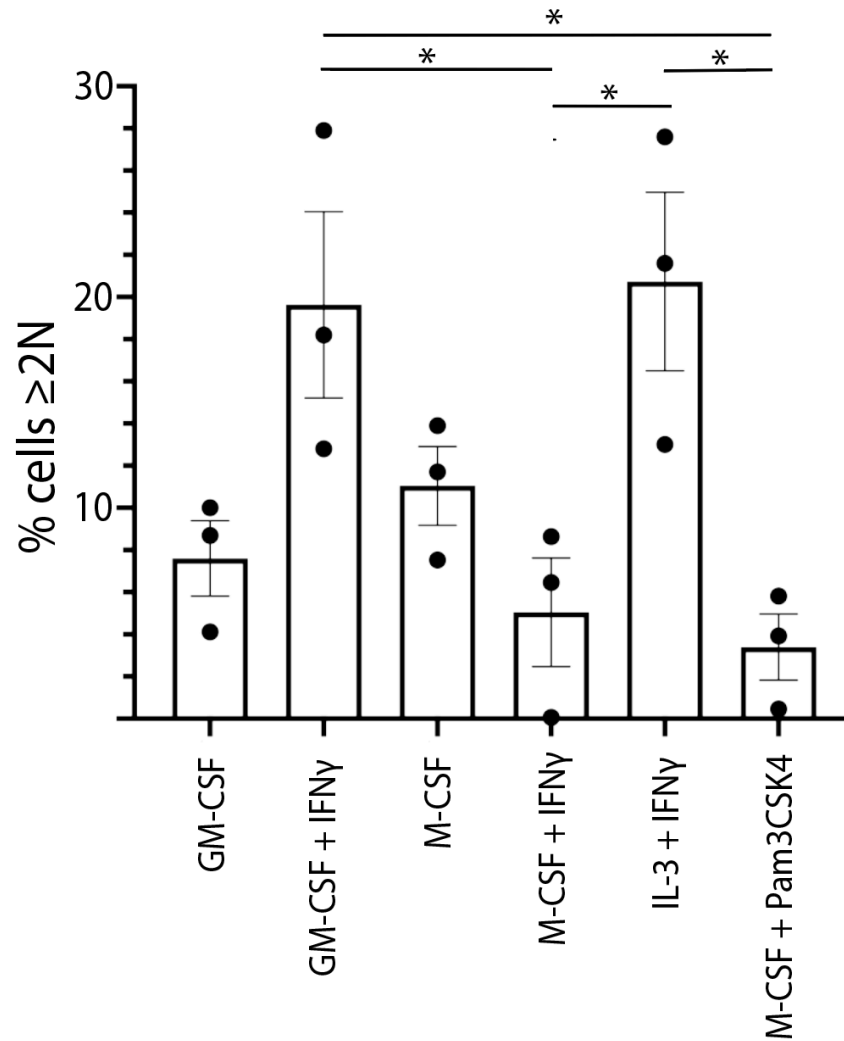


Figure 5. Comparison of *in vitro* LMG culture protocols from the literature.

Plot displaying relative multinucleation rate for outlined protocols. Statistical significance determined by one-way ANOVA with Tukey's multiple comparisons. * = $P < 0.05$. $n=3$.

The culture conditions leading to the highest yield of multinucleated cells were GM-CSF + IFN γ , and IL-3 + IFN γ . Both resulted in significantly higher yields than the combination of M-CSF and the toll-like receptor 2 (TLR2) agonist Pam3CSK4 ($p < 0.05$). I decided to take forward the use of GM-CSF and IFN γ for the next chapters of this thesis as one of the most effective combinations, and the immediate availability and reliability of these cytokines. Next, I aimed to optimise this protocol for maximal LMGC yield.

2.4. Optimisation of my chosen *in vitro* LMGC culture system

2.4.1. Titrating GM-CSF and IFN γ

A concentration titration for both of the factors used in the chosen culture system, GM-CSF and IFN γ , was carried out. The aim was to find the optimal concentrations, resulting in the highest yield of LMGCs without reaching hypertoxic levels. A range of 0.05 – 500ng/mL GM-CSF and 0.02-2000ng/mL IFN γ was used and again measured multinucleation with flow cytometry. The proportion of events captured by flow cytometry which were determined to be cellular debris using a forward scatter-area (FSC-A) vs side scatter-area (SSC-A) plot was used as a crude measure of culture health.

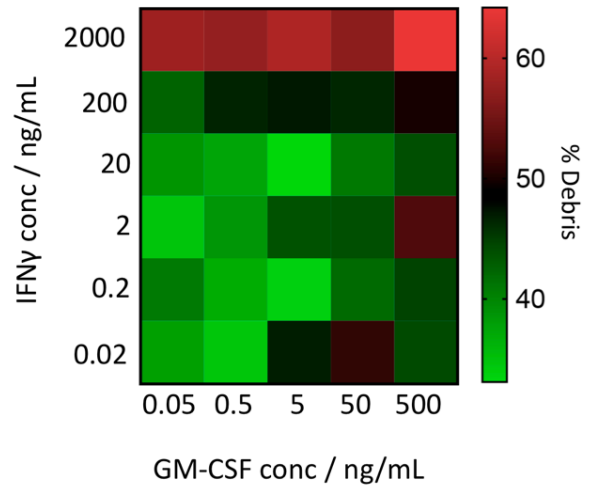
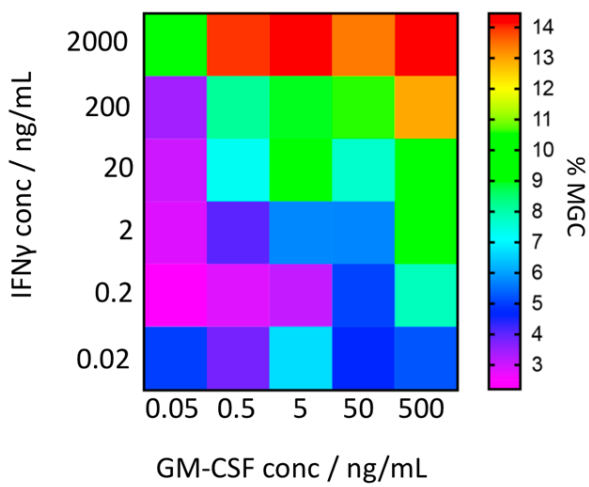


Figure 6. Optimising cytokine concentrations.

Heatmaps showing LMG formation rate (left) and % events captured debris (right) with different cytokine concentrations. Debris defined using A^{low} , $FSC-A^{\text{low}}$ gate. Values are mean of three donors (n=3).

As expected, higher concentrations of both factors correlated with increased multinucleation, with the highest yields observed in cultures with 2000ng/mL IFN γ and 500ng/mL GM-CSF. At this concentration there was little difference when GM-CSF concentration was increased. There was a large increase in debris in cultures with 2000ng/mL IFN γ compared with 200ng/mL. Similarly, there was an increase in debris from 50ng/mL to 500ng/mL GM-CSF. Going forward, 50ng/mL GM-CSF and 200ng/mL IFN γ were used, though lower concentrations could be used if necessary to improve culture health at the cost of a marginal decrease in yield.

2.4.2. Optimising culture time, monocyte seeding density and culture medium

In addition to finding the optimal concentrations of IFN γ and GM-CSF, three further factors were investigated in order to generate the highest yield of LMGCs; Culture time, seeding density and type of culture medium. A time course experiment was performed, culturing monocytes with GM-CSF and IFN γ , and using flow cytometry to measure the LMGC yield every 24 hours, beginning 144 hours after seeding, as this was when cultures began to take on a differentiated phenotype when observed using a standard light microscope. Monocytes were seeded at a range of densities, from 20,000 cells to 100,000 cells plated in each well of a 96 well flat-bottomed plate. In part, the premise behind this experiment was to investigate whether a higher monocyte seeding density would increase LMGC yield due to the close proximity of cells facilitating cell fusion, without having investigated the formation mechanism at this stage of the project. Finally, three different culture media were tested to grow LMGCs: RPMI, DMEM and α MEM. RPMI is typically used for the culture of primary monocytes, as well as numerous other primary cell types, DMEM is more commonly used for cell line culture, or for primary fibroblasts, neurons or smooth muscle cells, and α MEM is commonly used for cells grown in monolayers, in particular, the *in vitro* culture of osteoclasts.

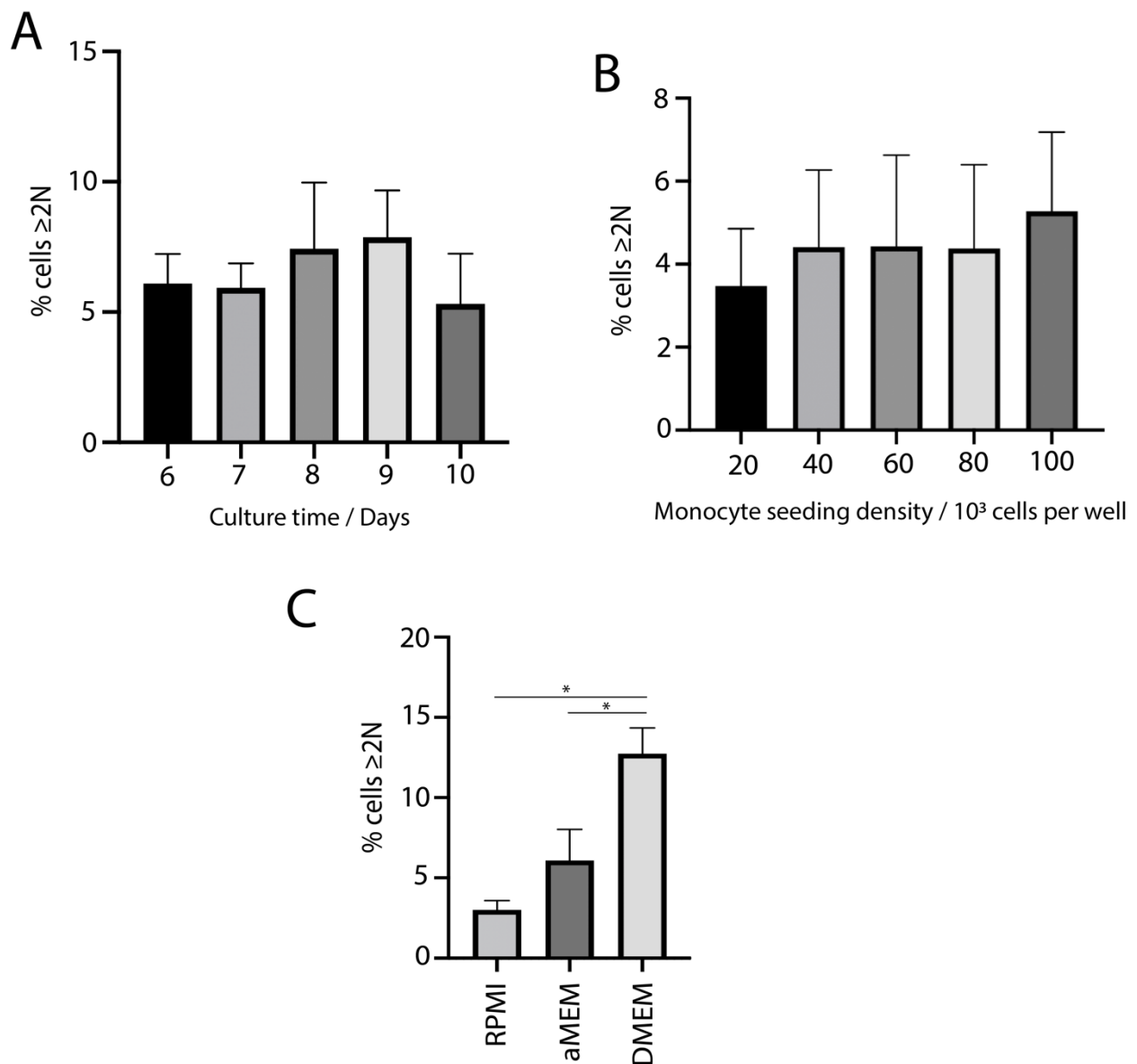


Figure 7. Optimisation of culture conditions.

Optimisation of culture time, cell seeding density and culture medium type for the generation of LMGs. A) Time course experiment. A non-statistically significant increase in multinucleated cells on days 8 and 9. $P = 0.838$ (One-way ANOVA). B) A non-statistically significant slight trend towards increased multinucleation with higher seeding densities. $P = 0.975$ (One-way ANOVA). C) DMEM was significantly more effective in the generation of multinucleated cells than both RPMI and α MEM (* = statistically significant, $P > 0.05$) statistics performed = One-way ANOVA with Tukey's multiple comparisons test).

As a result of these optimisation experiments, although non-significant, I decided to seed monocytes at 100,000 cells per well in 96 well plates, or equivalent densities in larger plates, and culture them for 8-9 days. Unexpectedly, of the culture media tested DMEM was most effective.

Combining these now optimised conditions would allow me to carry out the transcriptional and functional studies required for later chapters of this thesis and provides a relatively consistent high-yield protocol for future studies.

2.5. Morphological evaluation of *in vitro* LMGCs

For the final section of this chapter, I aimed to align the now optimised *in vitro* LMGC culture system with *in vivo* LMGCs. As LMGCs of pathology are described and identified only by their distinctive morphology by pathologists, I planned to determine whether cultured LMGCs possessed the same distinctive morphological characteristics. Cell size and the arrangement of nuclei are key factors used in diagnosis of GCA. Unlike other types of multinucleated cell, LMGCs have a distinctive horseshoe arrangement of nuclei around the periphery of the cytoplasm, and contain up to 20 nuclei. Immunocytochemistry was used to stain cultured LMGCs for beta-actin, a structural protein to visualise the cytoplasm, and co-stained with DAPI to visualise nuclei by confocal fluorescence microscopy.

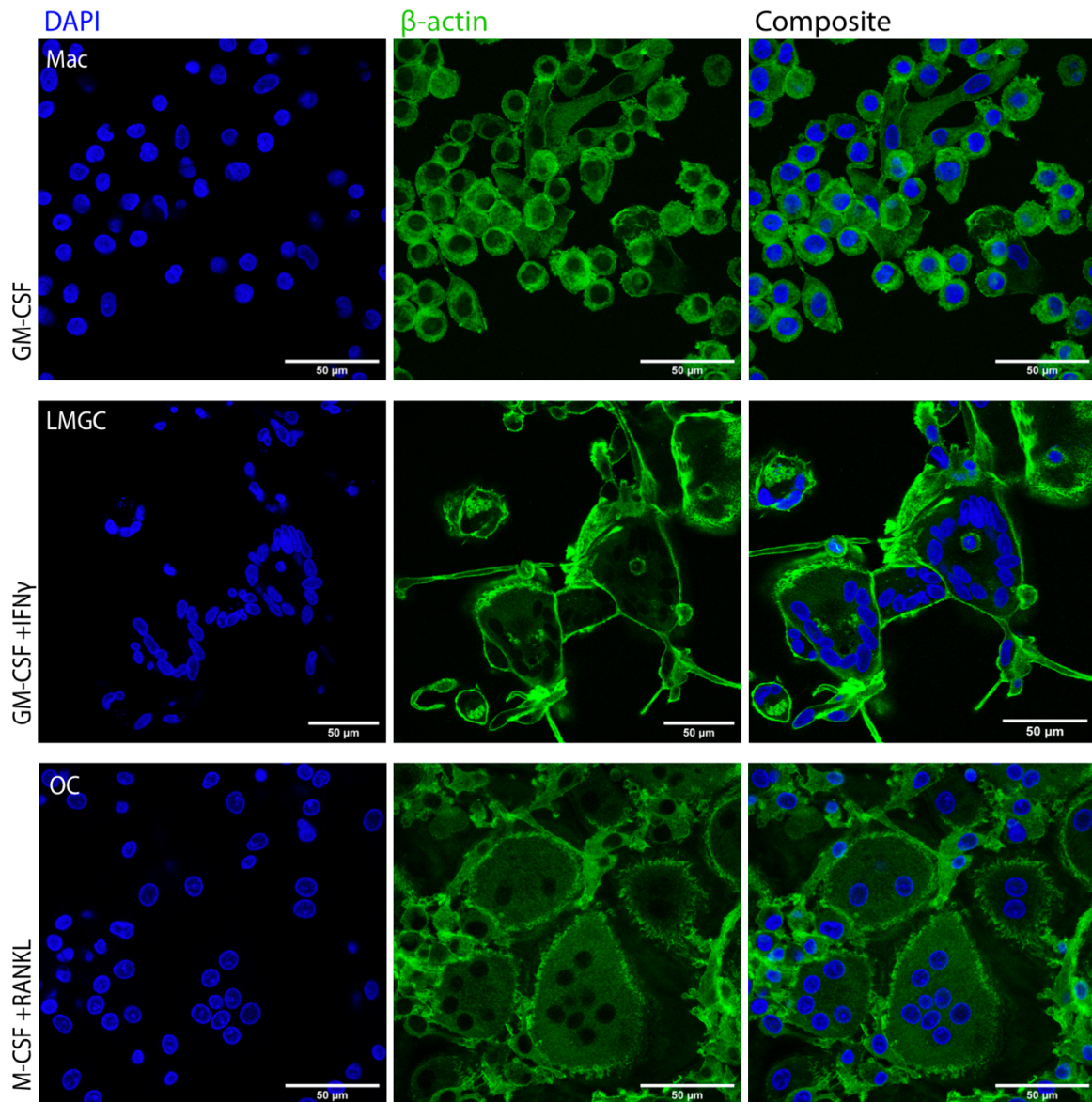


Figure 8. Morphological assessment of cultured macrophages, LMGCs and osteoclasts.

Top: control macrophages cultured in the presence of 50ng/mL GM-CSF only. Middle: Representative images of LMGCs cultured in the presence of 50ng/mL GM-CSF and 200ng/mL IFN γ . Bottom: Representative images of osteoclasts, cultured in the presence of 20ng/mL M-CSF and 50ng/mL RANKL. Blue = DAPI, Green = β -actin. SB = 50 μ m. Images taken using Leica SP8 confocal microscope with 63x objective magnification. LMGCs display morphological characteristics of tissue LMGCs, a horseshoe-like arrangement of nuclei around the periphery of the cell. Osteoclasts displayed a more random arrangement of nuclei throughout the cytoplasm. Control macrophages were exclusively mononucleated.

In vitro LMGCs were morphologically representative of those found in pathology, displaying the typical peripheral arrangement of nuclei. By visual assessment, cell size seemed to increase proportionally with number of nuclei, with the largest cells reaching upwards of 50 nuclei, and the ring/horseshoe arrangement becoming more pronounced in larger cells. These observations were consistent across cultured LMGCs from all donors studied in this thesis. In comparison, *in vitro* osteoclasts typically displayed a random arrangement of nuclei throughout the cytoplasm, the largest of these containing 30 nuclei.

2.6. Discussion

In this chapter I have adopted, optimised and morphologically validated an *in vitro* model culture system for the generation of LMGCs. Taking optimised culture conditions forward for the rest of this thesis, and thus achieving greater LMGC yields, will facilitate functional experiments. I have also demonstrated the power and limitations of flow cytometry as a technique for the measurement of multinucleation.

A common culture method used in the literature, but not shown in figure 5 is the use of concanavalin A (conA) alone or conA conditioned medium to differentiate primary monocytes to LMGCs. After attempting these protocols, I found that the monocytes did not survive long enough in culture to form LMGCs, and so were not included in the final analysis. A benefit of carrying out a cytokine titration is that it allows the use of lower concentrations in cases where culture health is more important than high LMGC yield, and vice versa.

There was a large degree of donor-donor variability. In many cases healthy donor monocytes did not survive the harsh culture conditions required for LMGC generation, which seemed to generally reoccur when next attempting to culture monocytes from the same donor. Often, for those healthy donor monocytes which did survive and produce LMGCs, yields were dramatically lower than for other donors. Again, this appeared to be persistent for specific individuals. Approximately 30% of all efforts to generate LMGCs resulted in culture death. Of the remaining roughly 70% of cases the LMGC yield varied greatly from as few as 2% cells binucleated or larger to as many as 30%. It is difficult to draw any meaningful conclusions in terms of the characteristics of those individuals whose monocytes were more or less effective, as the vast majority of blood obtained for this study was from anonymised donors making the sample sizes too small.

The difference in LMGC yield between different types of culture media was unexpectedly pronounced. Reading into the compositional differences of each media offers a potential explanation for the significant increase in multinucleation in DMEM compared with both RPMI and α MEM. Vitamin B12 deficiency has been implicated in increased risk of DNA damage. Later in this thesis I will discuss the role that DNA damage may play in the formation of LMGCs. As DMEM lacks vitamin B12, DNA damage may have been increased in these cultures, leading to higher rates of multinucleation. With more time, I would have liked to investigate this further, by quantifying DNA damage in cells cultured in different media, or by supplementing DMEM with additional vitamin B12 and measuring LMGC yield.

Due to a lack of reliable biomarkers, LMGCs are defined by their morphology. I chose to use their morphology to align our culture system to disease LMGCs, however, in order to more completely assess the extent to which these cells recapitulate those found in disease I next aimed to use transcriptomics to compare the RNA expression profiles of cultured LMGCs and LMGCs from disease tissue.

Chapter 3. Single cell RNA sequencing of *in vitro* LMGCs and GCA affected temporal artery tissue

3.1. Introduction

3.1.1. RNA sequencing of *in vitro* LMGCs

Single cell RNA sequencing is a powerful analytical tool which has come to prominence in recent years. While efforts are underway to sequence and characterise all of the cells of the human body in health and disease²³², there are currently few studies in which LMGCs have been sequenced. The information that this methodology provides could be instrumental in the efforts to characterise of LMGCs both in terms of their functional adaptations and formation mechanism.

In 2016, Herrtwich et al. used scRNAseq to sequence *in vitro* LMGCs cultured in the presence of M-CSF and FSL-1⁹⁹. They compared control macrophages cultured with M-CSF alone, to both mononucleated cells and cells with 2 or more nuclei cultured with M-CSF and FSL-1. They found differential gene expression patterns between mononucleated and multinucleated cells treated with FSL-1, although they were not able to separate these populations into distinct clusters using non-biased clustering techniques. This distinction in gene expression suggests a phenotypic change upon multinucleation of LMGCs. Genes significantly upregulated in multinucleated cells included *Cdk1*, *Tubb5* and *Mmp9*, whilst *ApoE* and *Csf1r* were downregulated. Pathway analysis suggested gene module upregulation in LMGCs relating to macrophage-attracting chemokines and ECM remodelling proteases, which is of particular interest due to the associations of these proteins with granuloma formation and arterial damage in GCA. These findings were expanded on in a different study four years later, with *in vitro* LMGCs displaying enrichment of genes relating to a number of interesting pathways including T cell receptor complexes such as *CD8A* and *CD40L*, T cell activation, IFN signalling, mitochondrial oxidative pathways, DNA replication and damage pathways²¹⁴.

In this chapter I aimed perform single cell RNA sequencing of *in vitro* LMGCs, in addition to four other cell types for comparison; Mononucleated cells and binucleated cells from the same cultures as LMGCs, macrophages grown in GM-CSF alone, and osteoclasts cultured with M-CSF and RANKL. By finding the gene expression profile of LMGCs I hoped to gain insight

into their mechanism of formation and functional adaptations, which will be discussed in chapters 4 and 5 of this thesis respectively. Here, the strategy used to sort, sequence, and analyse these different cultured populations will be discussed.

3.1.2. RNA sequencing of GCA-affected temporal artery tissue

Insights into the tissue microenvironment of GCA-affected temporal artery walls, which is poorly understood, can be gained using RNA sequencing. This methodology could also be used to identify systemic biomarkers for GCA. Gene expression profiling of peripheral CD4⁺ and CD8⁺ T cells has revealed transcriptional differences in GCA patients, which could even be used to predict long term prognosis though these biomarkers have not since been corroborated⁴⁷. Populations of CD66b⁺ CD15⁺ CD10^{lo/-} CD64⁻ neutrophils and CD66b^{hi} CD15⁺ CD10^{lo/-} CD64^{+/hi} myelocytes have also been identified as cell types associated with GCA using single cell technologies²³³.

I aimed to perform single cell RNA sequencing of temporal artery biopsies taken from patients with suspected GCA, to gain insights into the cell composition of affected arteries. I also aimed to identify tissue macrophages by their gene expression profile, and to investigate the possibility of identifying LMGCs within this population by comparing the gene expression profiles of macrophage populations with those of *in vitro* LMGCs.

3.1.3. Chapter aims

The aim of this chapter was to generate single cell sequencing datasets for both *in vitro* LMGCs, and unsorted temporal artery. I hypothesised that *in vitro* LMGCs would possess a unique gene expression profile which could be used to distinguish them from mononucleated cells cultured in the same conditions. As the only difference between LMGCs and these mononucleated cells is the fact that the LMGCs became multinucleated, the discrepancy between the gene expression of each population could provide insight into the mechanism of LMGC formation, or their functional adaptations, both of which are poorly understood. I further hypothesised that this unique gene expression profile could be then identified in temporal artery tissue, which would further demonstrate the extent to which *in vitro* LMGCs recapitulate the *in vivo* process.

The objectives of this chapter were as follows:

- To generate a single cell RNA sequencing dataset for *in vitro* LMGCs, to be used in subsequent chapters in the study of their formation mechanism and functional adaptations.
- To use single cell RNA sequencing to investigate the cellular composition of GCA-affected temporal artery tissue and matched blood.
- To identify an *in vitro* LMGC gene signature, and seek this signature in a sub-population of tissue macrophages in GCA-affected temporal artery tissue, to demonstrate that LMGCs can be identified transcriptionally in disease tissue.

3.2. Single cell RNA sequencing of *in vitro* LMGCs

3.2.1. Single cell sorting strategy

We aimed to compare the transcriptomes of *in vitro* LMGCs with other cell types to gain insight into their functional adaptations. FACS was used to isolate single cells from cell suspensions, sorting each cell into an individual well of a 96 well plate. DRAQ5 was used to ensure cells were sorted with the desired degree of ploidy. Three primary monocyte culture conditions were used; GM-CSF alone, from which mononucleated cells were sorted as control macrophages cultured without inflammatory stimulation, GM-CSF with IFN γ from which mononucleated and binucleated cells were sorted as further controls, cultured in the presence of inflammatory stimulation but without becoming polyploid as well as multinucleated LMGCs, and M-CSF with receptor activator of nuclear factor kappa-B ligand (RANKL) from which multinucleated osteoclasts were sorted as an alternative multinucleated giant cell for comparison.

Using mononucleated macrophages without any inflammatory stimulation would allow us to investigate the transcriptional effects of IFN γ , potentially revealing proteins or pathways involved in IFN γ induced macrophage multinucleation. Mononucleated and binucleated cells from stimulated wells were used to determine the functional adaptations of fully developed LMGCs, as they were cultured in identical conditions but did not become multinucleated. Using osteoclasts allows comparisons between LMGCs and this more well-characterised multinucleated cell type, and would allow us to demonstrate functional differences or similarities between different monocyte-derived multinucleated cell types. The culture systems & sorting strategy used are outlined in figure 9.

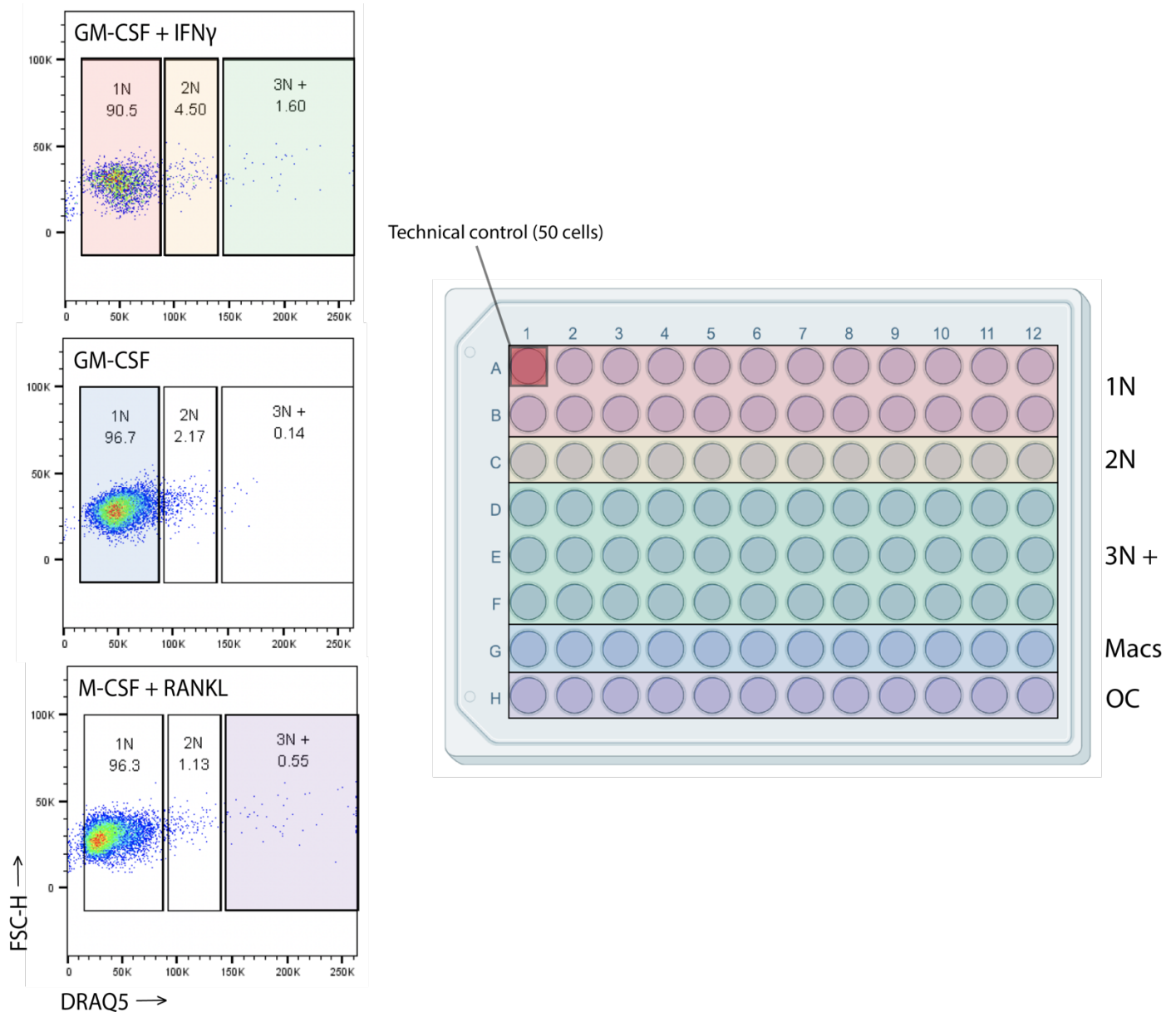


Figure 9. LMG Sorting strategy and plate layout for SS2.

Gating strategy and plate layout for single cell RNA sequencing of *in vitro* LMGCs and control cell types. Cultured cells were stained with DRAQ5 to distinguish populations based on nuclear content. From cultures grown in GM-CSF and IFN γ , mononucleated (1N, red), binucleated (2N, yellow) and multinucleated (3N +, green) populations were sorted. From cultures grown in GM-CSF only, mononucleated cells (1N, blue) were sorted and labelled “Macs”, and from cultures grown in M-CSF and RANKL, multinucleated cells (3N +, purple) were sorted and labelled “OC”. 50 cells were sorted into well A1 to be used as a technical control during generation of cDNA libraries.

The wells into which all cells were sorted contained pre-prepared lysis buffer (Buffer TCL – QIAGEN) containing 1% β -mercaptoethanol, to break apart the cell and make the DNA content accessible.

3.2.2. Dataset pre-processing

3.2.2.1. Applying quality control metrics

Using Seurat, a toolkit for the analysis of sequencing data in R developed by SatijaLab (<https://satijalab.org/>), Data pre-processing of the now aligned dataset was performed. Quality control was applied to remove low quality, unhealthy cells, and empty droplets from the final analysis.

First, the number of unique genes identified for each cell, 'nFeature_RNA' was plotted. Cells with an abnormally low number of different genes expressed were excluded as they are likely to be of low quality. Similarly, cells exhibiting abnormally high percentages of mitochondrial genes 'percent.mt' are excluded, as apoptotic cells typically exhibit a high degree of mitochondrial contamination. Following SatijaLab guidelines cells with unique gene counts fewer than 200 were excluded, as well as cells with mitochondrial gene percentages greater than 5%.

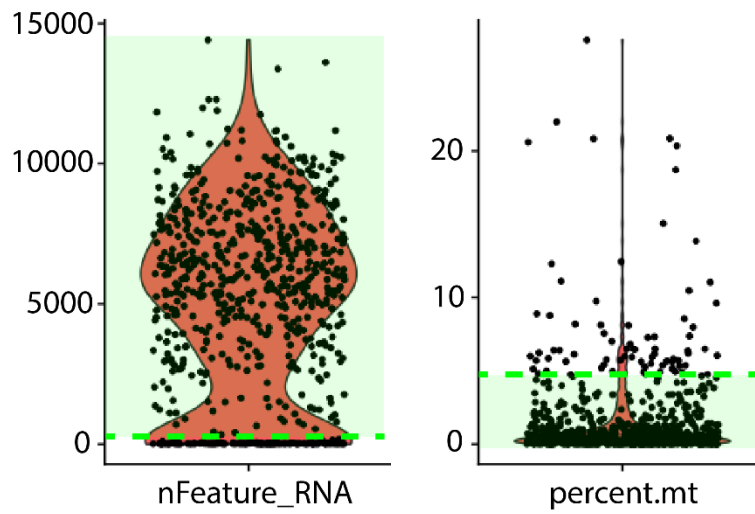


Figure 10. Quality control plots.

Plots showing the unique feature counts (nFeature_RNA), and percentage of total genes mitochondrial (percent.mt) for whole aligned dataset. Black dots represent single cells. Green areas show cells taken forward for downstream analysis, blank areas excluded at this stage.

With unwanted cells and empty droplets removed from the dataset, a normalization step in which the gene expression measurements for each cell is normalized by the total gene expression was performed. The result is then multiplied by a standard scaling factor of 10,000 (as demonstrated by the SatijaLab guidelines) and log transformed.

3.2.2.2. Identification of highly variable genes and principal component analysis

Following normalization, the dataset was further concentrated by selecting highly variable genes to be taken forward for downstream analysis. This was achieved by using the function *FindVariableFeatures* with the parameters *selection.method = "vst"* and *nFeatures = 2000*. This method plots mean gene expression against normalized gene dispersion in order to identify genes with high dispersion whilst controlling the innate correlation between variance and gene expression in single cell RNA sequencing data. The number of highly variable genes selected was 2000.

The dataset, now 2000 genes strong, was further simplified by performing principal component analysis (PCA). The benefits of this are reduction in the innate error generated by multiple test corrections, and a reduction in the computational power required for downstream analysis. PCA allows the simplification of complex datasets by identifying patterns such as phenotypic differences, and then transforming the data into objects with fewer dimensions, called principal components (PC). The goal of PCA is to simplify the data whilst maintaining the significant trends, by transforming it into as few principal components as possible. In Seurat a variance ratio plot is generated containing every PC identified. PCs before the point at which this plot plateaus, i.e. when each subsequent PC is no longer significantly different to the previous PC are then used for downstream analysis.

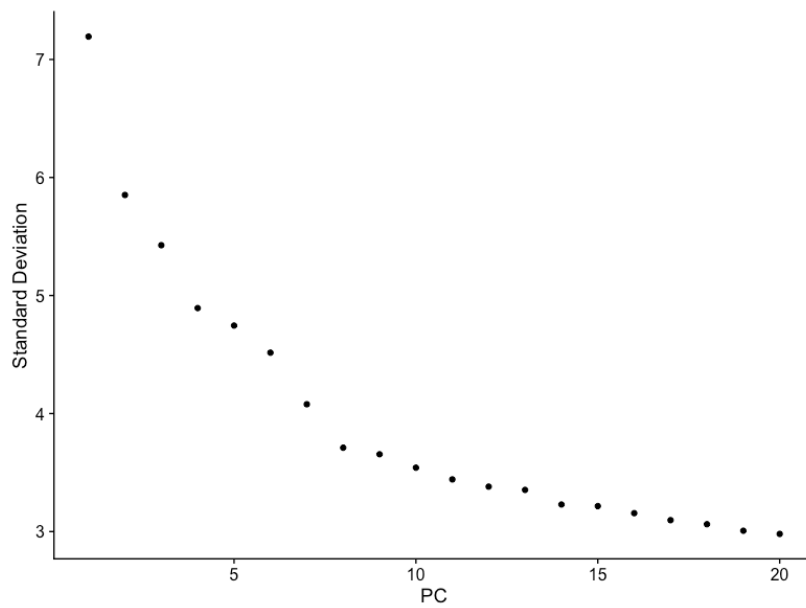
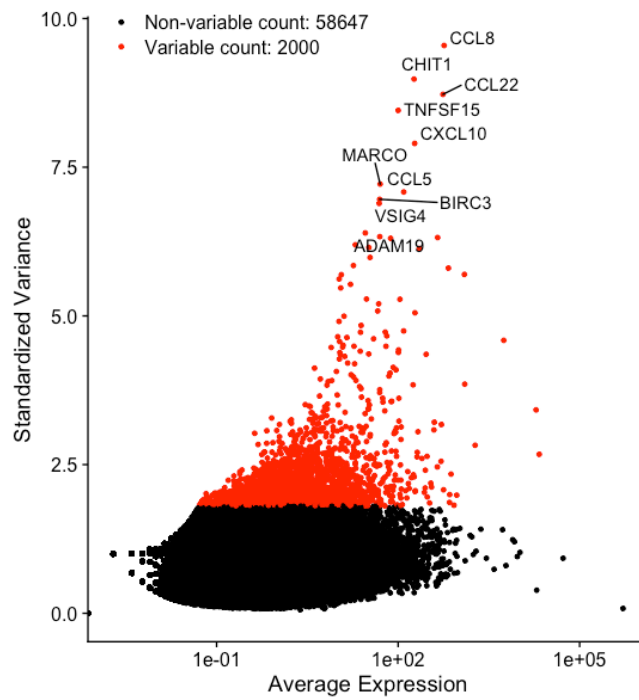


Figure 11. Variable gene identification and PCA.

A) Identification of 2000 highly variable genes (red) and non-variable genes (black). Top 10 highly variable genes labelled. B) Principal component plot showing the standard deviation of each PC generated during PCA

In later analyses the dimensionality of the dataset was defined at 30 PCs using the parameter *dims = 1:30* this was estimated to be the point at which the plot would have reached a plateau. In truth there is very little difference when the variance between PCs is so small and the majority of the true information is found in roughly the first 10 PCs. This was later confirmed when trying 'dims =' values ranging from 10-30 in later analyses and seeing very little difference in the outcome. With the dataset now at a manageable dimensionality, unbiased cell clustering was performed.

3.2.3. Unbiased cell clustering

To compare the sequenced cells types in an unbiased manner I performed non-linear dimensional reduction, a technique which clusters cells in 2D space based on their transcriptional similarity. Cells placed close together are more transcriptionally similar than those more distant, leading to the formation of clusters containing specific cell types. There are multiple non-linear dimensional reduction methods compatible with Seurat, the most commonly used being t-distributed stochastic neighbour embedding (t-SNE) and uniform manifold approximation and projection (UMAP). For our dataset UMAP projected four discrete clusters as shown in figure 12:

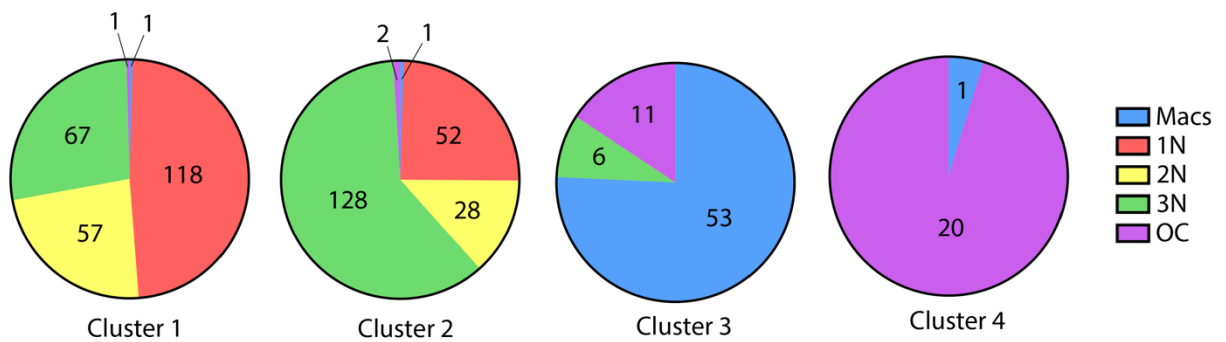
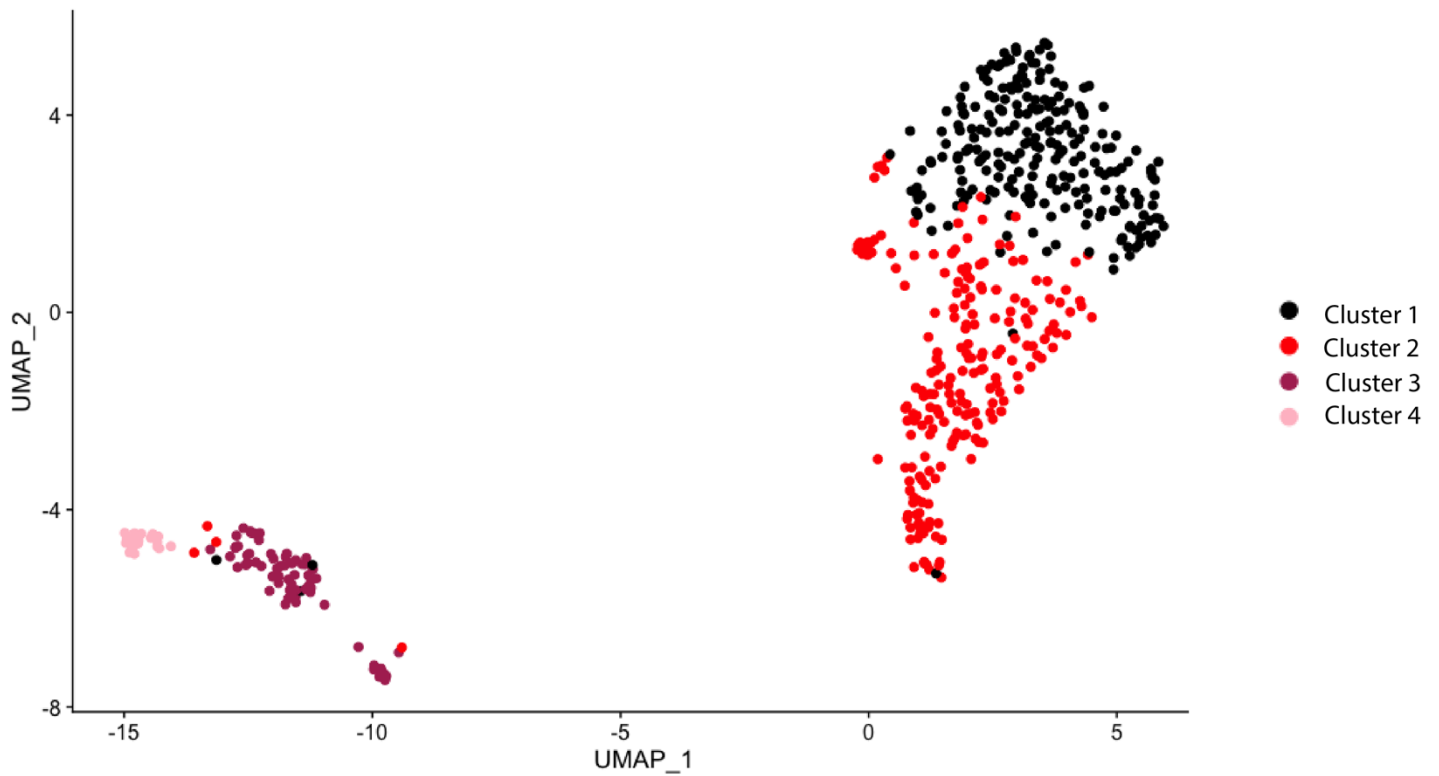


Figure 12. Unbiased population clustering by UMAP.

Above: non-linear dimensional reduction by UMAP. Four clusters projected in 2D space, clusters 1, 2, 3 and 4, coloured black, red, maroon and pink respectively. Below: Pie charts displaying the origin of cells comprising each cluster based on FACS sorting strategy. Blue = Control macrophages without inflammatory stimulation (Macs), Red = Mononucleated macrophages with inflammatory stimulation (1N), Yellow = Binucleated cells with inflammatory stimulation (2N), Green = LMGCS (3N), Purple = Osteoclasts (OC).

The number of cells from each FACS sorted population comprising each cluster is shown in figure 12. There was relatively high inter-cluster crossover between the cells subject to inflammatory stimulation during culture, likely due in part to the FACS gating impurities outlined in 2.2.2. Clusters were annotated by the prevailing cell type for each cluster; ‘Mononucleated LMGC’, ‘Multinucleated LMGC’, ‘Control macrophages’ and ‘Osteoclasts’ for clusters 1, 2, 3 and 4 respectively. Cells sorted as binucleated cells were not sufficiently transcriptionally distinct to form their own cluster, instead being shared between clusters 1 and 2.

3.2.4. Identification of cluster markers

The next stage of analysis was to identify the most differentially expressed genes for the cell clusters. Using Seurat to read gene expression levels, the top 10 differentially upregulated genes were found for each cluster and are displayed in figure 13. For a gene to be considered differentially expressed, it was required to be detected in a minimum of 25% of cells in every cluster.

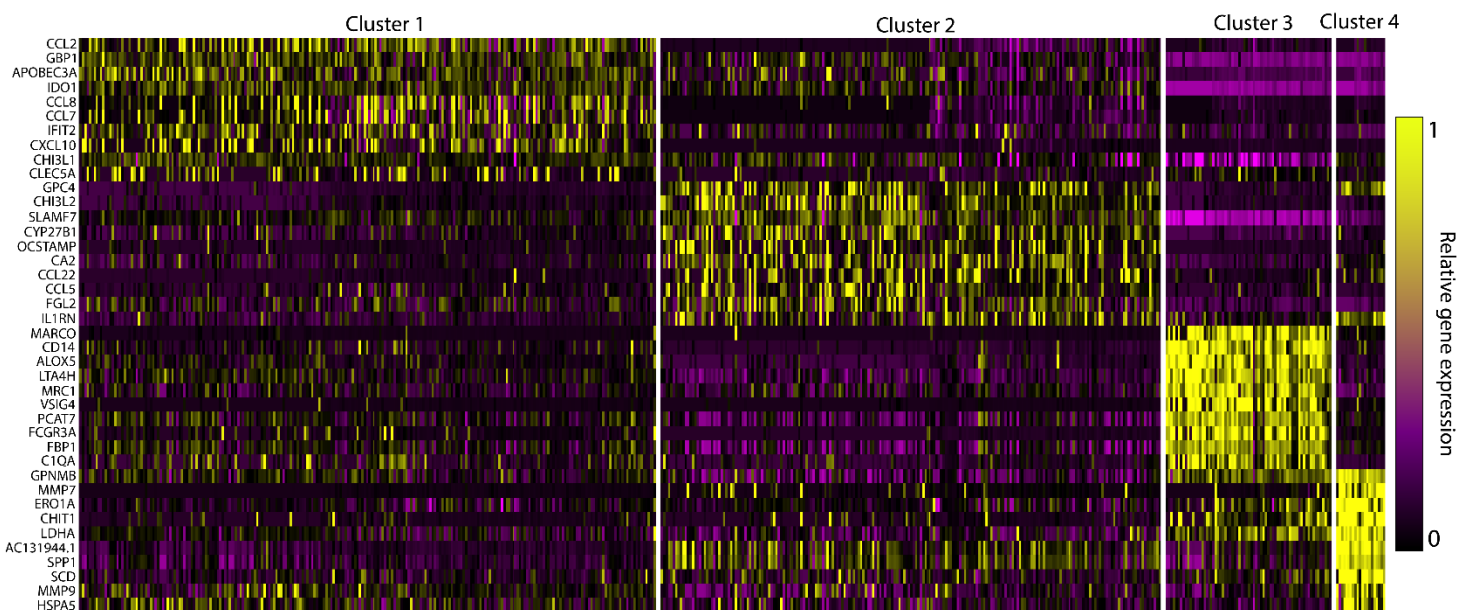


Figure 13. Identification of differentially expressed genes.

Heatmap displaying the ten most highly differentially expressed genes for each of the four clusters generated in 4.2.3. Yellow = High expression, purple = Low expression.

Reassuringly, a number of genes among the top differentially expressed genes for clusters 3 and 4, annotated 'control macrophages' and 'osteoclasts' respectively, were expected based on legacy knowledge. The control macrophage cluster had high expression of known monocyte/macrophage marker *CD14*, whilst the osteoclast cluster had high expression of metalloproteinases *MMP7* and *MMP9*, critical for the bone-resorptive properties of osteoclasts. Both clusters 1 and 2 showed expression of a more inflammatory phenotype, in keeping with having been cultured in the presence of IFN γ ; Different chemokines were highly differentially expressed in both clusters. With these top genes for the 'multinucleated LMGC' cluster we can infer their functional adaptations when compared with the 'mononucleated LMGC' cluster. Genes such as SLAM family member 7 (*SLAMF7*) and glypican 4 (*GPC4*) offer some insight into the ways these cells functionally adapt following multinucleation and their condition.

3.2.5. Pathway analysis

To investigate the functional adaptations of multinucleated LMGCs, pathway analysis was performed, using all of the significantly upregulated genes in the 'multinucleated LMGC' cluster compared with the 'mononucleated LMGC' cluster. Using the software 'Cytoscape' (version 3.8.2) This list of upregulated genes was input, and by searching the 'Gene Ontology' (GO) database of cellular pathways the software returned a selection of pathways in which some the selected genes are involved. There were many pathways implicated by this method including cellular responses to inflammatory stimulation and replicative stress. Amongst these there were some pathways relating to potential functional adaptations, four of these which are of particular interest based on our current understanding of LMGCs are outlined in figure 14.

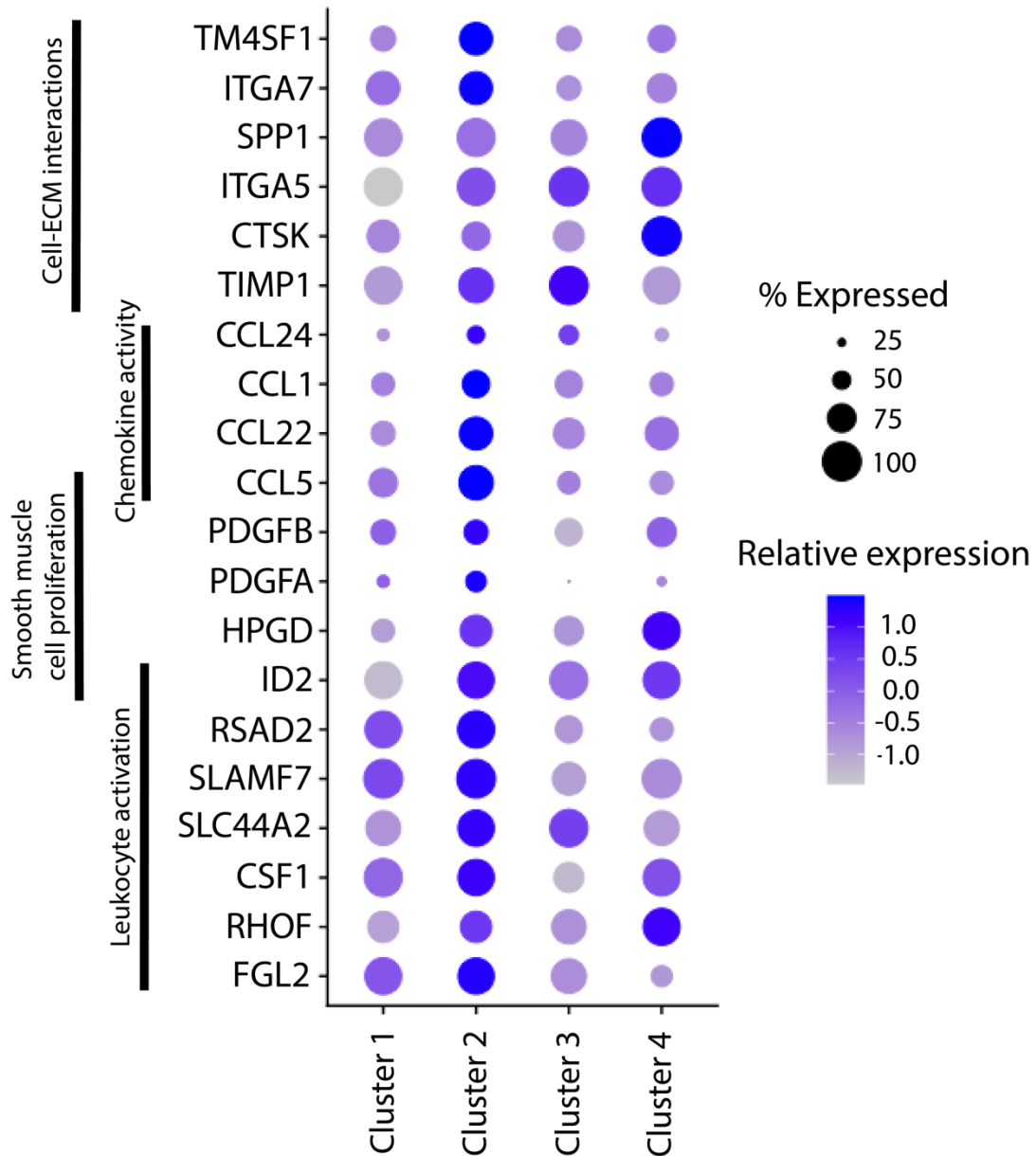


Figure 14. Upregulated gene modules in LMGs.

A dot plot indicating four functional pathways of interest which are seemingly upregulated in the transcriptome of our *in vitro* LMGs & and the upregulated genes involved in each pathway. Circle size = % of cells expressing that gene, Colour = relative expression, with blue - high expression and grey - low expression. Genes are differentially expressed (adjusted p value <0.05) between multinucleated cells and other cell types using the FindAllMarkers with Wilcoxon Rank Sum test in Seurat.

It is interesting that genes relating to Cell-ECM interactions are upregulated in cluster 2 (Multinucleated LMGC). In the literature, LMGCs have been implicated in remodelling of the extracellular matrix associated with granuloma formation; this data serves to reinforce that hypothesis. The upregulation of genes relating to chemokine activity and leukocyte activation suggests that LMGCs possess a pro-inflammatory phenotype, secreting mediators of inflammation which potentially drive the chronic inflammatory states of the conditions in which they're found, including GCA. The upregulation of genes relating to smooth muscle cell proliferation is particularly interesting in the context of GCA. As discussed in section **1.3.4**, in the pathogenesis of GCA it is clear that the vascular smooth muscle cells are driven to proliferate (intimal hyperplasia), leading to luminal narrowing and ultimately occlusion of the vessel. LMGCs have been implicated as one of the driving forces behind this and here we find supporting evidence for this.

I next aimed to perform RNA sequencing of sections of temporal artery, taken from patients with suspected GCA. We hoped to identify LMGCs transcriptionally by finding a sub-population of tissue macrophages expressing a similar gene expression profile to our *in vitro* LMGC cluster.

3.3. Sequencing of temporal artery

As discussed in 3.1.2, LMGCs from tissue have been seldom sequenced and transcriptionally analysed. To support our *in vitro* findings, sections of excised temporal artery tissue from patients with suspected GCA were processed for sequencing with matched blood samples. The cells from patients ultimately receiving positive diagnoses could be compared against cells from patients receiving negative diagnoses. With this data we also hoped to gain insight into the tissue microenvironment of the artery walls of affected arteries in GCA, measuring the quantities of different cell populations in cases and controls.

3.3.1. Temporal artery dissociation procedure

The receipt of temporal artery samples was arranged by Dr Gary Reynolds, including recruitment and consent of patients. Vessel sections, typically 1-2cm in length, were first bisected longitudinally in order for half of the section to be used by clinicians for diagnostic evaluation. The other half was transferred to an empty, sterile dish and manually cut into small pieces using a scalpel. A small volume of media was then added, and this mixture transferred to a 50mL tube. A cocktail of enzymes was then added; Collagenase I, Collagenase

XI, DNase I and Hyaluronidase, and this was incubated at 37°C for 50 minutes, with regular agitation. After this, red blood cells were lysed and remaining cells counted. Matched blood samples were simultaneously processed, isolating PBMCs by standard lymphoprep.

Cells from both blood and tissue were then loaded onto a 10X Genomics controller with chromium chips. This was performed by Emily Stephenson and Justin Engelbert of the Haniffa Lab, who also generated the cDNA libraries which were sent for sequencing.

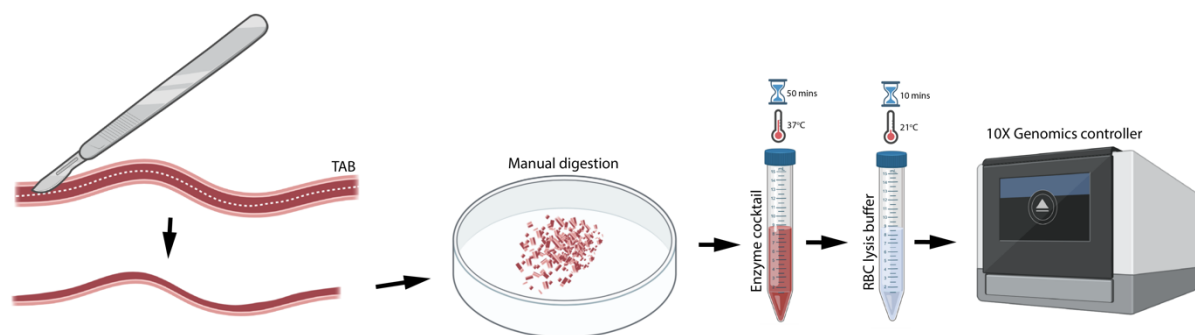


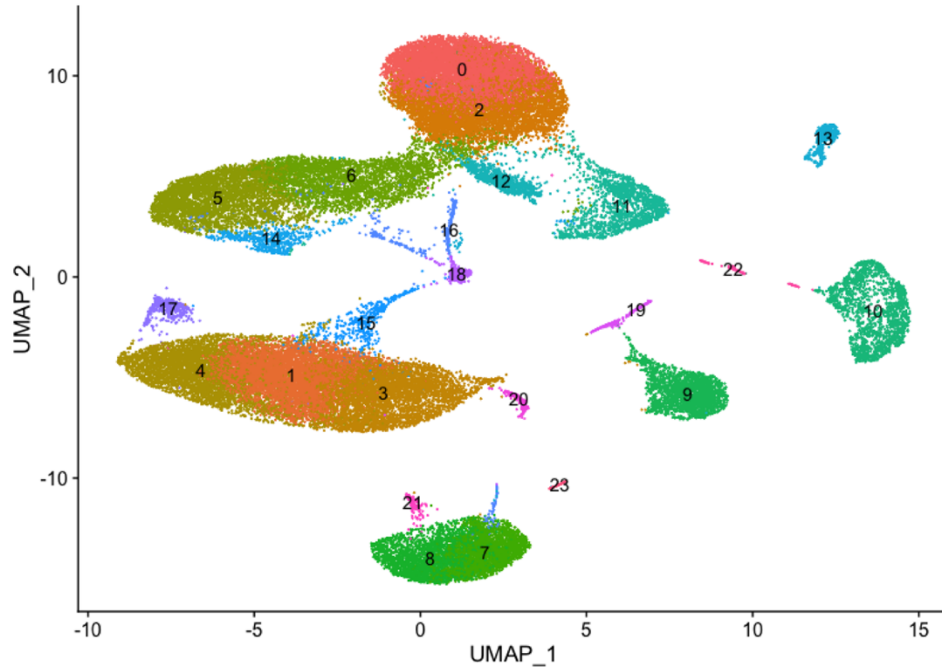
Figure 15. Temporal artery digestion workflow.

Tissue was digested manually initially, followed by enzymatic digestion and red blood cell lysis before being loaded on a 10X genomics controller.

Four biopsies from four patients were processed in total, with cells from blood and tissue all sequenced in the same way. Clinical assessment revealed that two of the patients received a positive diagnosis and two received a negative diagnosis, enabling the ability to analyse changes in the dataset by diagnosis to observe differences in health and disease.

3.3.2. Unbiased clustering and manual annotation of subsequent populations

The complete dataset was then clustered in an unbiased manner, as was done previously for *in vitro* LMGCs and controls. Again, UMAP was used as the non-linear dimensional reduction method and cells derived from both blood and tissue from all four samples were clustered together. The most differentially expressed genes for each cluster were then used to identify them combined with legacy knowledge of cell subset gene expression.



0	Blood CD4 ⁺ T cells	CD3E, LDHB, IL7R, NOSIP, MAL, SARAF, TCF7, LEF1, LTB, NDFIP1
1	Blood Monocytes	S100A9, S100A8, S100A12, LYZ, FCN1, VCAN, AIF1, LST1, CD14, TYROBP
2	Blood TRegs	IL7R, LTB, IL32, CD3E, LDHB, CD69, CD3D, MAL, SARAF, AQP3
3	Blood Monocytes	FCN1, CD14, VCAN, CTSS, PSAP, S100A9, AIF1, CFP, MS4A6A, GRN
4	Blood Monocytes	S100A12, NEAT1, COTL1, SLC11A1, CTSD, THBS1, LST1, CEBPD, CSF3R, AIF1
5	Blood NKs	GNLY, NKG7, FGFBP2, GZMB, PRF1, CTSW, CCL5, GZMA, SPON2, CLIC3
6	Blood CD8 ⁺ T cells	GZMK, CCL5, CD8A, DUSP2, GZMH, CD8B, NKG7, GZMA, CTSW, CMC1
7	Blood B Cells	CD79A, MS4A1, TCL1A, IGHM, CD74, JCHAIN, HLA-DRA, CD37, HLA-DPA1, CD79B
8	Blood B Cells	CD79A, MS4A1, CD74, TCL1A, CD37, HLA-DRA, HLA-DPA1, FCER2, CD79B, FAM129C
9	Blood & TAB DCs	TXN, CCL22, CXCL8, HLA-DRB5, IDO1, C15orf48, VMO1, FABP5, BIRC3, RAMP1
10	TAB VSMCs	APOD, DCN, COL1A1, GSN, CXCL14, COL1A2, CFD, PLA2G2A, IGFBP6, IGFBP5
11	TAB T cells	NR4A2, DUSP2, RGCC, CREM, TNF, DNAJB1, JUNB, GADD45B, BRD2, DNAJA1
12	TAB TRegs	BATF, MT2A, PRDX1, TIGIT, MIF, GAPDH, B2M, TXN, TNFRSF18, HINT1
13	TAB Endothelium	MGP, VWF, FN1, HSPG2, SPARCL1, CLU, BGN, ID1, SERPINE1, CCL14
14	Blood NKs	CCL4, CCL3, DUSP2, GNLY, NKG7, GZMB, SPON2, PRF1, KLRD1, IER2
15	Monocyte progenitor	PPBP, NRGN, PF4, CAVIN2, TUBB1, HIST1H2AC, F13A1, GP9, MPIG6B, ITGA2B
16	Lymphoid progenitor	PPBP, HIST1H2AC, PF4, CAVIN2, TUBB1, MPIG6B, TREML1, SPARC, GNG11, NRGN
17	Blood NK/Monocyte	GNLY, NKG7, PRF1, CCL5, GZMB, FGFBP2, RUNX3, GZMH, S100A9, KLRD1
18	Blood HSC/MMP	PF4, TUBB1, HIST1H2AC, CAVIN2, GP9, RGS18, GNG11, NCOA4, MPIG6B, MYL9
19	TAB Macrophages	IL1B, CXCL2, PLAUR, IER3, CXCL8, C1QC, C1QB, C1QA, CCL3, CCL20
20	Blood monocytes	IGHM, CD79A, IGKC, IGHD, MS4A1, TCL1A, TNFRSF13C, CD22, FAM129C, FCER2
21	Blood pDCs	CD79A, IGHM, MS4A1, TCL1A, FCER2, IGHD, LINC00926, NKG7, FAM129C, GNLY
22	TAB VSMCs	ACTA1, TAGLN, TPM2, CKM, ACTA2, TCAP, DES, ADIRF, TPM1, MB
23	TAB B cells	CXCR5, NFKBID, NR4A1, SPIB, BANK1, TGIF2, CD83, CKS2, NR4A2, CD79A

Figure 16. Unbiased clustering of TAB and matched blood.

Above: UMAP plot showing the unbiased clustering of all cells from blood and temporal artery tissue of four separate patients. Below: 23 clusters labelled and annotated based on differentially expressed genes. Top 10 markers for each cluster shown.

There were multiple clusters expressing genes of blood monocytes and blood B cells likely due to the innate heterogeneity within these populations. Cluster 17 highly expressed markers of both monocytes and natural killer (NK) cells from blood, and so has been labelled 'Blood NK/Monocyte'. Dendritic cells from blood and tissue were not sufficiently transcriptionally distinct to form separate clusters and have clustered together (cluster 9).

3.3.3. Cell population analysis

Using the annotated clusters, population analysis was performed by reading cell counts for each of the clusters generated in 3.3.2. For each cluster, the counts from two positive samples were compared with those from two negative samples, to investigate the differences in the cellular composition of GCA affected temporal arteries and healthy controls, as well as matched blood. It was expected that an increase in T cells and macrophages would be observed in tissue for positive samples, as the predominant cell types of granulomas. An increase in the number vascular smooth muscle cells (VSMCs) would also be indicative of intimal hyperplasia.

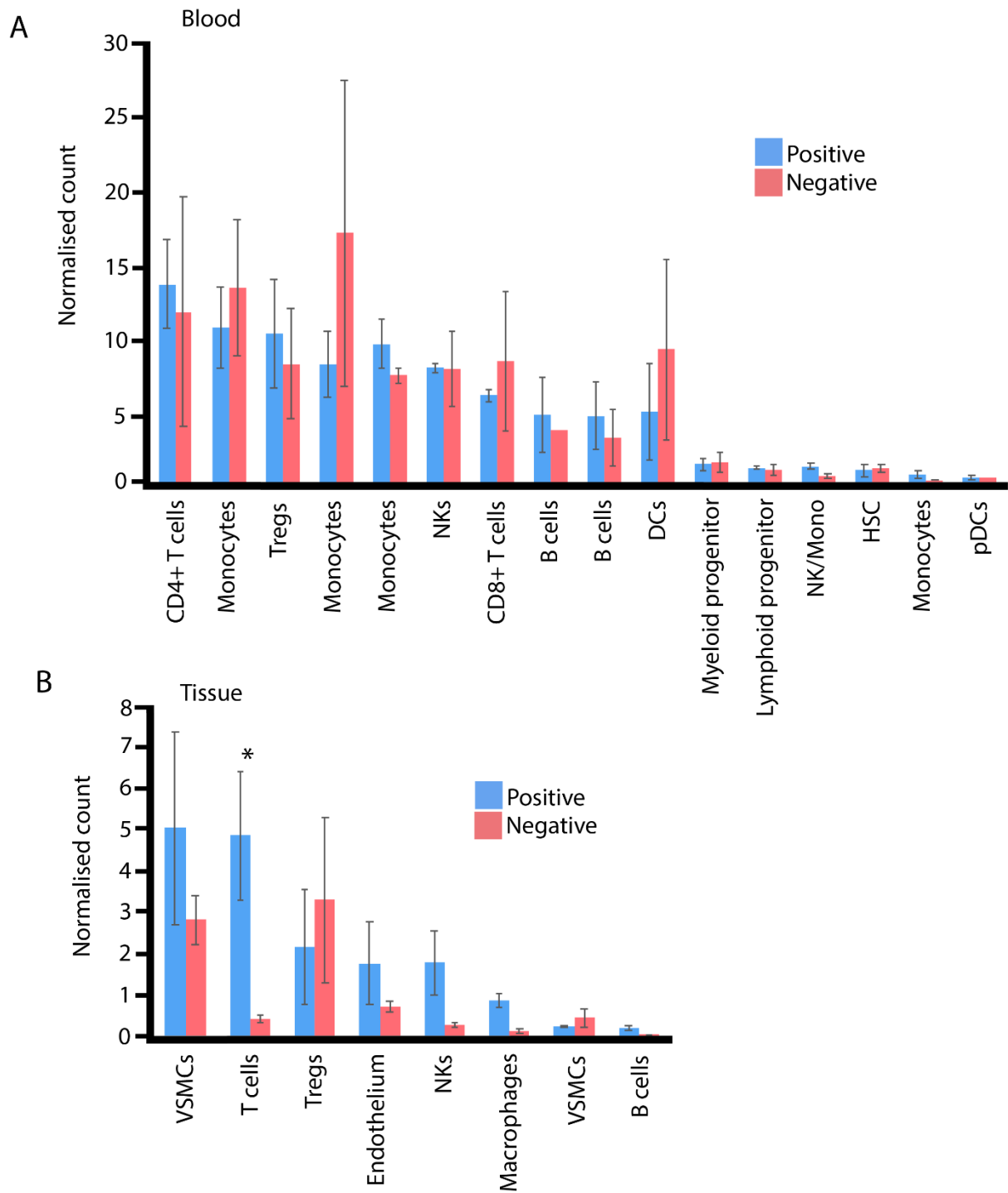


Figure 17. Population analysis of TAB and matched blood.

Mean cell counts for each population identified in 4.3.2. split by diagnosis. Values represent the mean counts for samples from 2 positive (blue) and 2 negative (red) diagnoses. Normalised by Min-Max scaling. Error bars = SEM. * = statistically significant, $p < 0.05$. Mann-Whitney U tests.

In blood samples, there was a greater number of CD4+ T cells, Tregs, a monocyte population (cluster 5), and B cells in the peripheral blood of patients who received positive diagnoses, although these increases were not statistically significant, with P values invariably greater than 0.05 determined by a Kruskal-Wallis test. Conversely, these blood samples contained fewer CD8+ T cells, and certain populations of monocytes (Clusters 2 and 4), although again these were not statistically significant. In tissue, T cells were significantly elevated in positive samples ($P < 0.05$). Macrophages and NK cells were also elevated, albeit not significantly. Vascular smooth muscle cells were also non-significantly elevated.

We hypothesised that LMGCs may lie within the tissue population of macrophages, but were not sufficiently transcriptionally distinct to form their own cluster given the complexity of the whole dataset. In order to identify and isolate LMGCs by this method, the TAB macrophage cluster was taken in isolation, and re-clustered using UMAP.

3.3.4. Identification of a LMGC gene signature in tissue

A new Seurat object was created containing only the cells from cluster 19, tissue macrophages. This object was then re-clustered, using the same UMAP method as in 3.3.2 to generate sub-clusters within this population. The aim was to reveal heterogeneity amongst tissue macrophages, and to find a population expressing a similar gene expression profile to *in vitro* LMGCs. Four clusters were generated, each with a unique gene signature. Differentially expressed genes were then identified for each cluster to be compared with the *in vitro* LMGC gene profile generated in 3.2.

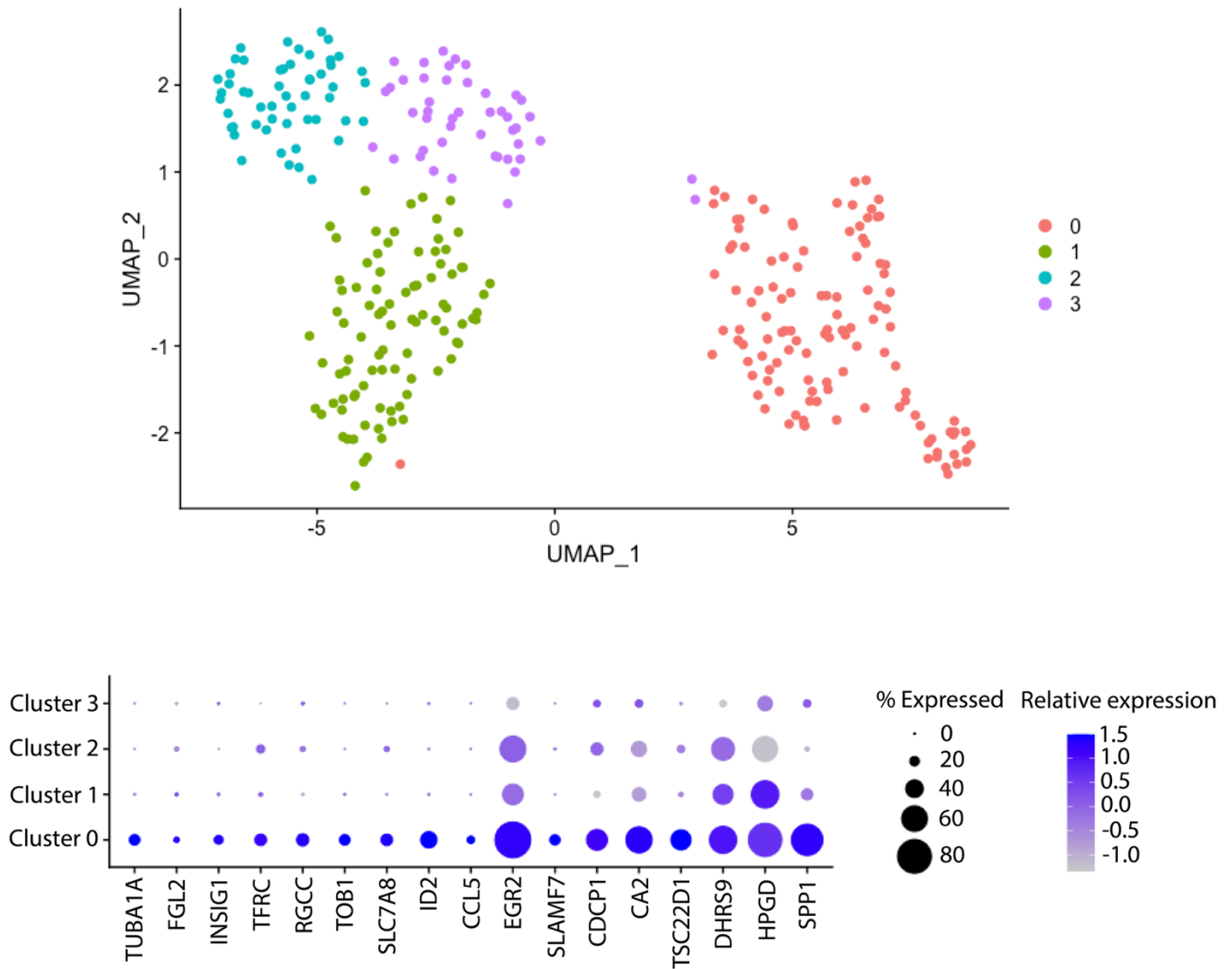


Figure 18a. Unbiased re-clustering of TAB macrophages, and shared DEGs with *in vitro* LMGCs.

Above: Unbiased re-clustering of tissue macrophage cluster by UMAP method. Four transcriptionally distinct clusters produced. Below: Genes upregulated in cultured LMGCs. Dot size = percentage of cells expressing that gene. Blue = High expression. Grey = Low expression.

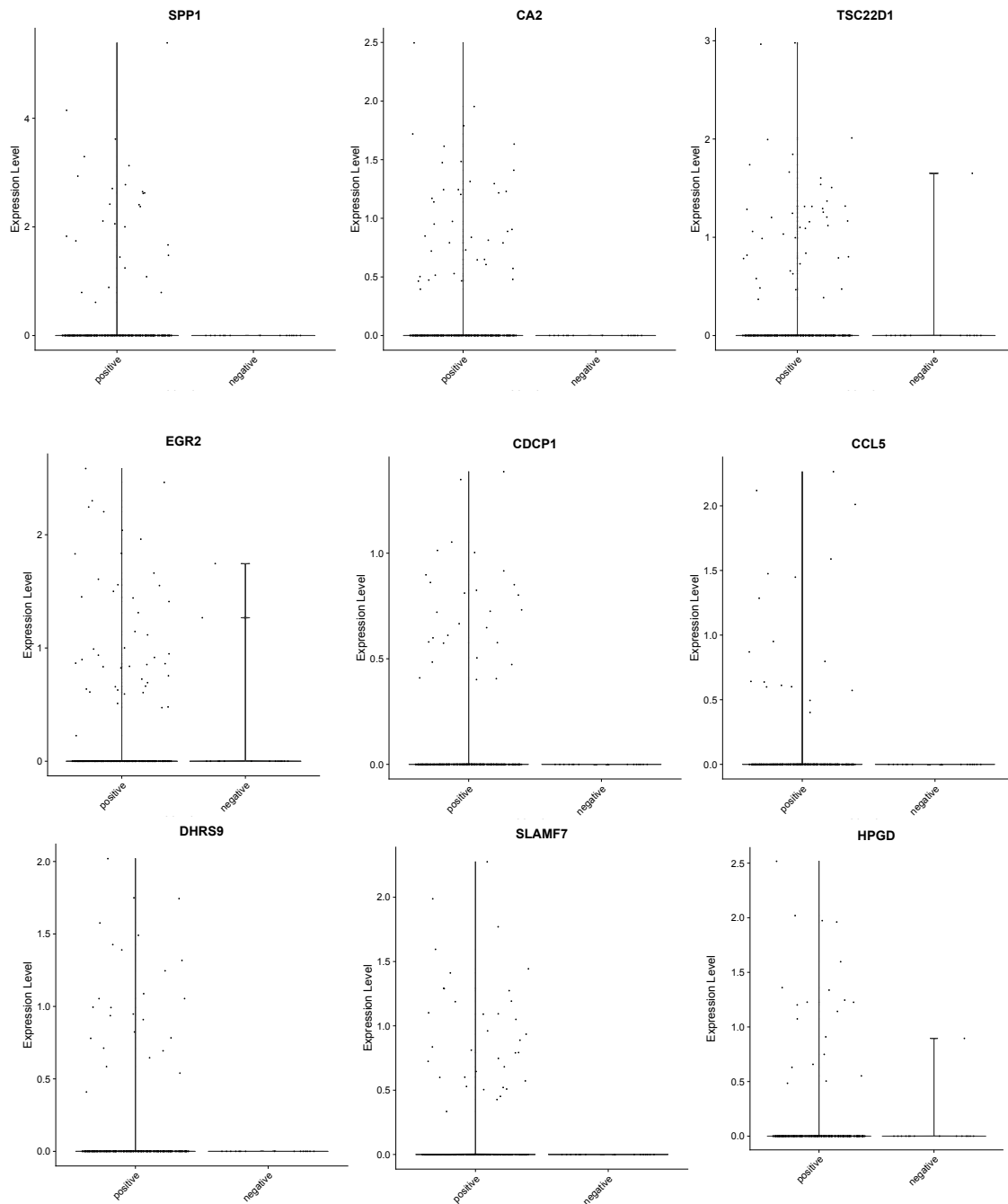


Figure 18b. Lack of an in vitro LMGC gene signature in GCA negative patients

Gene expression in the macrophage tissue sub-cluster (cluster 19, Figure 16). Nine genes outlined in figure 18a, differentially upregulated by both in vitro LMGCs and tissue macrophage cluster 0 are upregulated by a number of cells in GCA positive patients compared with GCA negative patients.

Four clusters were generated by UMAP indicating four transcriptionally distinct macrophage sub-populations. Of these, cluster 0 was the most transcriptionally distinct, as represented by its physical separation in 2D space. In cluster 0 there was high expression of numerous genes identified earlier as *in vitro* LMGC markers. Relatively low expression percentages for some genes could represent heterogeneity between tissue LMGCs themselves, or impurity of the cluster due to insufficient clustering power. With this finding we demonstrate that LMGCs can potentially be isolated by their transcriptomes from temporal artery tissue, though proteomic validation of markers will be necessary to make this claim reliably. We also further validate our *in vitro* LMGC model by showing cultured LMGCs may recapitulate tissue LMGCs effectively, displaying a similar gene expression profile. Furthermore, I have demonstrated that components of this transcriptional crossover are only expressed in patients with confirmed GCA, and not those who received negative diagnosis. The relatively small proportion of cells expressing the genes could represent the fact that LMGCs are scarce in tissue compared with the total number of macrophages.

3.4. Discussion

In this chapter we show that *in vitro* LMGCs are transcriptionally distinct from mononucleated cells from the same cultures, macrophages, and osteoclasts, and they can be computationally isolated and analysed using this distinction. Whilst this data alone may be insufficient to draw robust conclusions regarding the functional adaptations of tissue LMGCs in the artery walls of GCA patients, we have demonstrated that the *in vitro* model recapitulates tissue LMGCs both morphologically in section 2.5 and now transcriptionally. Sequencing of temporal artery cells from GCA patients revealed a macrophage sub-population expressing a similar gene expression profile to our *in vitro* LMGCs, demonstrating the potential to transcriptionally isolate tissue LMGCs. This finding also further demonstrates the validity of our optimised *in vitro* LMGC culture system as a means of characterising these cells in future studies.

This data could also be used to identify specific biomarkers for tissue LMGCs, by taking highly upregulated genes in the tissue macrophage sub-population of interest and using immunohistochemistry to validate associated protein expression in biopsied sections of temporal artery. Effective identification of biomarkers would benefit both the study of the conditions in which LMGCs are found and their clinical diagnosis and treatment. Insights into

the pathogenesis of GCA are difficult to glean from this data with a limited number of samples and time. With a greater number of samples, and more time for analysis, the populations of cells identified could be scrutinised in greater detail.

In the next chapters of this thesis, the *in vitro* LMGC sequencing data generated here will be used to build hypotheses and support molecular and functional data relating to LMGC formation and functional adaptations.

Chapter 4. The mechanism of LMGC formation; The role of DNA damage in failed cytokinesis

4.1. Introduction

4.1.1. *The mechanism of LMGC formation*

The molecular pathways which instruct macrophage polyploidy in chronic inflammation are likely to be a salient factor in the understanding of the pathogenesis of the conditions in which LMGCs are found. Until recent studies, the consensus in the literature was that they form exclusively by cell-to-cell fusion, as their myeloid derived equivalents have been shown to do^{201, 215, 234}. As of 2021 the LMGC formation mechanism is contested, with evidence in the literature for both cell to cell fusion and incomplete cell division due to failed cytokinesis.

Early studies into macrophage fusion used electron microscopy and radiolabelling. ³H-thymidine incorporation of tissue in live animals resulted in LMGCs with both labelled and unlabelled nuclei, suggesting fusion of labelled and unlabelled mononuclear precursors²¹⁶. The presence of intracellular vacuoles was demonstrated by electron microscopy, and with the lack of a phagocytic phenotype questions were raised as to their origin. It was suggested they may have been autophagic vacuoles, or that they may have been introduced during macrophage fusion²¹⁷. These findings alone were far from conclusive, and it took advances in laboratory techniques years later to amass further supporting evidence for macrophage fusion in the generation of LMGCs.

Mediators of cell fusion appear to play a role in LMGC formation. The protein DC-STAMP, known to be critical for the formation of both osteoclasts and foreign body type giant cells, is necessary for LMGC formation, and proteins of cell fusion machinery CD40, ADAM9 and β 1-integrin have all also been implicated^{159, 215, 229}. In addition, stimulation of macrophages with IFN γ has been shown to increase the expression of the protein ICAM1, which localises on areas of cell to cell contact during monocyte aggregation leading to LMGC formation¹⁶⁸. This evidence together led many scientists to accept cell fusion as the sole formation mechanism, despite the lack of direct experimental evidence. The use of live cell imaging has now revealed the increased complexity of the story, demonstrating the involvement of an alternative mechanism; incomplete cell division with failed cytokinesis.

Murine bone marrow derived macrophages have been shown to undergo modified cell division when cultured *in vitro* in the presence of the toll like receptor 2 agonist FSL-1⁹⁹. Live

cell fluorescence imaging with a DNA-dye revealed multiple instances of mononucleated macrophages entering mitosis, completing DNA synthesis and separation of daughter nuclei, but then failing to abscise, leaving cells polyploid. In this study, successful divisions also occurred at a rate of approximately 40% of total mitoses compared with above 80% in unstimulated controls. Micronuclei (MN) were observed in 10% of FSL-1 stimulated cells compared with 2% in controls, a possible result of anaphase lagging chromosomes due to spindle misalignment, or the formation and subsequent resolution of chromatin bridges. The presence of MN is a strong indication of genome instability²³⁵. The macrophages used to demonstrate this mechanism were of murine origin, it is not clear whether the same mechanism is active in humans.

There is a precedent for cell-cycle dependent polyploidy in a number of well characterised multinucleated cell types in humans. Megakaryocytes are multinucleated cells found in human bone marrow, and are crucial for the process of coagulation by producing platelets. They form by endomitosis (mitosis without cytokinesis), exhibiting deficiencies in cleavage furrow formation and Rho/Rock signalling during the action of the contractile ring, and even failure during karyokinesis^{218, 236, 237}. Hepatocytes, polygonal epithelial cells of the liver, have also been shown to undergo cytokinesis failure, while trophoblasts, key cells of human developmental processes, display rounds of endoreduplication to achieve polyploidy^{100, 219}. It seems that these cells express these differentiation pathways with the distinct purpose of bypassing cell cycle checkpoints which ordinarily would safeguard against this modified mitotic activity, in order to obtain specific functional adaptations beneficial to the organism. It is unclear whether the process of LMGC formation by failed cytokinesis is specialised in this way or whether it's a segregated by-product of the inflammatory environments which drive it. The generation of genomic instability during LMGC formation, which is absent during the differentiation of the other multinucleated cell types mentioned, perhaps suggests the latter^{99, 238}.

4.1.2. The role of DNA damage signalling in macrophage polyploidy

The molecular pathways by which chronic inflammatory stimulation leads to failed cytokinesis of macrophages are poorly understood, however, the DNA damage response (DDR) is thought to play a key role. Stimulation of macrophage precursors with bacterial lipoproteins (BLP) is effective at inducing polyploidy, and these polyploid macrophages exhibit significantly

increased levels of phosphorylation of the histone variant H2AX (γ H2AX), indicating increased DNA damage^{99, 239}. *In vivo* γ H2AX was found in greater quantities in tissue LMGCs in human M.tuberculosis biopsies⁹⁹. This H2AX phosphorylation pathway as a result of DNA damage is mediated predominantly by the ataxia telangiectasia and Rad3 related protein (ATR)²⁴⁰.

While the specific mechanism underlying DNA damage-induced polyploidy is unclear in the case of granulomatous macrophages, parallels may be drawn from a telomere damage-associated pathway which has been implicated in tetraploidisation of human cancer cells²⁴¹. Persistent damage signalling as a result of telomere damage in p53-deficient cells correlates with increased rates of tetraploidy. As cells progress through the cell cycle, abnormalities begin at the G2 phase, which is prolonged, before resolving by bypassing cytokinesis and beginning a new cycle at G1. This appears to be achieved by suppression of the Cdk1/CycB protein complex, which under unperturbed conditions is involved in progression into, and out of, the 'M' phase of the cell cycle²⁴². The protein ATR plays a role here, responsible in combination with the related kinase ataxia-telangiectasia mutated (ATM) for Cdk1/CycB suppression²⁴¹.

Additionally, DNA damage may lead to cytokinesis failure indirectly by promoting mitotic defects involving aberrant strands of chromatin. As discussed in section 1.1.1, chromosome ends are protected by telomeres, tandem repeats of the DNA base sequence TTAGGG. In the absence of telomeres, or when telomeres are damaged or dysfunctional, catastrophic chromosome fusion events can occur leading to failure of complete chromosome segregation during the G2 phase of the cell cycle^{243, 244}. Chromosome fusion is thought to be a protective mechanism serving to prevent further chromosome degradation in the event of telomere damage or dysfunction, however, it leads to significant genome instability when it occurs during the S phase of the cell cycle, as the majority of telomere fusions do^{245, 246}. As the cell cycle progresses into G2/M phases, daughter chromosomes, now fused at telomeres, attempt to segregate. This leaves strands of chromatin, often highly condensed, spanning the cell and connecting the daughter nuclei. These condensed strands are known as chromatin bridges, or anaphase bridges, as they bridge the midbody of a mitotic cell following anaphase.

Chromatin bridges can be resolved as the cell enters the M phase of the cell cycle through sufficient physical tension induced by actomyosin, which provides the hyperextension

necessary for bridge rupture²⁴⁷. This breaking of the bridge often leaves behind micronuclei (MN), cytoplasmic chromosome fragments of varying sizes contributing to genome instability and potentially activating cytoplasmic DNA-sensing senescence pathways²⁴⁸. The exonuclease TREX1 has been implicated in chromatin bridge resolution, suggesting that there may also be protein-mediated chromatin bridge resolution pathways, although this is not well understood, and physical rupture appears to be more common^{245, 247}.

Without the force necessary for rupture, or sufficient enzymatic intervention, chromatin bridges persist into cytokinesis. As chromatin is now present in the midbody of the cell as it attempts to initiate cleavage furrow regression proteins of the abscission checkpoint are activated, predominantly the protein kinase aurora B, which then acts downstream on other factors including ANCHR and ULK3, ultimately delaying abscission. Perturbations in the abscission checkpoint can result in binucleation, as the cell attempts cytokinesis regardless of the presence of chromatin bridges, and daughter cells are physically unable to abscise^{97, 249}.

It is unclear whether LMGC formation by cytokinesis failure involves either the suppression of Cdk1/CycB protein complex or the formation of chromatin bridges and perturbation of the abscission checkpoint. In this chapter I aimed to address this by performing a combination of high-resolution imaging techniques to observe *in vitro* LMGCs as they form, and their nuclear morphology once formed.

4.1.3. Chapter aims

The aim of this chapter was to investigate the formation mechanism of LMGCs. I hypothesised that DNA damage signalling plays a role in their formation by failed cytokinesis, as was demonstrated recently by Herrtwich et al. in a murine model⁹⁹. I further hypothesised that failed cytokinesis would arise following, and due to, the formation of DNA damage-induced chromatin bridges between nuclei.

The objectives of this chapter were as follows:

- To use live cell imaging to observe *in vitro* LMGC formation and gain evidence for cell fusion and/or cytokinesis failure.
- To explore the molecular pathway for LMGC formation by DDR-signalling-induced cell cycle modification proposed by Herrtwich et al. in our *in vitro*

human LMGC culture system by finding evidence for DNA damage and replicative stress.

- To investigate the mechanism by which DNA damage signalling may promote polyploidy in response to chronic inflammatory stimulation.

4.2. Live cell imaging: *In vitro* LMGCs appear to form by a combination of cell fusion and incomplete cell division

To investigate the formation mechanism of LMGCs our optimised model of LMGC formation was used to perform live cell imaging to capture time-lapse footage of the multinucleation process. Primary monocyte cultures were prepared as described in chapter 2, however, standard culture plates were replaced by glass-bottomed dishes suitable for live confocal imaging (CELLview imaging dishes, Greiner Bio-one). Live imaging was performed after 7 days of culture growth, a time point at which we expected LMGCs at various stages of their differentiation to exist. Cells were stained with SiR DNA, a dye with low enough toxicity levels to enable the visualisation of nuclei in live cells with fluorescence microscopy. In order to see the effect of culture conditions on cell division, images were taken every 5 minutes to ensure resultant time-lapse footage possessed a frame-rate high enough to clearly observe any mitotic events. Imaging was performed for a total time period of 17 hours. As well as our optimised LMGC culture conditions, imaged cells were cultured in the presence of GM-CSF only as a control. Four fields of view were captured for both conditions (GM-CSF +/- IFN γ), and for each field of 8 images were taken at a range of heights (Z focal planes), to ensure entire cells were captured even whilst 'rounding up' during any mitoses. Time lapse footage was compiled and analysed using Nikon Elements Viewer software, and annotated in Adobe Illustrator.

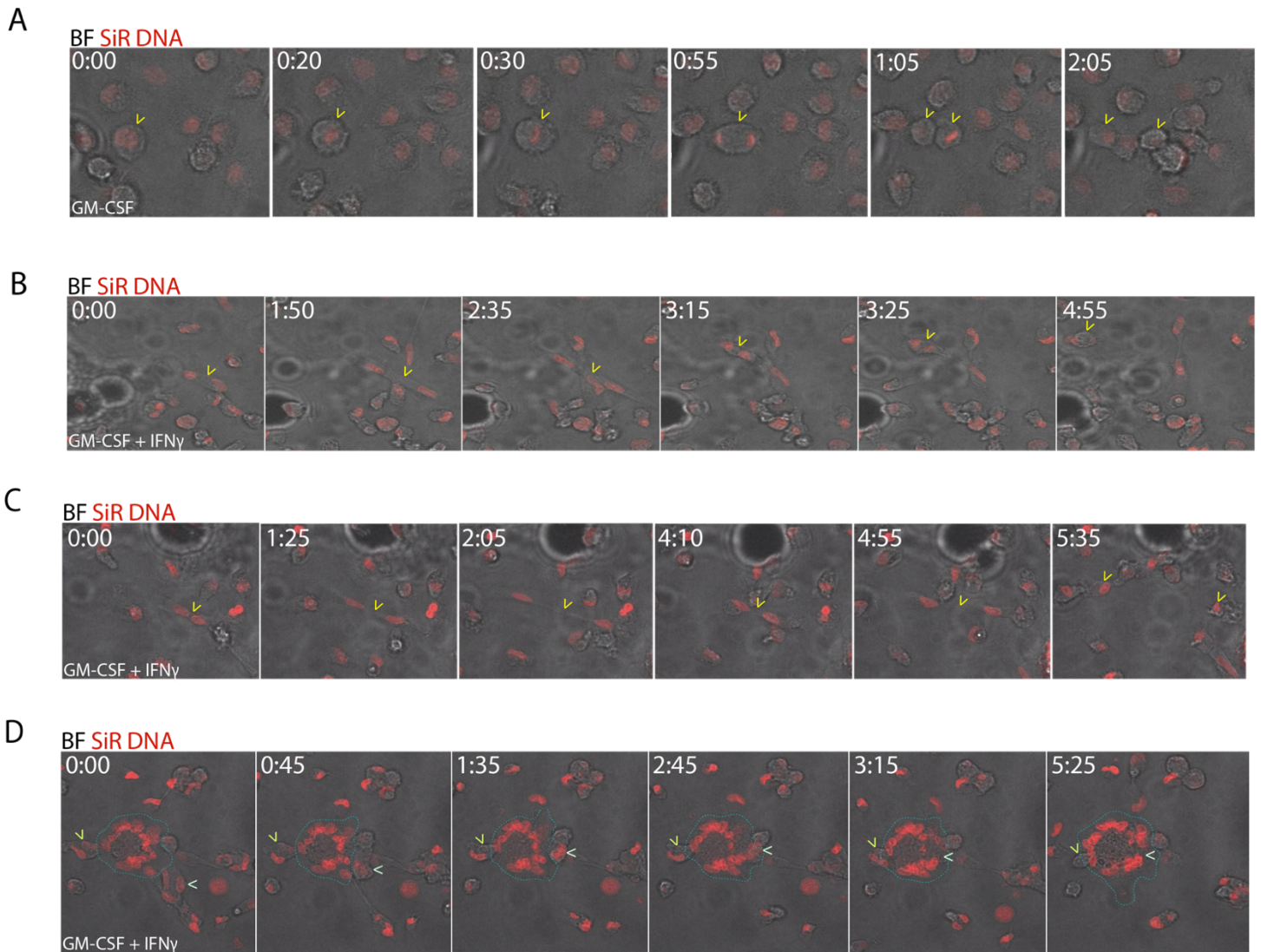


Figure 19. Capturing LMGC formation by live confocal imaging.

Live cell imaging suggests a combination of cell fusion and incomplete cell division with failed cytokinesis as the formation mechanism of *in vitro* LMGCs. Imaging initiated after 7 days of culture. A) Control macrophages, cultured in the presence of GM-CSF alone demonstrating successful mitosis. Arrows indicate a mitotic cell in panels 1-4, and resultant daughter cells in panels 5-6. B) In the presence of IFN γ , a binucleated cell seemingly enters abscission and is unable to complete cytokinesis, resulting in a binucleated cell. Arrow indicates the cell midbody. C) In the presence of IFN γ , a binucleated cell seemingly enters abscission and after multiple attempts, cytokinesis is completed. Arrows indicate the cell midbody in panel 1-5, and resultant daughter cells in panel 6. D) In the presence of IFN γ , multiple mononuclear cells (yellow and white arrows) fuse with a large LMGC (cyan outline). BF = Brightfield, Red = nuclei (SiR DNA). Imaging time shown as Hours:Minutes.

Analysis of the time-lapse footage revealed that complete and normal mitoses occurred, albeit infrequently, in the absence of IFN γ . Each round of mitosis took between one and two hours to complete. These mitotic events were not observed in in cultures with IFN γ , however, there were many examples of polyploid cells undergoing attempted cytokinesis. In some instances, cytokinesis was eventually successful, after prolonged cytokinesis with what appeared to be multiple attempts at abscission, whereas in other instances cytokinesis was ultimately unsuccessful and cells remained binucleated. Cell fusion events were clearly evident and frequent in cultures with IFN γ . Fusion of mononucleated cells with each other, mononucleated cells with binucleated cells, and mononucleated cells with already large multinucleated cells was observed.

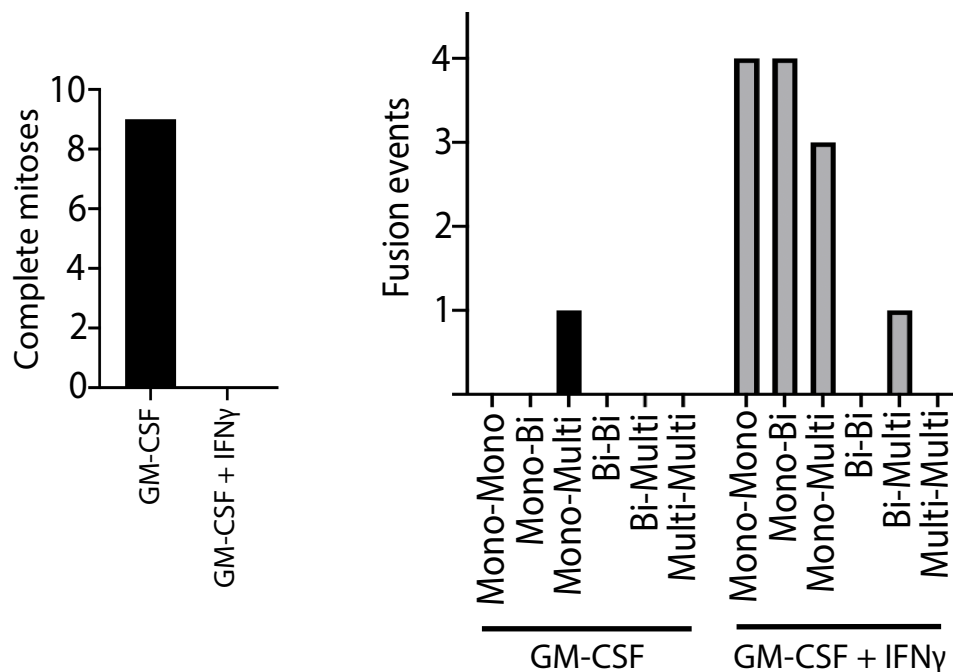


Figure 20. Live cell imaging quantification of mitoses and fusion events.

Quantification of (A) complete mitoses and (B) cell fusion events in LMGC culture conditions and control conditions. Complete mitoses and cell fusion events shown as the number observed in total across four fields of view at 40X objective magnification. In the presence of GM-CSF alone, Complete mitoses totalled 8 and there was a single fusion event between a mononucleated cell and multinucleated cell. The addition of IFN γ led to complete absence of complete mitoses, and a higher number of fusion events between mononucleated, binucleated and multinucleated cells. N=1.

Quantification is limited by the low number of cells it was possible to image. Five-minute intervals were maintained to ensure mitotic events could be fully captured (So that stages were not missed between frames), and this limited the number of fields of view it was possible to capture. Complete mitoses were absent in the presence of IFN γ . While time lapse footage demonstrated evidence of prolonged cytokinesis in this condition we were unable to conclusively identify this at mitosis as we did not observe G1, S or G2 phases of the cell cycle in these cells. Whilst this time lapse evidence suggests the possibility of cytokinesis failure, alone it was inconclusive.

4.3. The presence of chromatin bridges supports incomplete cell division

4.3.1. In vitro LMGCs exhibit large chromatin bridges between pairs of nuclei

To further investigate the possibility of cytokinesis failure we used confocal microscopy was used to study the morphology of nuclei within LMGCs. As discussed in 4.1.2, chromatin bridges can arise as a result of catastrophic DNA damage, specifically telomere damage, and can cause cytokinesis failure when chromatin is detected in the midbody during abscission. LMGCs were cultured as previously described, on glass coverslips. Once sufficiently grown for maximal LMGC yield, coverslips were removed from culture plates, fixed with a formaldehyde-based fixative, permeabilised with triton-X and stained with the DNA-dye DAPI to visualise DNA. Coverslips were mounted on microscope slides to allow images to be taken by confocal microscopy. Taking Z-stack images allowed the rendering of DAPI fluorescence in 3 dimensions, so we could view the full extent of the nuclei and their connections which weren't necessarily apparent single slices.

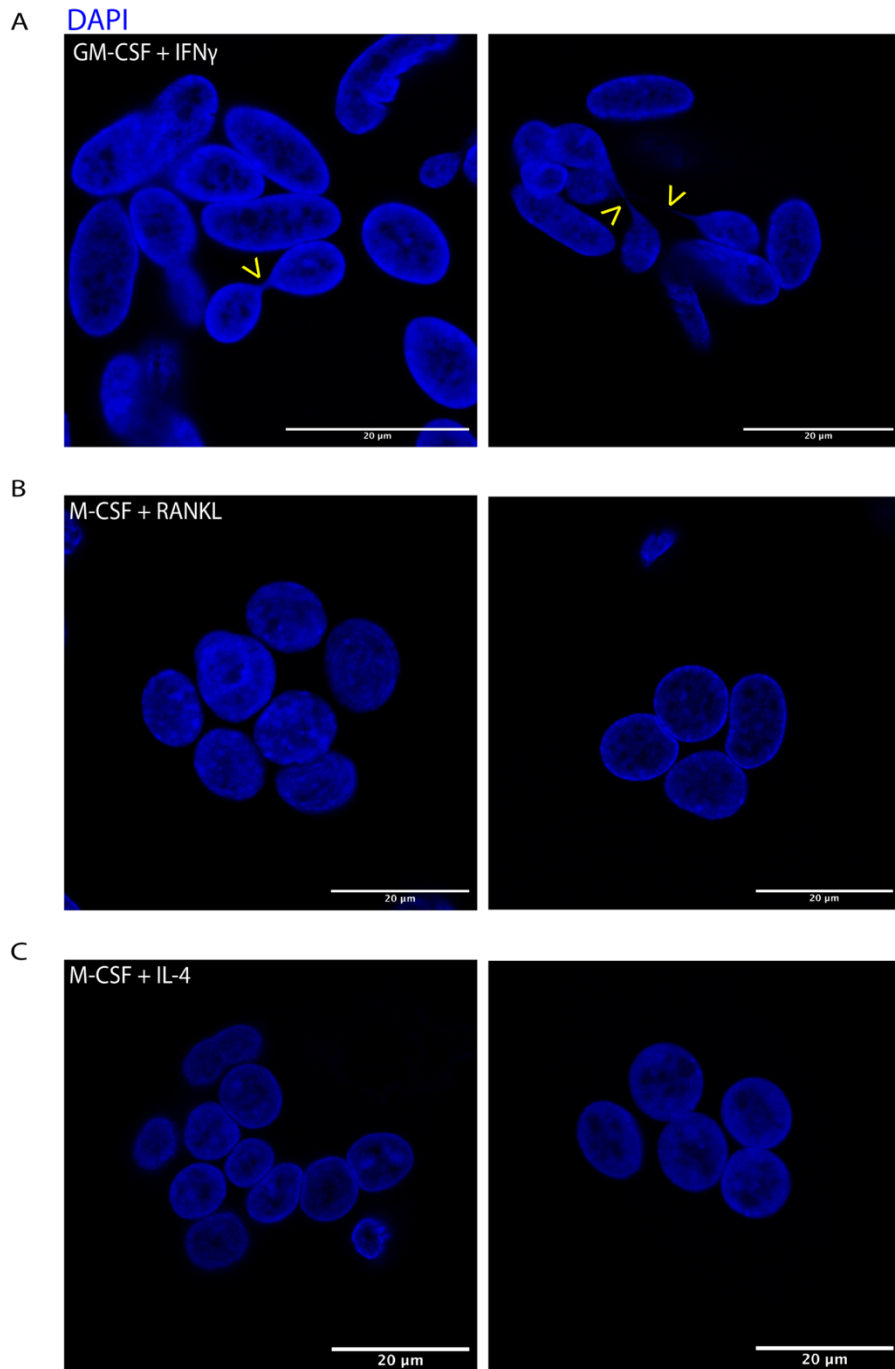


Figure 21. Confocal imaging of *in vitro* LMGs, osteoclasts and FBGCs.

A) Nuclei within cultured LMGs containing large chromatin bridges connecting pairs of nuclei. B) Nuclei within cultured osteoclasts (OC) with M-CSF and RANKL. Chromatin bridges were absent within OCs. C) Nuclei within cultured foreign body giant cells (FBGCs) with M-CSF and IL-4. Chromatin bridges were absent within FBGCs. Nuclei stained with DAPI. Scale bars = 20 μ m.

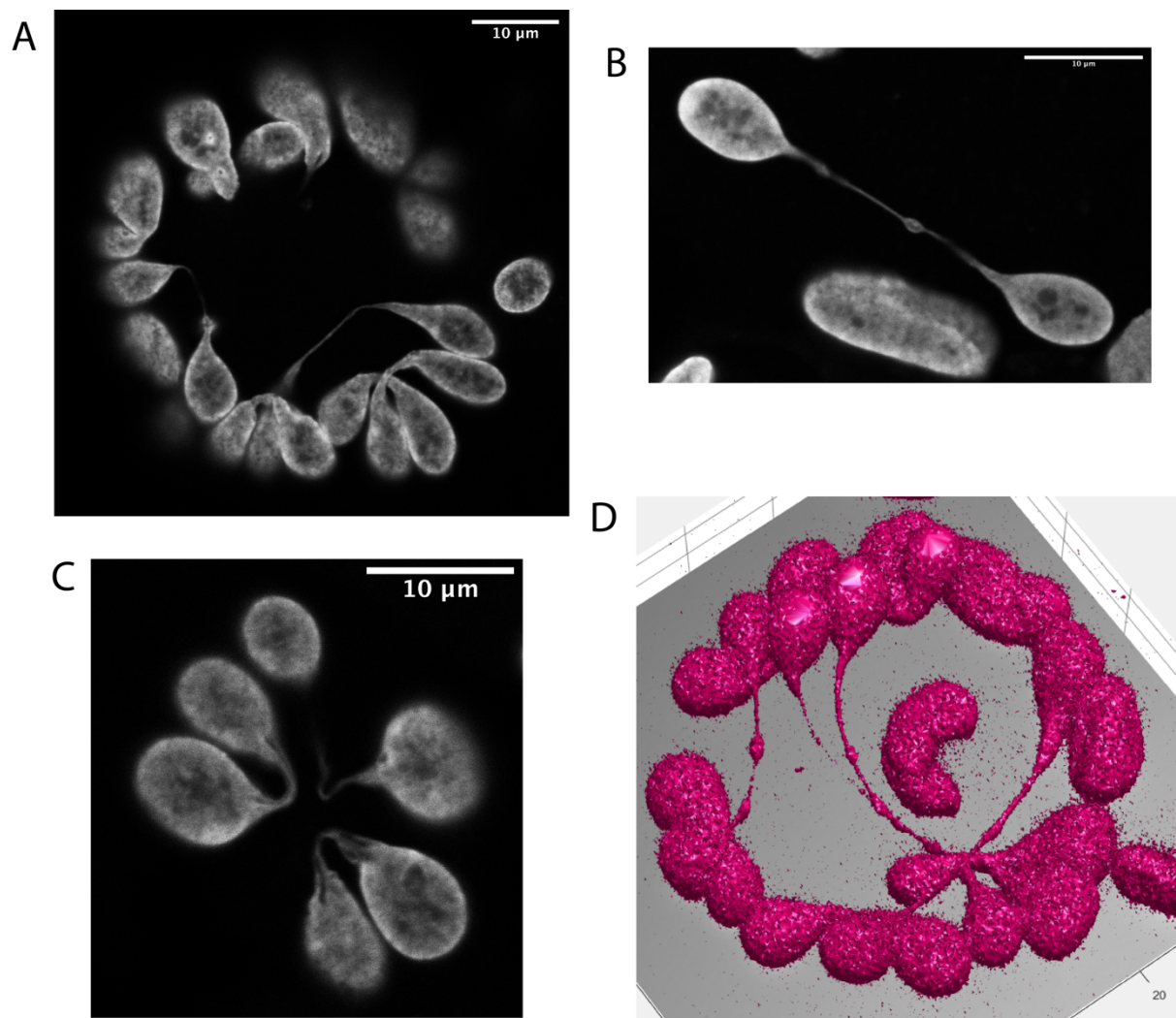


Figure 22. Chromatin bridges within *in vitro* LMGCs by confocal imaging.

A, B, C) Polyploid LMGCs of different sizes. Grey = Chromatin (DAPI). Images grey-scaled for clear visualisation of chromatin bridges. Images taken with Leica SP8 confocal microscope with 63x objective lens with oil immersion. Scale bars = 10um. D) 3D reconstruction of an LMGC Z stack image. Slices were analysed in Microscopy Image Browser software (MIB Helsinki), and DAPI positive pixels were highlighted and segmented by contrast thresholding (pink). This was repeated for all slices, and the resultant segmented object was rendered as a 3D model in MIB, before being visualised using Matlab volume viewer.

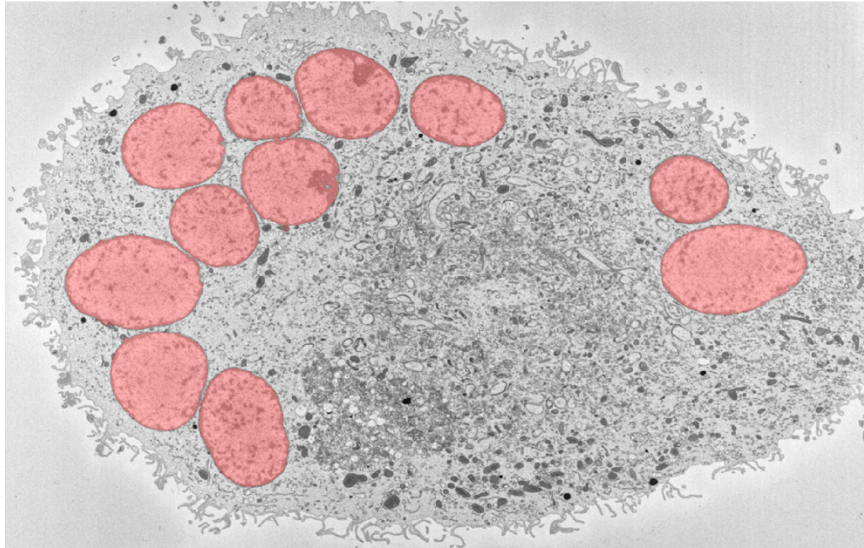
Chromatin bridges were large and extensive within *in vitro* LMGCs, connecting pairs of nuclei only. Connected nuclei were commonly adjacent within LMGCs, although there were also examples of more distal pairs with chromatin bridges spanning the centre of the cell. The absence of chromatin bridges within osteoclasts and foreign body giant cells supports the hypothesis that polyploidy resulting from chronic inflammation is by a distinct mechanism to other macrophage-derived MGCs. We next aimed to align this finding to LMGCs from GCA affected temporal artery tissue.

4.3.2. Electron microscopy reveals chromatin bridges between pairs of nuclei in LMGCs from GCA affected temporal artery tissue

With the presence of chromatin bridges within *in vitro* LMGCs established by fluorescence microscopy, we aimed to match this finding in LMGCs from GCA affected temporal artery tissue. Scanning electron microscopy was used to investigate the morphology of nuclei within tissue LMGCs and *in vitro* LMGCs to support fluorescence microscopy findings and to act as a comparison. Electron microscopy would also allow the identification of any changes in the gross morphology of *in vitro* LMGCs when compared to mononucleated cells from the same cultures.

A small section, roughly 1mm² in volume was dissected from a temporal artery biopsy (TAB) sample from a patient with suspected (and later confirmed) GCA. This was placed in glutaraldehyde to fix the tissue, before being prepared and imaged by the Electron Microscopy Service at Newcastle University. Images were pre-processed in Microscopy Image Browser (MIB) software, where Z stack images were cropped to show only the region of interest, corrected to have consistent contrast, and aligned to allow 3D rendering. Segmentation of nuclei was performed in the same software, using the '2D watershed' function in combination with a manual brush tool to highlight and segment nuclei slice by slice.

A



B

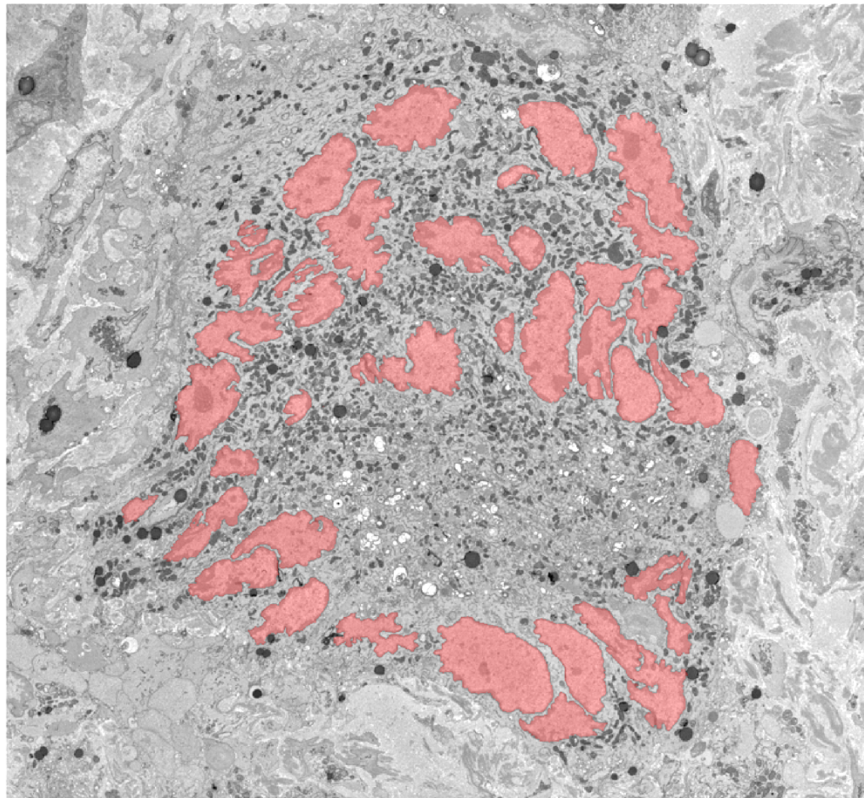


Figure 23. Nucleus segmentation from scanning electron microscopy images of *in vitro*, and TAB LMGCs.

Scanning electron microscopy images of (A) An *in vitro* LMGC, and (B) An LMGC from GCA affected temporal artery tissue. Images shown are single sections of full Z stacks. Nuclei (highlighted in red) were manually segmented using MIB software. Nuclei display characteristic peripheral ring/horseshoe arrangement. Images taken using a Zeiss Sigma Scanning Electron Microscope.

In total, three LMGs from *in vitro* cultures from two different donors, a single mononucleated macrophage taken from one of these cultures, and a single tissue LMGC were imaged. It was not possible to image entire cells, instead sectioning began part way through. This was because LMGCs had to be manually identified while sectioning was taking place, and it was not clear whether a cell was multinucleated or mononucleated until a certain amount had already been processed and ploidy could be determined.

A number of morphological observations were made. All imaged multinucleated cells, both from *in vitro* cultures and TAB tissue, displayed the peripheral ring/horseshoe arrangement of nuclei characteristic of LMGCs. *In vitro* LMGCs contained numerous vacuoles and a distinctive spherical section in the very centre of each cell, seemingly separated from the rest of the cell by a sphere of organelle-free cytoplasm. This is displayed and discussed in further detail in the following chapter of this thesis (5.4). Both of these characteristics were absent in the TAB LMGC. Within the unusual spherical sections were what appeared to be fragmented or disformed organelles, and cellular debris, although this was unclear. *In vitro* LMGCs also possessed distinctively long projections emanating from their plasma membranes, similar to those observed on healthy dendritic cells. The TAB LMGC imaged was larger than cultured LMGCs, and contained nuclei which were not as spherical as cultured LMGCs, taking on more of a creased, distorted appearance. Nucleoli were observed as dark areas within each nucleus, and were used to confirm single nuclei.

When the chromatin of all sections had been highlighted and segmented as shown in figure 23, the segments were compiled into three dimensional objects using the 'Models with Matlab isosurfaces' function within MIB, and visualised in Matlab volume viewer.

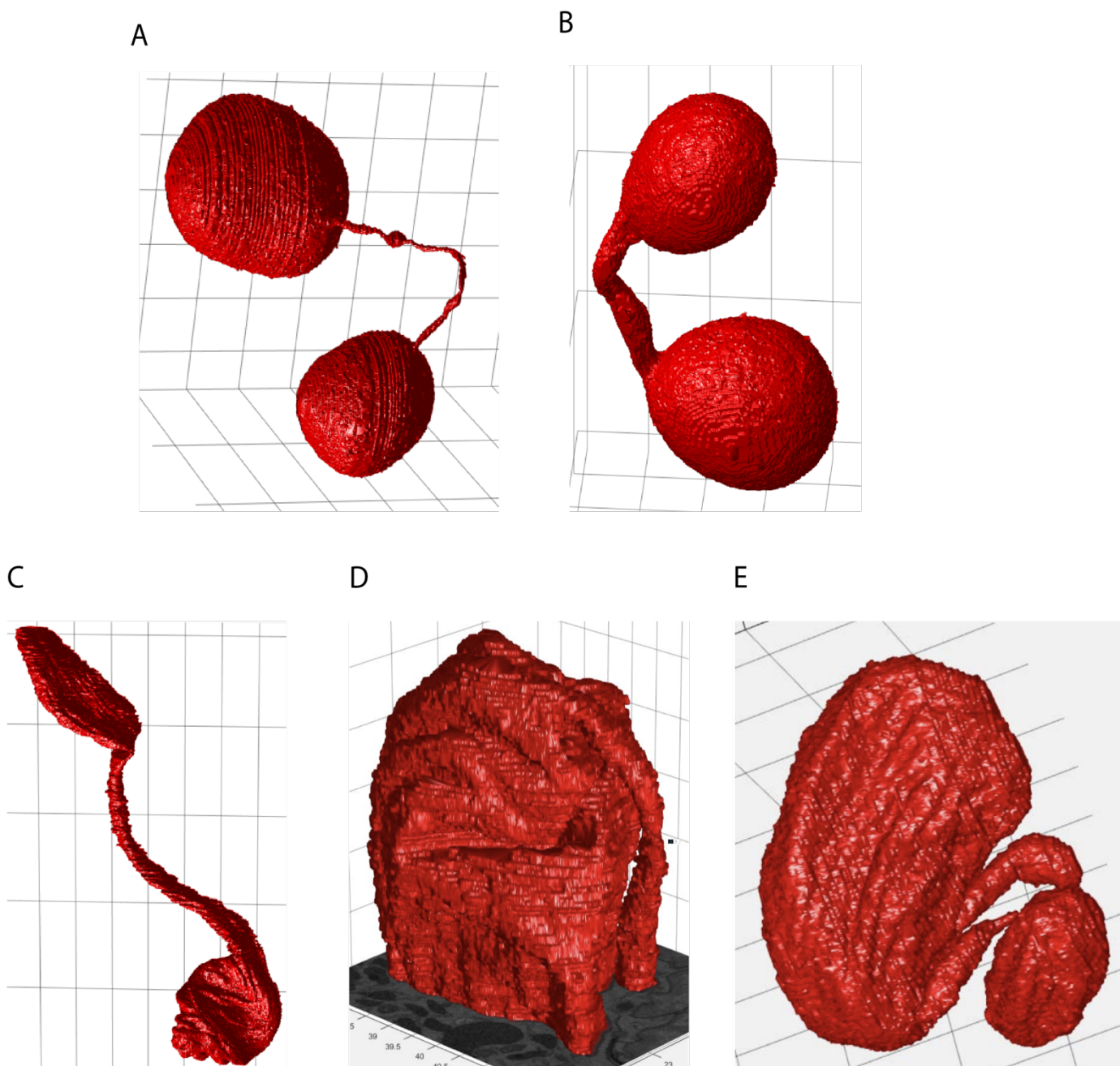


Figure 24. Reconstructing chromatin bridges from scanning electron microscopy images in 3D.

Confirming the presence of chromatin bridges within LMGCs using electron microscopy. A, B) Chromatin bridges of different sizes connecting pairs of nuclei within *in vitro* cultured LMGCs. Examples from two separate donors. C, D, E) Chromatin bridges within a LMGC from the artery wall of a temporal artery biopsy taken from a patient with confirmed GCA. All examples taken from a single LMGC. Electron microscopy images processed, segmented and rendered as 3D models using microscopy image browser (MIB) software and visualised using Matlab.

In vitro LMGCs displayed clear chromatin bridges, supporting what we observed by fluorescence microscopy. All chromatin bridges connected two distinct nuclei but never more. In three cells analysed, four chromatin bridges were found, two of which are shown above (Figure 24A, Figure 24B). Chromatin bridges varied in thickness and length.

Like *in vitro* LMGCs, the imaged cell from TAB tissue displayed the characteristic morphology of a LMGC, with a horseshoe shaped arrangement of nuclei around the periphery of the cell. Within this cell, three examples of chromatin bridges were identified, bearing a resemblance to those observed in our cultured LMGCs when rendered as 3D models. The imaging of this cell began part-way through the nucleus shown in figure 24D, and so the beginning of a possible chromatin bridge was seen but was not confirmed to have been connected with a second nucleus. Figure 24E shows two nuclei, one significantly greater in volume than the other, connected by two separate chromatin bridges.

As discussed, chromatin bridges can arise as a result of catastrophic telomeric DNA damage. Next, I aimed to investigate whether this was the case in the formation of LMGCs by looking for evidence of DNA damage and replicative stress in IFN γ treated cultures.

4.4. IFN γ driven DNA damage and replicative stress in LMGCs

4.4.1. LMGCs express 'DNA damage response' gene signature

To investigate the hypothesis that DNA damage plays a role in chromatin bridge development and LMGC formation we first analysed the single cell RNA sequencing dataset generated in 3.2. Among the differentially expressed genes of the LMGC cluster, a number of genes relating to the activation of the DNA damage response and cellular responses to oxidative damage were found.

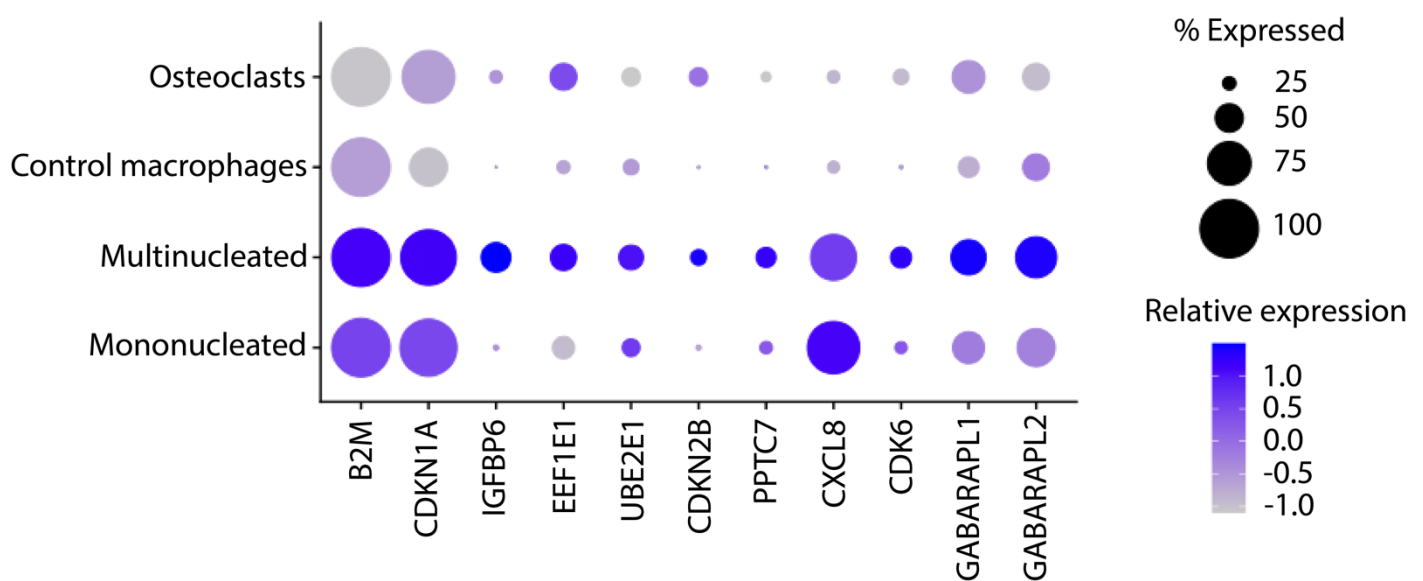


Figure 25. Differentially expressed genes of LMGCs relating to the DNA damage response.

Dot plot displaying eleven differentially expressed genes for the LMGC (Multinucleated) cluster. Genes relate to or are involved in the activation of the DNA damage response. Circle size represents the percentage of cells expressing the gene within the cluster, and colour represents relative gene expression, blue = high and grey = low. Clusters assigned to osteoclasts, control macrophages (GM-CSF only) and mononucleated cells from the same cultures as LMGCs were included as comparators. Genes are differentially expressed (adjusted p value <0.05) between multinucleated cells and other cell types using the FindAllMarkers with Wilcoxon Rank Sum test in Seurat.

The eleven genes identified within LMGC cluster differentially expressed genes (DEGs) are all known to play a role in the activation of the DNA damage response, suggesting that LMGCs do exhibit a degree of DNA damage or replicative stress. Interestingly, mononucleated cells from the same cultures typically expressed these same genes to a slightly lesser extent than LMGCs, although still significantly greater than control macrophages and osteoclasts. This points to the IFN γ as the cause, present in the culture media of those cells highly expressing these genes and absent in those not. It is possible that DNA damage must reach a certain threshold before chromatin bridges are likely to form, which would explain why the 'multinucleated' cell cluster exhibit marginally higher levels of gene expression than the 'mononucleated' cluster. To support this transcriptional evidence of DNA damage, we next aimed to perform immunocytochemistry to measure protein expression of the DNA double strand break marker 53BP1.

4.4.2. IFN γ induces DNA double strand breaks

Immunocytochemistry was used to measure 53BP1 expression, a protein upregulated in response to DNA double strand breaks and an indication that the DNA damage response is activated under replicative stress²⁵⁰. LMGCs and control macrophages were cultured as described in 7.2.1.5. After 8 days of culture, coverslips with now adherent cells attached were removed from the culture plates, and prepared for immunocytochemistry by fixation with a formaldehyde-based fixative, and subsequent blocking and permeabilization as described in methods section 7.2.5. After this, primary antibody staining was performed with an anti-53BP1 antibody (Novus Bio) at a dilution of 1:100 in 0.5% BSA. This concentration was determined to be optimal following a titration experiment not shown. One coverslip was incubated in the absence of the primary antibody to serve as a negative imaging control (Secondary only). Secondary antibody staining was then performed with an anti-rabbit, AF647 conjugated secondary antibody (Abcam), at a 1:200 dilution in 0.5% BSA, as recommended by the supplier. Coverslips were finally stained for 20 minutes with DAPI (Sigma), at 1 μ g/mL in PBS, rinsed with PBS, and mounted onto microscopy slides. Images were captured with the Zeiss AxioImager wide field fluorescence microscope with 63X objective magnification with oil immersion.

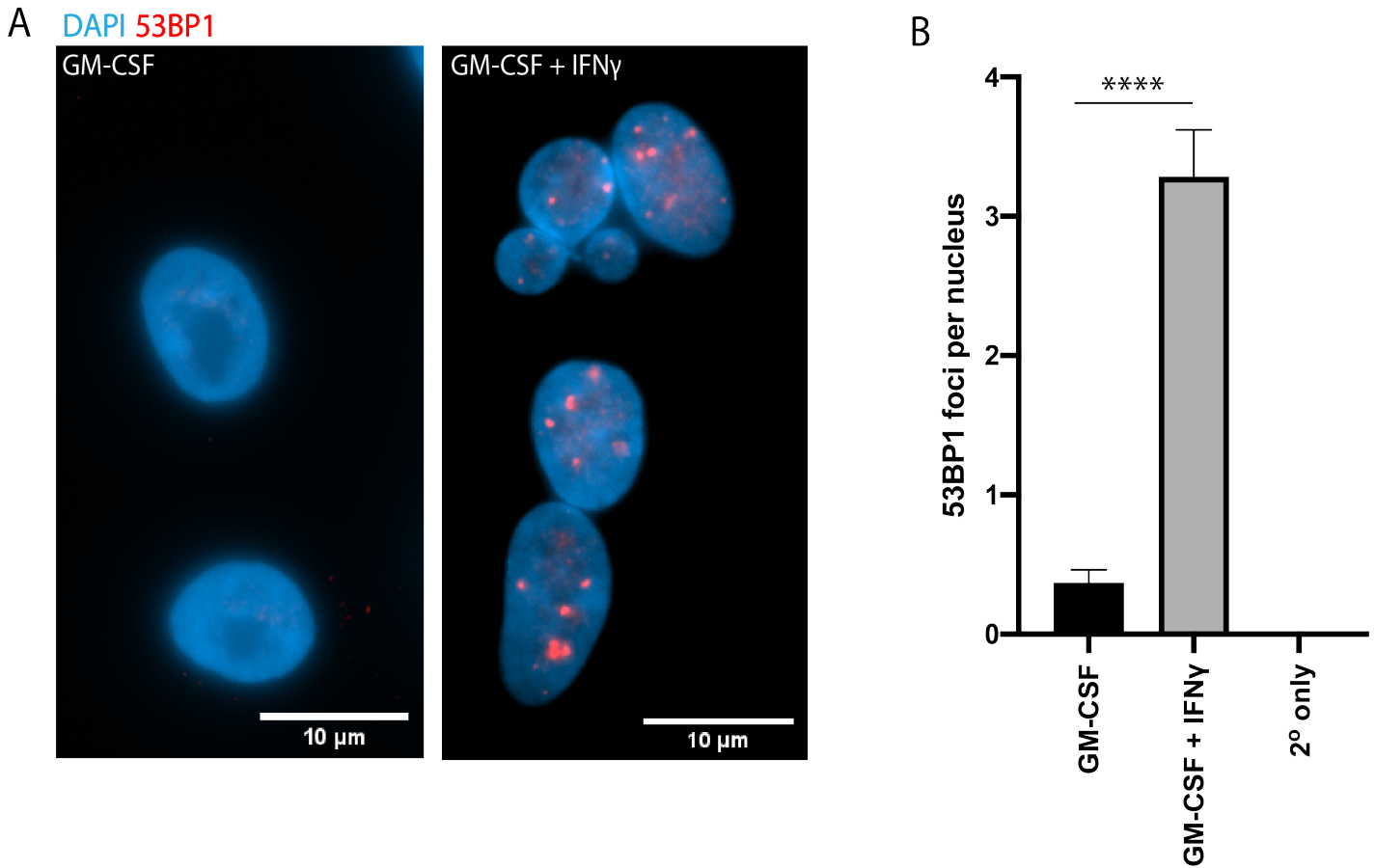


Figure 26. Measuring IFN γ induced DNA damage by 53BP1 immunofluorescence.

IFN γ induces DNA damage and activation of the DNA damage response (DDR). A) Representative images of nuclei within cells cultured in GM-CSF only (left) and GM-CSF with IFN γ (right). Numerous 53BP1 foci are visible in cultures containing IFN γ . B) The mean number of foci per nucleus was found for 100 nuclei in each condition. The mean of these means for all three samples was then calculated. Laser power set using secondary only (2° only) as negative control. Foci were manually counted using ImageJ. Values represent the means of the means for cells from three donors (n=3). **** = statistically significant, $p < 0.0001$ using Mann-Whitney U tests. Error bars = SEM. Scale bars = 10 μ m.

The number of 53BP1 foci were counted per nucleus, for 100 nuclei per condition. Microscope settings were determined using secondary only (2° only) as a negative control. Cells cultured in the presence of IFN γ contained significantly greater quantities of 53BP1 foci per nucleus than those cultured in the absence of IFN γ , suggesting that IFN γ induces DNA double strand breaks. Furthermore, 53BP1 nuclear bodies can be an indication of mitotic transmission of chromosomes during a state of replicative stress²⁵⁰. To further explore the mechanism by which IFN γ signalling leads to DNA damage, we next investigated the hypothesis that IFN γ leads to oxidative damage via the generation of reactive oxygen species (ROS).

4.4.3. Culture with a reactive oxygen species scavenger has no effect on LMGC formation

To investigate the role ROS may play in IFN γ induced DNA damage and multinucleation, LMGC culture assays were performed in the presence or absence of a ROS scavenger, MitoTEMPO (Sigma) at a range of concentrations. Concentrations were chosen based on ranges used in a study where similar culture assays were performed with MitoTEMPO²⁵¹. Cultures were maintained for 9 days before being harvested as described in 7.2.2.1, and stained with DRAQ5 before measuring multinucleation using the Fortessa X20 flow cytometer. This was repeated with monocytes from four separate donors.

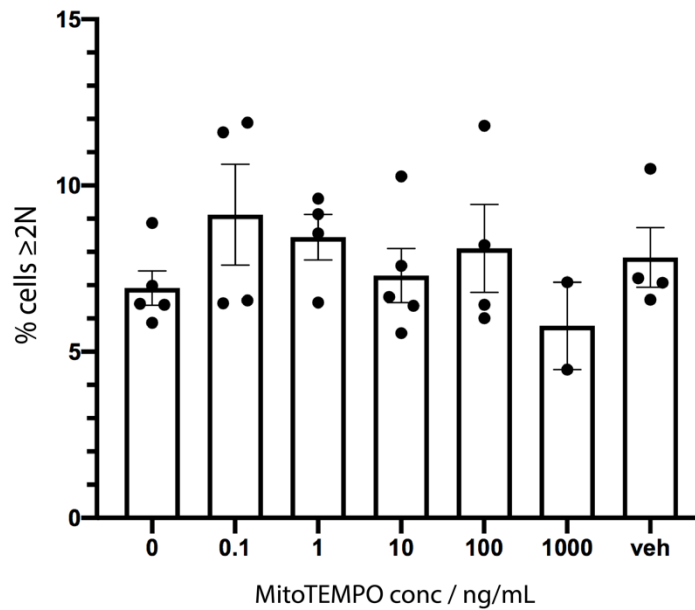


Figure 27. The effect of MitoTEMPO in culture on LMGC formation.

Measuring multinucleation of primary monocytes cultured to generate LMGCs (50ng/mL GM-CSF + 200ng/mL IFN γ) in the presence of MitoTEMPO. MitoTEMPO concentrations used were 0.1, 1, 10, 100 and 1000ng/mL. veh = DMSO. There was no significant change in multinucleation with increasing concentrations of mitoTEMPO, $p > 0.05$ determined by Kruskal Wallace test. $n=4$.

Culture with the (ROS) scavenger MitoTEMPO had no significant effect on LMGC formation. There were only two values at a concentration of 1000ng/mL mitoTEMPO as the mitoTEMPO became hypertoxic at this concentration and cultures from two of the donors did not survive. This may indicate that IFN γ causes DNA damage through a mechanism independent of ROS mediated oxidative damage.

4.5. Discussion

In this chapter we aimed to investigate the mechanism of LMGC formation using the *in vitro* LMGC culture system optimised in chapter 2. We have demonstrated that *in vitro* LMGCs form convincingly by cell fusion, and have found compelling evidence that incomplete cell division with cytokinesis failure is also involved. Our findings suggest that human macrophages have the same capacity for polyploidy by induction of replicative stress and activation of the DNA

damage response as was demonstrated by Herrtwich et al. in murine macrophages, although unlike this study we also demonstrate the contribution of cell fusion events⁹⁹.

With the data generated in this chapter I propose a potential mechanism by which chronic inflammation promotes cytokinesis failure and macrophage polyploidy. IFN γ , the cytokine responsible for driving LMGC formation, induces DNA damage in macrophages by an unknown pathway, which may be ROS-independent. Telomeric DNA damage may then lead to the formation of chromatin bridges through chromosomal fusion events during anaphase as discussed in 4.1.2, although it is not clear from this data whether the DNA damage observed is localised to telomeres, and further experimentation is required to confirm this. The presence of chromatin bridges in both *in vitro* LMGCs and those from GCA affected temporal artery tissue further validates our *in vitro* LMGC culture system, and indicates that the same pathways are active in human granulomas.

As chromatin bridges were almost exclusively observed between pairs of nuclei, it suggests that the mechanism of incomplete cell division occurs exclusively in mononucleated cells, which go on to fuse with other cells to generate large LMGCs. This would suggest that cells with two or more nuclei are no longer mitotically active, exhibiting a more pro-fusion, prematurely senescent phenotype.

Chapter 5. Investigating the functional phenotype of LMGCs

5.1. Introduction

5.1.1. The role of LMGCs in GCA pathogenesis

LMGCs are associated with arterial damage in GCA. Damage to the vascular smooth muscle cells (VSMCs) of the artery wall intima can cause vessel fragmentation, and ultimately rupture. The damage observed may be mediated by ROS as 4-Hydroxy-2-nonenal adducts, products of lipid peroxidation, can be found on VSMCs in GCA affected temporal artery tissue⁵⁸. LMGCs are implicated in this damage due to their proximity to areas of lipid peroxidation⁵⁸. In support of this hypothesis, a number of studies demonstrate enhanced capacity for the production of ROS by multinucleated giant cells, both osteoclasts and LMGCs^{228, 252-254}.

In addition to ROS, LMGCs are proposed to produce a number of pro-inflammatory mediators, contributing to granulomatous infiltration. Metalloproteinase 9 (MMP-9) and platelet derived growth factor (PDGF) are implicated in GCA pathogenesis, associated with degradation of the elastic lamina and VSMC hyperproliferation respectively^{220, 221}. LMGCs have been shown to release both of these factors in GCA affected temporal artery tissue, though evidence suggested PDGF was also produced by VSMCs and mononucleated macrophages^{221, 255}. In combination these factors may contribute to intimal hyperplasia and luminal occlusion by promoting vascular remodelling and the hyperproliferation of VSMCs. LMGCs are also the main source of vascular endothelial growth factor (VEGF) in GCA affected temporal arteries, levels of which are elevated in rheumatic diseases including GCA^{40, 222}. This suggests a role for LMGCs in promoting the formation of medial and intimal vasa vasorum, contributing to granulomatous inflammation by driving the recruitment of immune cells⁴⁰.

5.1.2. Premature senescence and the senescence associated secretory phenotype

Eukaryotic cells typically possess the capacity to proliferate. However, in response cellular stresses including persistent DDR signalling, dysfunctional telomere signalling or oncogene activation they can enter a state of permanent cell cycle arrest; Senescence²⁵⁶. Senescence was first demonstrated in human fibroblasts, which were shown to have a limited number of cell cycles before entering a terminal non-proliferative state²⁵⁷. There is a clear relationship between the programs of apoptosis and senescence as there is a significant overlap between

the principal proteins involved, in particular those of the p53 pathway, and senescent cells have improved viability due to increased apoptotic resistance^{258, 259}.

Telomere shortening, which occurs naturally in proliferative cells as we age, is strongly associated with the induction of cellular senescence²⁶⁰. As telomeres shorten or DNA damage accumulates over time the DDR is activated, which signals through a cascade including ATM, ATR, CHK1, CHK2 and p53 to arrest the cell cycle²⁶¹. While this process naturally becomes more common with age, it also occurs prematurely in instances of sudden atypical telomeric damage, regardless of telomere length²⁶².

Recently an alternative senescence induction pathway has been identified, in which cyclic GMP-AMP synthase (cGAS) senses cytosolic chromatin fragments and promotes senescence via the stimulator of interferon genes (STING) pathway²⁶³. cGAS undergoes a conformation change upon binding with phosphate-sugar backbone of double stranded DNA, allowing the stimulation of STING by cGAMP following catalysis of the second messenger GMP-AMP²⁶⁴. STING activates interferon-regulatory factor 3 (IRF3) and nuclear factor kappa B (NF- κ B), and causes their translocation to the nucleus where they exert transcriptional changes^{265, 266}. This results in an enhanced secretory, pro-inflammatory phenotype with increased expression of pro-inflammatory mediators including chemokines and cytokines²⁶⁷. This cell state is known as the senescence associated secretory phenotype (SASP), and is associated with the increased secretion of a number of factors including type 1 interferons, chemokines such as CXCL8, CCL2 and CCL8, cytokines IL-1, IL-6, and other inflammatory factors, proteases and soluble factors such as GM-CSF, metalloproteinases and IGFbps²⁶⁷⁻²⁷⁵.

The presence of chromatin bridges within LMGCs is suggestive of catastrophic telomere damage and the physical rupture of these bridges may result in fragments of cytoplasmic DNA, both of which can cause premature senescence through different molecular pathways. Evidence in the literature indicates increased secretion of numerous pathology-driving factors by LMGCs in GCA affected temporal arteries. I hypothesise that LMGCs enter a state of premature senescence following cytokinesis failure, and exhibit an enhanced senescence-associated secretory phenotype.

5.1.3. Chapter aims

The aim of this chapter was to characterise LMGCs in terms of their functional phenotype. I hypothesised, based on data generated in previous chapters and evidence for an increased secretory phenotype demonstrated in the literature, that LMGCs enter a state of premature senescence and exhibit a senescence-associated secretory phenotype. I further hypothesised that cytokines involved in the pathogenesis of GCA, namely TNF α , IL-6 and IL-1 β , as well as reactive oxygen species, would be constituents of their secretome. I additionally hypothesised that, based on electron microscopy data generated in the previous chapter, LMGCs may be specialised for enhanced phagocytosis.

The objectives of this chapter were as follows:

- To measure the protein expression of the senescence marker p21 to investigate the premature senescence of *in vitro* LMGCs.
- To gain experimental evidence exploring the expression of a senescence associated secretory phenotype by *in vitro* LMGCs.
- To investigate the capacity for the production of ROS by *in vitro* LMGCs.
- To further characterise the functional adaptations of *in vitro* LMGCs by measuring their phagocytic capabilities.

5.2. LMGCs exhibit increased P21 expression

To investigate the senescence of LMGCs, they were cultured as described in chapter 2 on glass coverslips, and immunofluorescence staining for the senescence marker p21 was performed. The kinase inhibitor p21 (CIP1/WAF1) is used as an intracellular marker of cellular senescence; As a key downstream component of the p53 pathway it is upregulated during cell cycle arrest^{276, 277}. The cells were fixed with a formaldehyde-based fixative (BD) and blocked before consecutive primary and secondary antibody incubations, which were performed at 1:100 and 1:200 dilutions in 0.5% BSA respectively. The primary antibody was raised against p21 (Cell Signalling) and the secondary, AF647 conjugated, against the rabbit mAb primary (Abcam). A secondary antibody only (2^o) control was used by incubating a coverslip in the absence of the primary antibody, in order to eliminate imaging artefacts due to non-specific secondary antibody binding. Cells were then briefly stained with DAPI as previously described and mounted onto microscopy slides using VECTASHIELD (Vectorlabs). Images were taken

using the Zeiss AxioImager fluorescence microscope with 63x objective magnification with oil immersion. Images were analysed by outlining nuclei first in the DAPI channel, before overlaying the measured area onto the p21 channel and taking an MPI measurement. This step was taken to eliminate a degree of input bias, ‘blinding’ the measurements as much as possible.

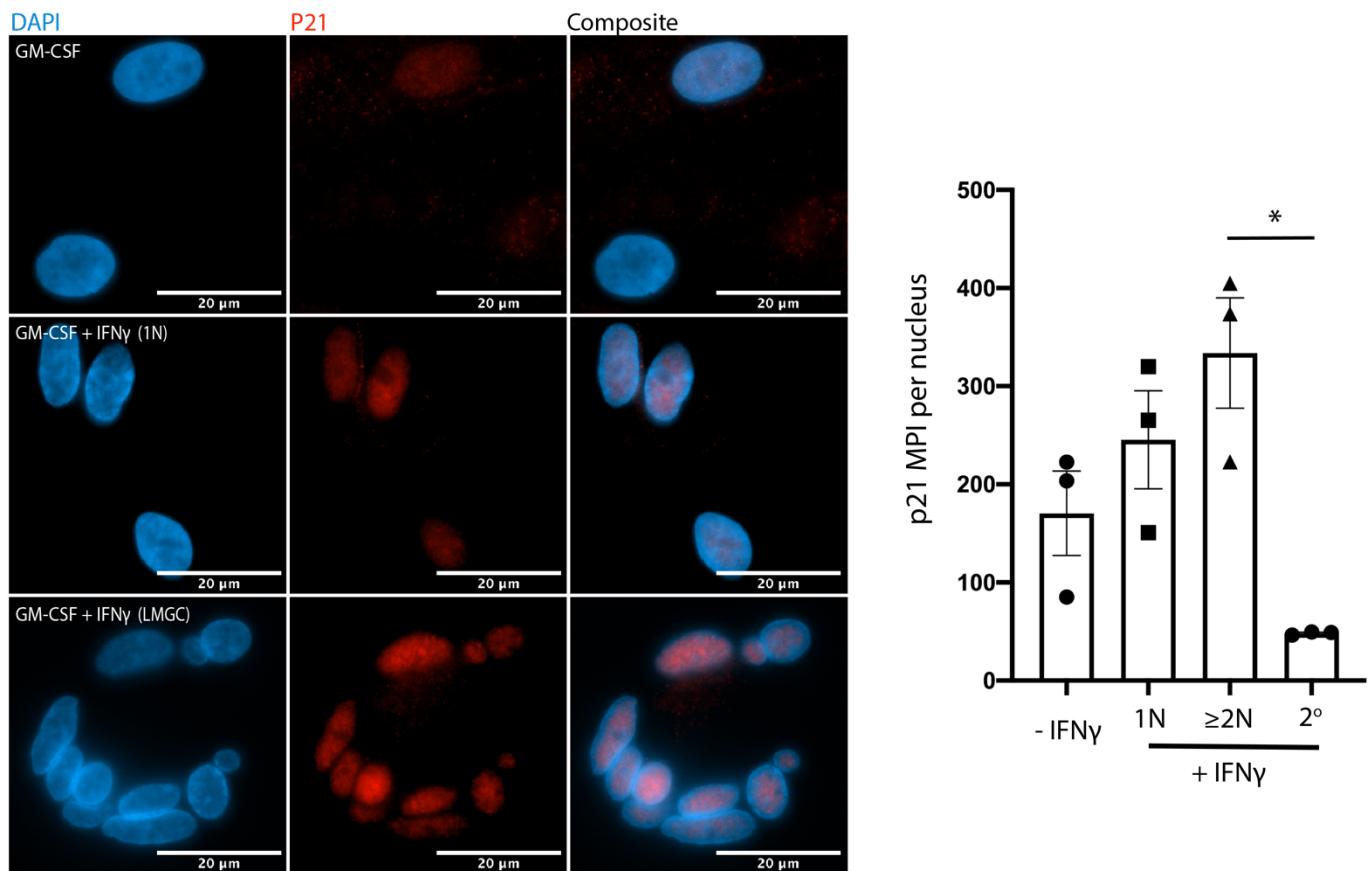


Figure 28. P21 immunofluorescence.

Immunofluorescence showing the expression of protein P21 in response to IFN γ treatment and multinucleation. Cells were cultured as previously described on glass coverslips for immunofluorescence. Cells were fixed and stained with DAPI to visualise nuclei (blue) and with a primary antibody against the protein P21 with an AF568 conjugated secondary antibody (red). Mean pixel intensity (MPI) measured for individual nuclei of a minimum of 15 cells per condition using ImageJ software, and the mean values for three separate donors calculated. Error bars = SEM. • = $p < 0.05$ determined by Mann-Whitney U test). No statistical significance between any other groups.

Of the conditions measured only multinucleated cells cultured in the presence of IFN γ ($\geq 2N$) showed significantly increased p21 expression compared with the negative control (2 $^{\circ}$). There was a non-significant increase in cells cultured with IFN γ compared with those cultured in the absence of IFN γ . Of the cells cultured with IFN γ there was non-significant increased expression in multinucleated cells compared with mononucleated cells. Although lacking statistical power, this data suggests that LMGCs have increased p21 signalling and therefore greater inhibition of the cell cycle. Next, I aimed to determine whether this heightened state of cell cycle arrest is associated with SASP in LMGCs.

5.3. Investigating the exhibition of senescence associated secretory phenotype by LMGCs

5.3.1. Secretion gene module upregulation by LMGCs

The single cell RNA sequencing dataset of *in vitro* LMGCs generated in 3.2 was studied to investigate any transcriptional evidence for SASP. Several genes relating to the process of cell secretion were upregulated amongst the differentially expressed genes of the LMGC cluster. These are displayed in figure 29, with the clusters of osteoclasts, control macrophages (GM-CSF only), and mononucleated cells from LMGC cultures for comparison.

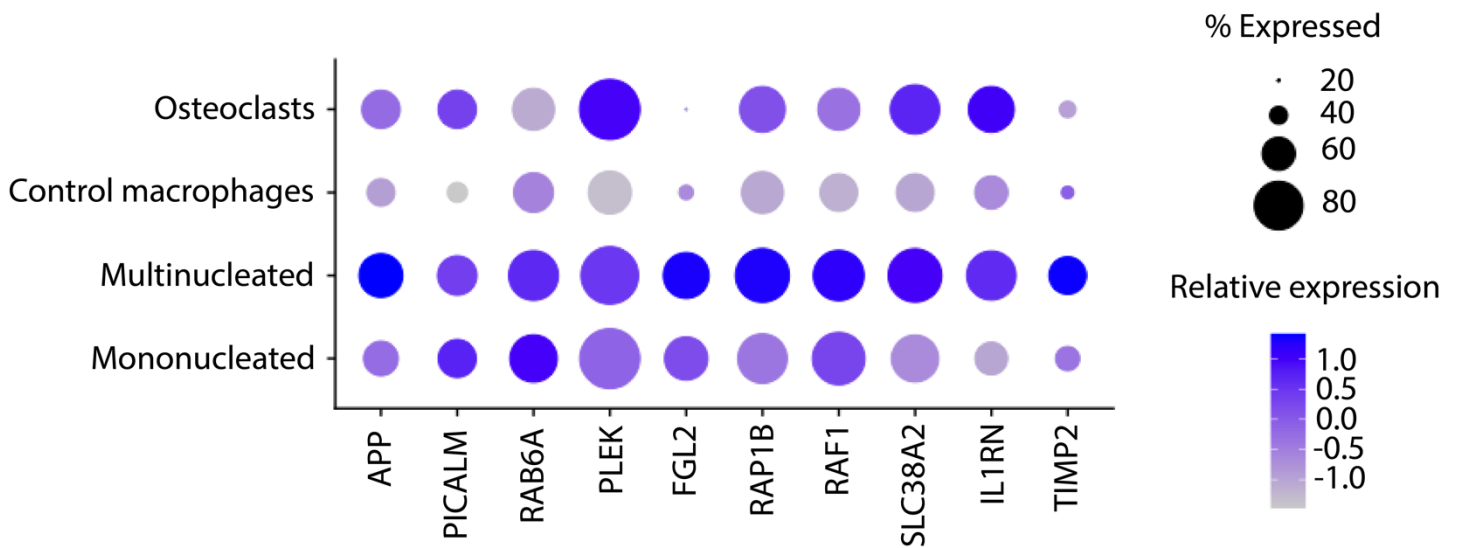


Figure 29. Secretory gene module upregulation by *in vitro* LMGCs.

Dotplot displaying genes relating to the process of secretion, upregulated in the LMGC cluster (multinucleated). All genes were amongst the significantly differentially expressed genes of the LMGC cluster. Circle size = percentage of the cells expressing the gene. Colour = relative gene expression of that gene, blue = high expression, grey = low expression. Genes are differentially expressed (adjusted p value <0.05) between multinucleated cells and other cell types using the FindAllMarkers with Wilcoxon Rank Sum test in Seurat.

The genes identified in figure 29 were identified as part of the ‘secretion’ pathway in the gene ontology pathway database, and are known to have roles in cytoplasmic vesicle formation, trafficking and membrane fusion. This transcriptional evidence supports the hypothesis that LMGCs may exhibit SASP. Whilst this suggests *in vitro* LMGCs have increased secretion, the constituents of the secretome were still unclear, so we next aimed to measure the production of specific factors by *in vitro* LMGCs.

5.3.2. Measuring cytokine production by LMGCs

The increased production of cytokines is a characteristic of cells exhibiting SASP, and in the tissue microenvironment of GCA affected temporal arteries a number of cytokines are enriched. This includes key drivers of inflammation TNF α , IL-6 and IL-1 β ^{34, 278}. The capacity for production of these three cytokines by *in vitro* LMGCs was investigated using flow cytometry.

LMGCs were cultured as described in chapter 2, including control wells of monocytes cultured in the absence of IFN γ . Once LMGCs had formed the media was aspirated and replaced with fresh media containing 20ng/mL GM-CSF only to maintain the cultures in the absence of inflammatory stimulation for 48 hours. The purpose of this was to allow the cells a recovery period before the next step, which was to stimulate the cells with 1 μ g/mL LPS for 6 hours at 37°C. Brefeldin A (BFA) was also added at a concentration of 10 μ g/mL for the duration of this incubation. LPS was added to induce cytokine production, and BFA to block secretion via inhibition of vesicle assembly and protein transport from the endoplasmic reticulum, ensuring any cytokines produced remained intracellular to be measured. Control wells were included, incubated in the absence of LPS and in the presence of BFA. Following this incubation, cells were removed from wells using Accutase incubation, fixed and permeabilised using a formaldehyde-based fixative (BD), and stained with antibodies raised against TNF α , IL-6 and IL-1 β conjugated to AF647, PE, and FITC fluorophores respectively (all Biolegend) at 1:100 dilutions in permeabilization buffer (BD). After 1 hour at room temperature, cells were washed with permeabilization buffer and DAPI was then added at a concentration of 1 μ g/mL. Samples were analysed using the BD symphony flow cytometer.

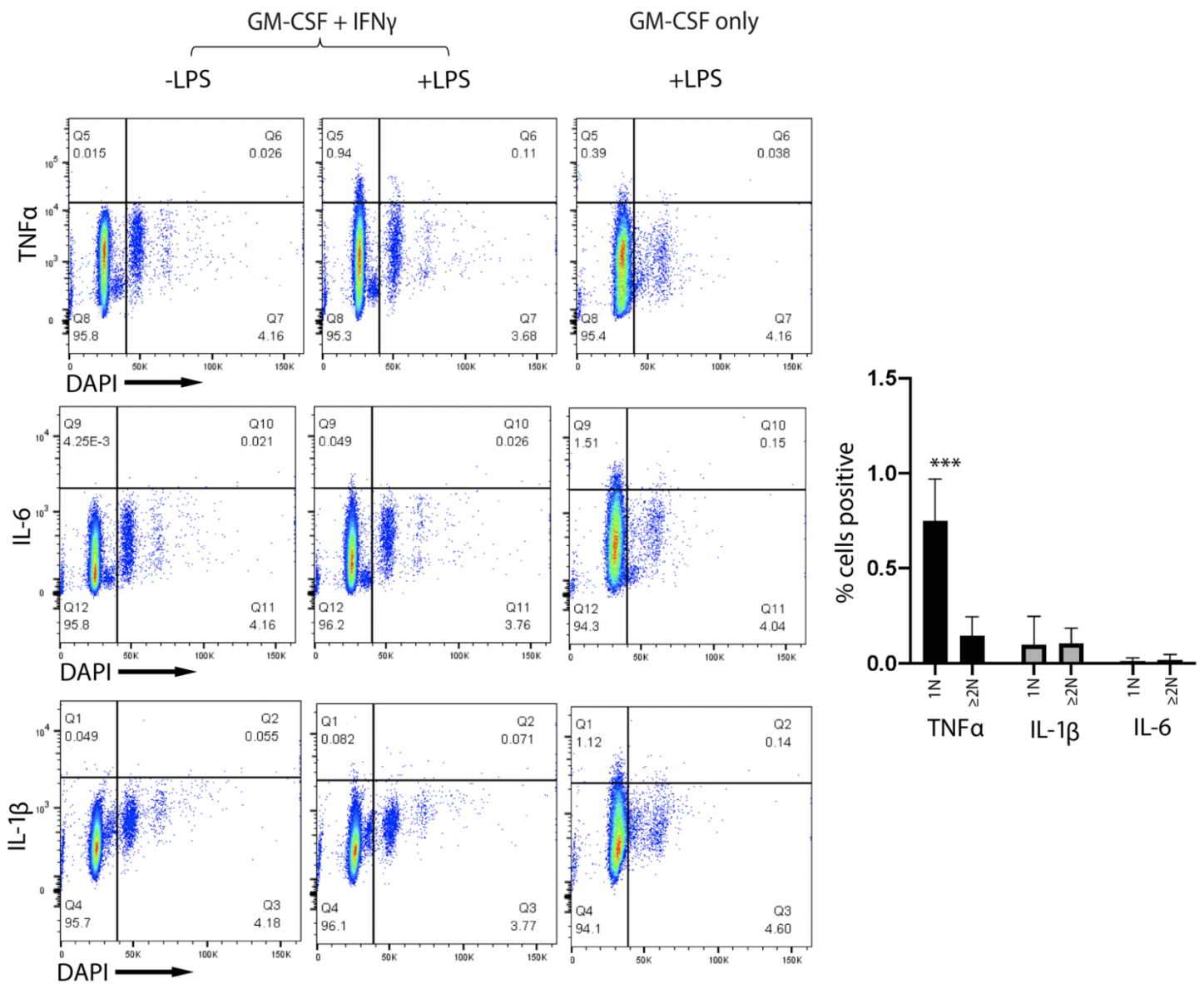


Figure 30. Measuring the production capacity of TNF α , IL-6 and IL-1 β by *in vitro* LMGCs.

GM-CSF only well was used to set gate in the DAPI channel to separate 1N from $\geq 2N$, unstimulated control (-LPS) was used to set cytokine gates. The percentages of cytokine positive cells in 1N and $\geq 2N$ quadrants were measured and the mean values of three experiments with different donors were calculated (n=3). There was significantly reduced expression of TNF α by multinucleated cells ($\geq 2N$) compared with mononucleated (1N). •••p < 0.05 determined Mann-Whitney U test.

The data shown in figure 30 demonstrates that despite increased expression of a secretory gene module, *in vitro* LMGCs do not have increased capacity for the production of the GCA associated pro-inflammatory cytokines measured, and in the case of TNF α their capacity was reduced. This would suggest that LMGCs are not the source of these mediators of inflammation in GCA, though further studies in tissue are required to substantiate this. It also opposes the hypothesis that LMGCs exhibit SASP, though they still may secrete alternative pathology driving factors. We next investigated their capacity for the production of ROS.

5.3.3. LMGCs exhibit high capacity for ROS production

To measure the capacity for ROS production by LMGCs, the fluorogenic dye MitoSOX Red (Biolegend) was used. This dye emits red fluorescence upon oxidation, therefore, when taken up by cells it can be used as an indicator of intracellular superoxide. LMGCs were cultured as before, and once grown were incubated with 5 μ M MitoSOX red reagent for 30 minutes at 37 $^{\circ}$ C to allow dye uptake. Cells were then gently washed and trypsinised, before being pipetted into FACS tubes containing FACS buffer and 5 μ M DRAQ5. In order to induce maximal ROS production cells were then incubated with antimycin A at a range of concentrations (0, 1 μ M, 5 μ M, 10 μ M and 20 μ M). Antimycin A inhibits complex III of the electron transport chain, leading to high rates of superoxide production²⁷⁹. DRAQ5 intensity was used to determine ploidy, and compare the MitoSOX fluorescence of mononucleated and multinucleated cells.

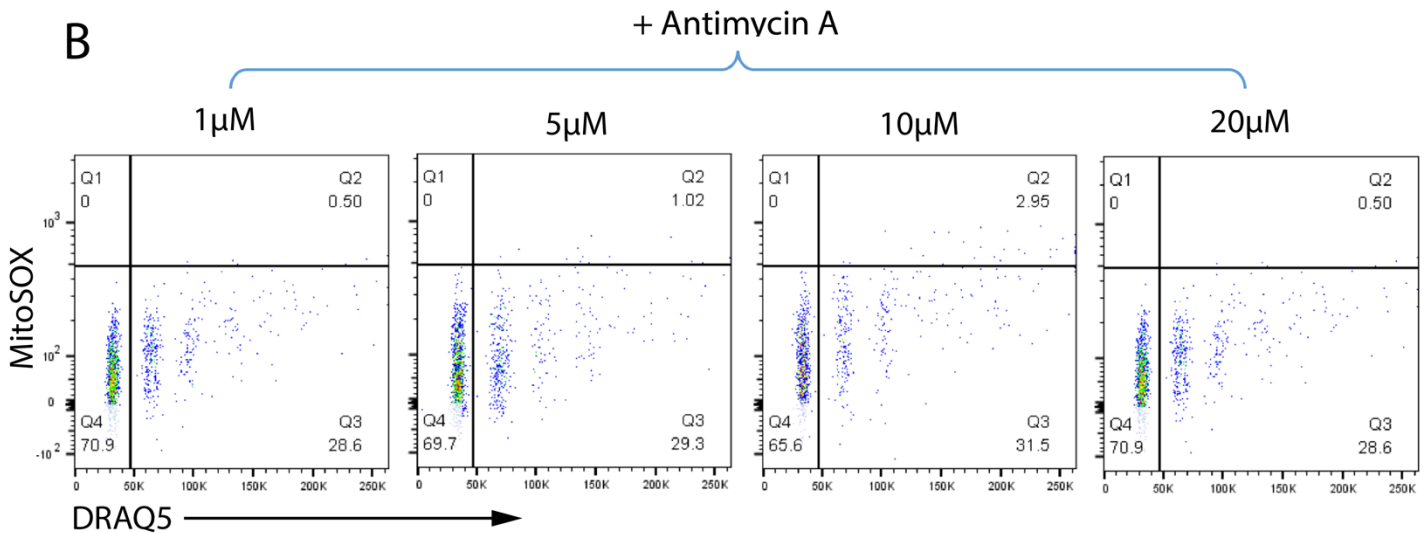
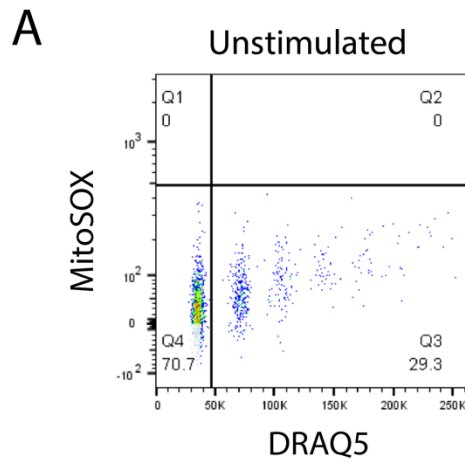


Figure 31. Measuring capacity for ROS production by LMGs using MitoSOX.

low cytometry plots showing MitoSOX intensity of cells treated with or without antimycin A at a range of concentrations. A) Cells without antimycin A treatment, used as unstimulated control to determine gating strategy. B) Cells with antimycin A treatment at 1 μ M, 5 μ M, 10 μ M and 20 μ M concentrations. There was no change in mononuclear cell mitoSOX intensity with increasing Antimycin A concentration, whereas multinucleated cells showed an increase in intensity, maximal at 10 μ M (2.95% of events). N=1.

This data suggests that LMGCs may have increased capacity for ROS production compared with mononucleated cells of the same culture, supporting the evidence in the literature for ROS production by LMGCs in lesions of GCA^{228, 252, 253}. Attempts to repeat this experiment were unsuccessful, due to both poor culture viability or hypertoxicity following Antimycin A administration. These may have been the result of donor variability, as all other variables were consistent. We were therefore unable to use statistical testing to reinforce this finding, and sought an alternative methodology for the measurement of ROS producing capacity in support.

CellROX Green, like MitoSOX, is a fluorescent probe used to measure intracellular superoxide. It emits green fluorescence upon oxidation and binds DNA, and because it is fixable it can be detected by fluorescence microscopy which was chosen due to its strengths over flow cytometry for the morphological confirmation of LMGCs. Primary monocytes were cultured as before to generate LMGCs on glass coverslips. Once grown, wells were incubated with 400 μ M tert-butyl hydroperoxide (TBHP) (Thermofisher) for 30 minutes at 37°C, to stimulate ROS production. Like Antimycin A, TBHP induces superoxide production, but through the alternative mechanism of inducing oxidative stress²⁸⁰. Following this, CellROX green reagent was added at a final concentration of 1 μ M, and cells were incubated for a further 30 minutes at 37°C. TBHP and CellROX concentrations used were as suggested in the supplier's guidelines. After this, cells were gently washed with PBS, fixed and permeabilised with a formaldehyde-based fixative (BD), washed again, and incubated with PBS containing 1 μ g/mL DAPI for 10 minutes at room temperature to stain nuclei. Coverslips were then removed from wells and mounted onto microscopy slides with VECTASHIELD, before being imaged with the Leica SP8 confocal microscope with 40x objective magnification and oil immersion.

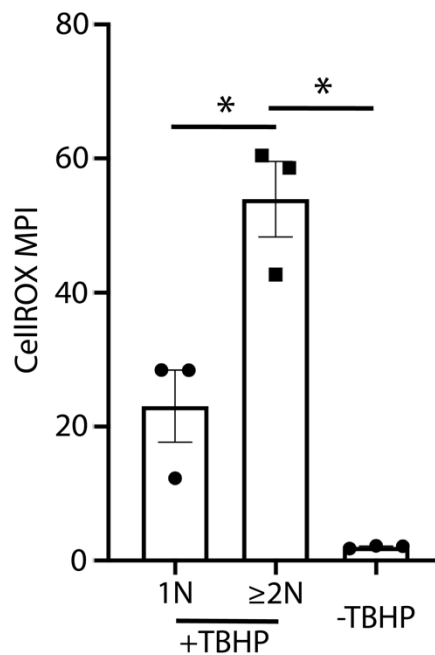
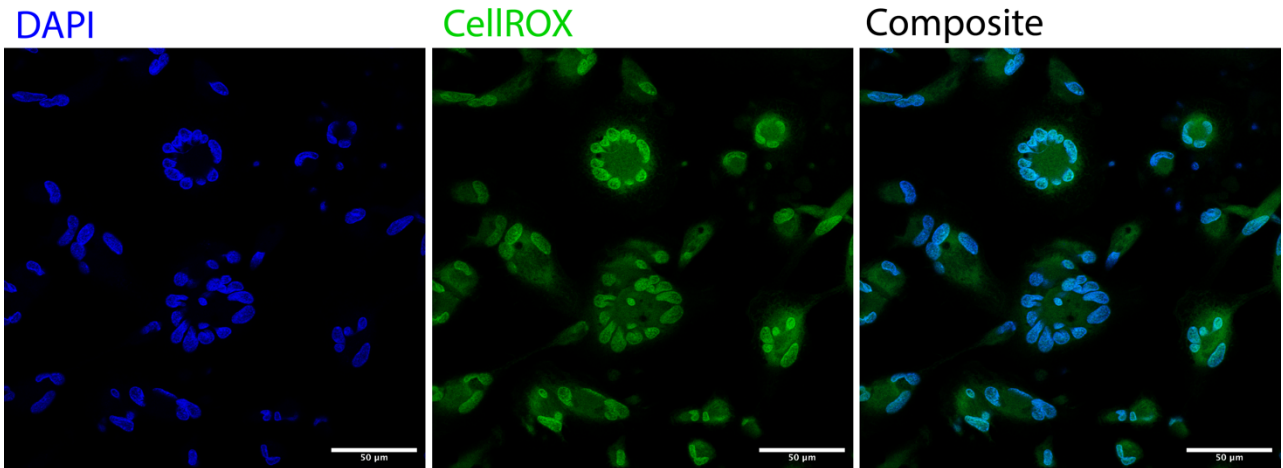


Figure 32. Measuring the capacity for ROS production by LMGCs using CellROX.

CellROX staining of LMGC cultures and measurement by confocal microscopy. Above: Representative image of LMGC culture stained with DAPI and CellROX GREEN reagent, stimulated with TBHP, blue = DAPI, green = CellROX. Scale bars = 50 μ M. Shown are both mononucleated (1N) and multinucleated (\geq 2N) cells. Below: Mean pixel intensity (MPI) for cellROX GREEN channel. Means of the mean values for three donors shown. Comparison between cells treated with TBHP, both mononucleated (1N), and multinucleated (\geq 2N) and cells not treated with TBHP as an unstimulated control. Multinucleated cells exhibited greater CellROX intensity than both mononucleated cells from the same fields of view and unstimulated controls ($p < 0.05$). P values determined by Mann-Whitney U tests. N=3.

This data supports the hypothesis that LMGCs have higher capacity for the production of superoxide than mononuclear cells from the same cultures. The MPI was calculated for a minimum of ten whole cells of each group taken from a range of areas on the coverslip, and this was repeated for cells from three separate donors to calculate the values shown in figure 32. CellROX staining was also performed on LMGC cultures to be analysed by imaging flow cytometry (ImageStream X Mark II), by the same staining protocol. We found further supporting evidence of the increased capacity for ROS production by LMGCs, which has significantly increased CellROX intensity than mononucleated cells from the same cultures.

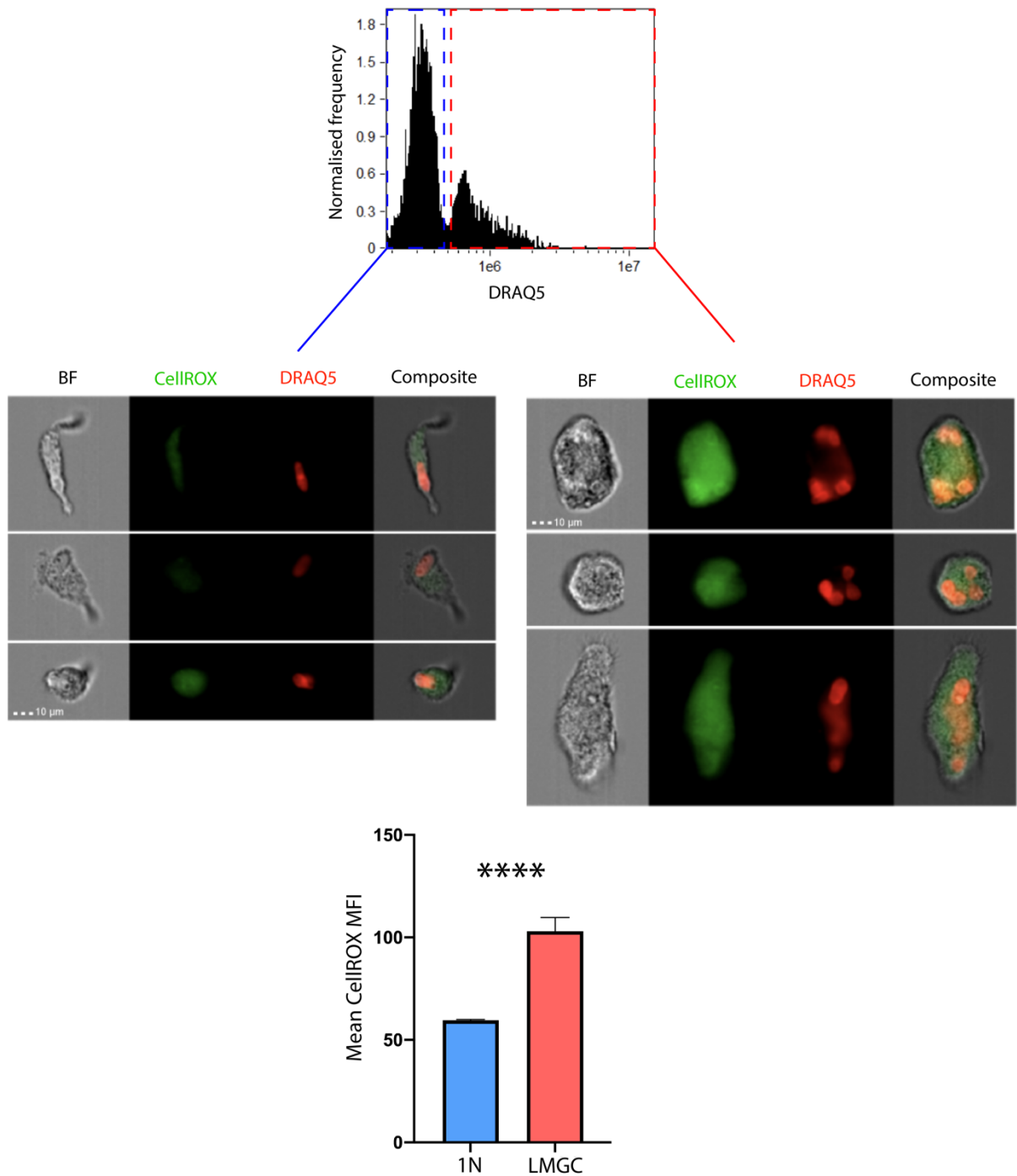


Figure 33. Analysing CellIROX-stained LMGCs by ImageStream.

LMGC cultures stained with CellIROX GREEN following TBHP stimulation and analysed by imaging flow cytometry. Top: cytometry plot and gating strategy to separate mononucleated and multinucleated cell populations using DRAQ5 intensity. Middle: Representative images taken of events from the resultant gates, showing brightfield (BF), CellIROX (Green) and DRAQ5 (Red), and a composite of all three. Below: Mean fluorescence intensity (MFI) of the CellIROX channel for all mononucleated cells, and all LMGCs confirmed by their morphology. 4446 mononucleated cells and 23 LMGCs were measured. There was a significant difference, ●●●● $p < 0.0001$, determined by Welch's T test. N=1.

These data together demonstrate that LMGCs have a higher capacity for the production of ROS than mononucleated cells of the same cultures, and supports evidence in the literature which suggests that they may be the source of ROS mediated damage in GCA affected temporal arteries. It also supports the hypothesis that LMGCs enter premature senescence and exhibit SASP, as ROS are known to be secreted by cells with this phenotype, though further studies are required to identify their full secretome. With more time, it would have been of particular interest to measure other factors associated with LMGCs in GCA including MMP9, various chemokines, PDGF and VEGF, as well as other common SASP factors mentioned in 5.1.2.

5.4. Investigating the phagocytic properties of *in vitro* LMGCs

In addition to SASP, we aimed to investigate the phagocytic properties of *in vitro* LMGCs. Phagocytosis is a form of endocytosis, and is a key effector function of tissue macrophages whereby they remove damaged, apoptotic cells or foreign particles from areas of infection or damage. This function is enhanced by the multinucleation of macrophages into foreign body type multinucleated giant cells, which are specialised for enhanced complement uptake²⁰¹. However, this may not be true of LMGCs which are unable to perform mycobacterial uptake in granulomas of tuberculosis, suggesting divergent specialisation of these multinucleated cell types²²⁸. We used SEM images taken of LMGCs, generated in 4.3.2, to observe any intracellular morphology which could indicate a phagocytic phenotype.

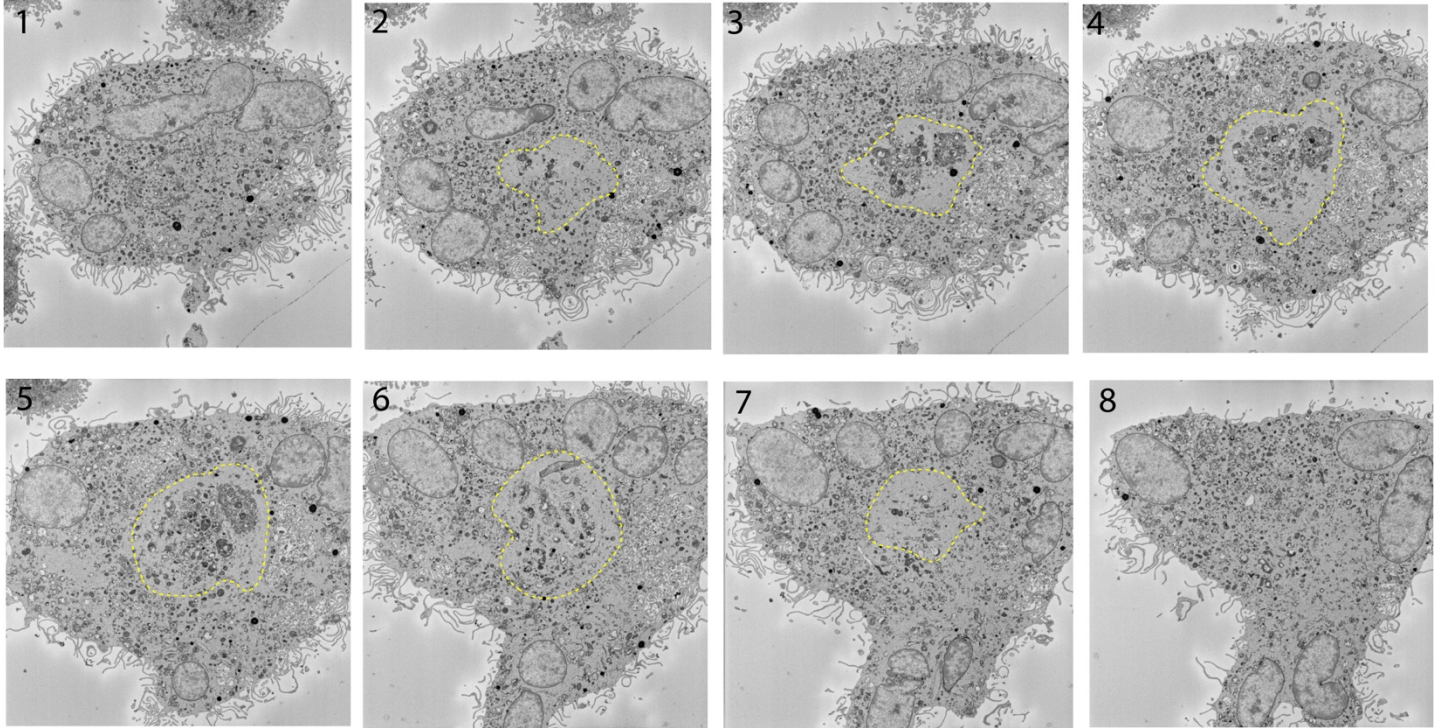


Figure 34. Scanning electron microscopy sections of a single LMGC at a range of heights.

Unusual central area identified containing mixed organelles with damaged morphology and cellular debris (Yellow dashed line). Images taken with Zeiss Sigma Scanning Electron Microscope, performed by Dr K. White of the Electron Microscopy Service at Newcastle University.

Cross sectional SEM imaging revealed a previously unidentified, unusual intracellular structure in the centre of LMGCs. This roughly spherical area was 'walled off' from the rest of the cell by a boundary of cytoplasm which was absent of organelles. Within this area was a darker, denser region containing morphologically irregular organelles, and debris. It is difficult to discern the specific contents of this structure, though it is a possibility that it may be specialised for the degradation of intracellular debris and phagocytosed material, proposing a novel LMGC functional adaptation. To test the phagocytic phenotype of *in vitro* LMGCs a FITC dextran endocytosis assay was performed.

Primary monocytes were cultured as described in chapter 2 to generate LMGCs, in addition to a control well cultured in the absence of IFN γ . Once grown, 2mg/mL FITC dextran (Sigma) with an average molecular weight of 10kDa, was added to the culture medium. Cells were then incubated for 30 minutes at 37°C, or on ice as a negative uptake control. The ice reduces the temperature of the cells in order to inhibit cellular processes including endocytosis, so cells positive for FITC dextran under this condition are not considered true measures of endocytic activity. Following this incubation, cells were trypsinised to lift them from the wells, washed with PBS and resuspended in flow buffer containing 5 μ M DRAQ5. Samples were then analysed using the BD Symphony flow cytometer using DRAQ5 intensity to determine ploidy.

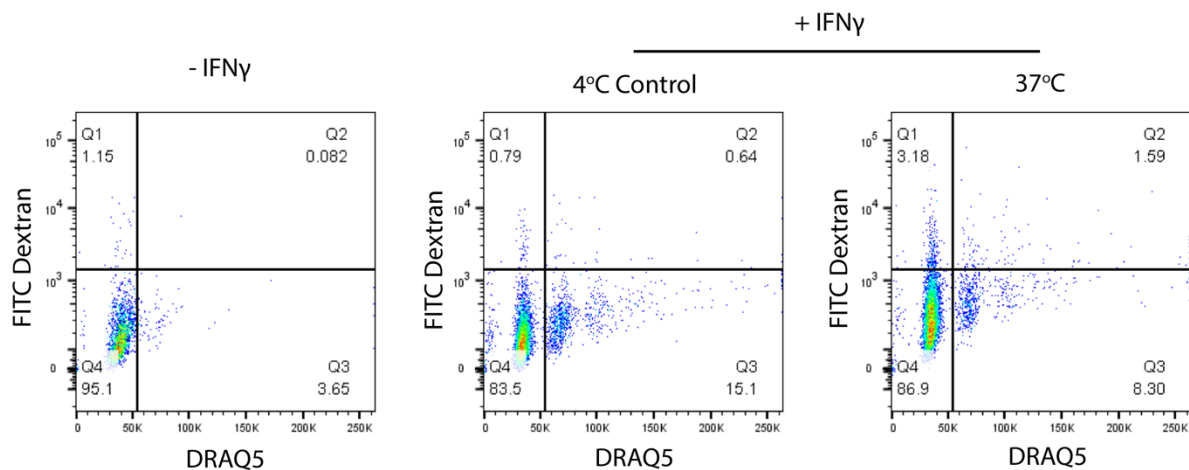


Figure 35. FITC dextran uptake assay of *in vitro* LMG cultures.

Flow cytometry plots for primary monocyte cultures grown with or without IFN γ and incubated with FITC dextran to measure endocytosis. FITC Dextran incubation was performed on ice (4°C Control) as a negative control. DRAQ5 was used to determine ploidy. In the 4°C control, 0.946% of mononucleated cells were FITC dextran positive, compared with 4.24% of multinucleated cells. In 37°C samples 3.66% of mononucleated cells were FITC dextran positive, compared with 19.16% of multinucleated cells. n=1.

Although cells incubated at 4°C were not completely negative for FITC dextran uptake (later confirmed by fluorescence microscopy), there was an increase when incubated at 37°C. The ratio of positive events between mononucleated and multinucleated cells in the negative control was 1 : 4.48. Applying this ratio to adjust the 37°C sample in order to account for false positives results in 3.66% positive mononucleated cells to 4.28% positive multinucleated cells. This marginal increase in endocytosis by LMGCs is not significant, however, I next aimed to observe the intracellular localisation of endocytosed FITC dextran using fluorescence microscopy. SiR DNA was used to stain nuclei, added at a concentration of 250 μ M to culture medium simultaneously with FITC dextran, and incubating together for 30 minutes.

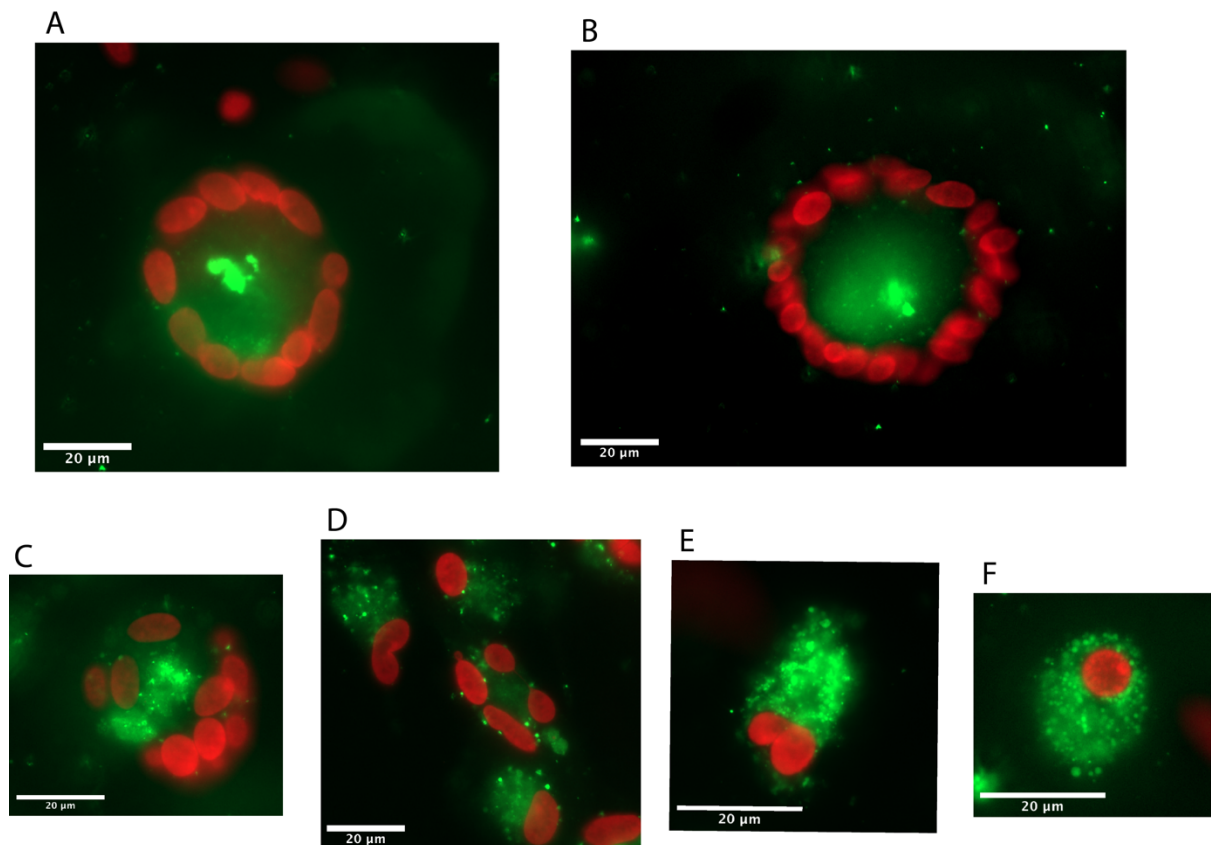


Figure 36. Representative fluorescence microscopy images taken of FITC dextran incubated LMGC cultures.

Red: Nuclei (SiR DNA), Green = FITC dextran. A, B, C) Large LMGCs exhibit central localisation of FITC dextran at distinct locations within nuclei ring. D, E, F) Smaller multinucleated cells, binucleated cells and mononucleated cells exhibit FITC dextran dispersed throughout the cytoplasm. Images taken using Zeiss Axioimager fluorescence microscope with 63x objective magnification and oil immersion. Scale bars = 20μm.

Although repeated experiments are required to draw meaningful conclusions, this data suggests that *in vitro* LMGCs do not exhibit a significant change in endocytic activity compared with mononucleated macrophages from the same cultures, though they may be specialised to contain a central intracellular region to which endocytosed material is trafficked. The purpose of this is unclear, and further experimentation is required to determine whether material in this area is degraded, and whether this is more or less efficient than the phagocytosis process of diploid tissue macrophages. While present in all four *in vitro* LMGCs, this central area was not observed in the single tissue LMGC imaged by SEM in 4.3.2, so this phenomenon may not be aligned to disease. Again, further experiments are necessary to explore this, particularly as imaging began halfway through this cell and it may have been missed.

5.5. Discussion

In this chapter we have explored the functional phenotype of *in vitro* LMGCs. First, in keeping with the findings of chapter 4, we have found evidence that they enter a state of premature senescence upon polyploidy, likely relating to the DNA damage and chromatin bridge formation which we previously observed. Further experiments are required to identify the specific mechanism by which this occurs, in particular whether the cytosolic-DNA-sensing cGAS pathway plays a role following the physical rupture of chromatin bridges. With more time, p21 upregulation would have been validated at protein level by proteomic techniques such as western blot, and further senescence assays performed such as β -galactosidase staining.

We have investigated the exhibition of SASP by *in vitro* LMGCs. Single cell RNA sequencing data indicates increased expression of genes relating to the machinery responsible for the formation, trafficking and membrane fusion of intracellular vesicles, suggesting an increase in secretion. However, the contents of the secretome are unclear. Investigating some of the key cytokines involved in the tissue microenvironment of GCA-affected temporal artery, we have found that the secretion of both IL-6 and IL-1 β is unchanged in LMGCs compared with mononucleated cells from the same cultures, and secretion of TNF α was reduced. While the upregulated secretory gene module cannot be attributed to increased secretion of these cytokines, it may be associated with increased ROS production. With a combination of flow

cytometry, ImageStream, and fluorescence microscopy we have found evidence that *in vitro* LMGCs possess an increased capacity for the production of superoxide.

Finally, we have made preliminary investigation into the phagocytotic properties of *in vitro* LMGCs, a primary function of mononucleated tissue macrophages and a process shown to be enhanced by polyploidy in the case of FBGCs²⁰¹. Our findings suggest that *in vitro* LMGCs do not possess increased phagocytic activity, though may traffic endocytosed material to a specific intracellular structure found in the centre of each cell. This may also provide some insight into the reason behind the distinctive nuclear arrangement of LMGCs, in a ring around the periphery of the cell. It is not possible to draw significant conclusions from this data, however, until performed with sufficient repeated measures.

Chapter 6. General discussion and future work

6.1. General discussion

LMGCs are a poorly characterised polyploid cell type arising from monocyte/macrophage precursors through an unclear mechanism. They appear in a number of idiopathic diseases including GCA. Investigations into their characteristics are challenging due to the scarcity of disease tissue available for research, although these efforts have been facilitated by a number of *in vitro* culture systems. In this thesis, a number of *in vitro* culture systems which have been previously used for LMGC generation were tested and optimised, and facilitated by the use of an optimised model, the mechanism of formation and functional adaptations of LMGCs were investigated. The initial aim of this research was to develop an optimised *in vitro* culture system for the generation of LMGCs, and to validate this against disease LMGCs across multiple levels, including morphologically and transcriptionally. A secondary aim was to explore function of LMGCs by investigating common gene modules active in *in vitro* LMGCs and temporal artery tissue LMGCs compared with control populations. The third aim of the project was to study the formation mechanism of *in vitro* LMGCs with imaging techniques, with reference to the transcriptional data derived in earlier sections. The final aim was to perform functional assays in order to investigate their functional adaptations and potential roles in disease.

An optimal method of *in vitro* LMGC generation from primary monocytes, using GM-CSF and IFN γ was found and then adopted for subsequent experimentation. The mechanism of LMGC was identified as a combination of cell-to-cell fusion and incomplete cell division, with evidence for DNA-damage induced chromatin bridge formation contributing to the latter. A transcriptional programme of DNA damage response activation was identified in these cells, in keeping with recent findings in the literature linking activation of the DDR to LMGC formation by modified mitoses⁹⁹. The upregulation of proteins 53BP1 and p21, indicating DNA double strand breaks and premature senescence respectively, was also found in these cells. Additionally, upregulation of genes relating to vesicular transport and secretion was identified, as well as an increased capacity for the production of ROS, though other constituents of the secretome were not found. Overall, these data further our understanding of the transcriptional control of, and the role that DNA damage signalling plays in LMGC formation, and provide supporting evidence for a tissue-destructive role in GCA and other

pathologies in which they're found by enhanced ROS production. LMGCs appear to form by a combination of binucleation by incomplete cell division, and cell fusion events. Incomplete cell division may be the result of DNA-damage induced chromatin bridge formation, preventing cytokinesis due to the presence of chromatin at the midbody. LMGCs undergo transcriptional changes supporting the involvement of DNA damage response signalling in their formation, and hinting at functional adaptations including a heightened secretory phenotype. Both senescence associated genes and anti-apoptotic genes were shown to be upregulated suggesting that LMGCs may escape the programmed cell death that DNA damage would typically induce and persist in a prematurely senescent state, producing factors which mediate inflammation and drive tissue damage.

6.1.1. *In vitro* model generation and validation

The relative rarity of LMGC-related pathologies and the invasive nature of tissue acquisition are significant barriers to investigations into the characteristics of LMGCs, highlighting the need for an effective, reliable *in vitro* culture system. There have been a multitude of culture systems used to induce LMGC differentiation from primary monocytes, resulting in difficulties in selecting the most effective or suitable for new investigations, and with standardisation across studies. Many studies have used isolated PBMCs to develop LMGC cultures, growing them in the presence of conA, which stimulates T cells to produce the factors which drive LMGC differentiation. A number of studies differentiated LMGCs from purified populations of monocytes, with T cells depleted, by adding specific factors such as IFN γ , GM-CSF, M-CSF, IL-3 and TLR2 agonists to drive LMGC differentiation. The measures of output introduce an additional hurdle to the standardisation of LMGC cultures across studies, with investigations using either flow cytometry or microscopy, and measure LMGC yield by either fusion rate (the total number of nuclei as a function of the number of cells), or by counting the sheer numbers of multinucleated cells.

The data presented in this thesis demonstrate that, of cytokine combinations used previously in the literature for the generation of *in vitro* LMGCs from primary monocytes, GM-CSF and IFN γ was most effective, and this culture system was subsequently optimised for maximal LMGC yield. Optimisation of culture conditions led to the use of DMEM as culture medium, a monocyte seeding density of 100,000 cells per well of a 96 well plate, and increased concentrations of both IFN γ and GM-CSF to those used in the literature, up to 200ng/mL and

50ng/mL respectively. As concentrations increased the LMGC yield also increased, at the cost of culture viability. These concentrations were chosen as a reasonable middle ground between high yield and preserved culture viability. Flow cytometry was used to assess polyploidy, which was first used for this purpose in a recent study on murine LMGC formation⁹⁹. It was therefore necessary to assess the suitability of flow cytometry for this purpose, which was achieved using ImageStream and FACS. Of the conditions tested, the combination of M-CSF and Pam3CSK4 was found to be least effective for the generation of LMGCs. As murine macrophages were used in the study from which this protocol was adopted, this disparity could be the result of interspecies variation. There was also high donor variability throughout the study; cultures grown from the primary monocytes of different donors in identical conditions exhibited a wide range of LMGC yields. Furthermore, a significant proportion of cultures lost viability before sufficient time had passed for LMGC differentiation. It is unclear whether this high donor variability is any indication of an individual's susceptibility to the pathologies in which LMGCs form, and the demographic information for the donors used in this study was not available as donations were often made anonymously. It would perhaps be of interest to assess the rate of LMGC differentiation of primary monocytes taken from groups with higher predisposition to GCA, and even from patients with confirmed GCA. It may also provide valuable insight to conduct a study in which the predisposition to form LMGCs of peripheral monocytes from patients with GCA, and those from patients with alternative inflammatory pathologies is compared. This may reveal whether propensity to form LMGCs is innate to individuals with GCA or whether the environment the cells are in is what drives LMGC formation. Various clinical metrics could also be measured to assess whether LMGCs form more readily in individuals who are, for example, older or a particular sex. I would hypothesise that, with GCA being an age-associated pathology and now we've demonstrated that DNA damage plays a role in LMGC formation, the monocytes of older individuals would return greater LMGC yields. ConA is a factor commonly used in the literature for the generation of *in vitro* LMGCs, but was excluded here due to consistent loss of culture viability. Neither conA conditioned media or conA alone was sufficient to maintain the health of primary monocyte cultures for more than 48 hours, falling short of the time period required for LMGC differentiation.

The alignment of the now optimised *in vitro* culture system to tissue LMGCs was two-fold. Morphological assessment by confocal microscopy revealed consistent, distinctive horseshoe-like nuclear arrangement within LMGCs in keeping with previous analysis of disease tissue LMGCs²⁸¹, and this was absent in cultured osteoclasts. The distinctive nuclear morphology was consistent throughout this study, with examples displayed in chapters 4 and 5. In chapter 3, the gene signature of cultured LMGCs was identified and sought within tissue macrophage population of dissociated GCA-affected temporal artery tissue. This included a number of gene modules relating to inflammatory processes such as leukocyte activation and chemokine activity, as well as cell-ECM interactions and smooth muscle cell proliferation which are both of biological significance, implicating LMGCs in the propagation of intimal hyperplasia in GCA. This gene signature was partially identified within a population of macrophages from GCA-affected temporal artery tissue, providing further support that the chosen *in vitro* culture system recapitulates the disease process. The sequencing data generated from temporal artery biopsies could be further interrogated to gain insight into the pathogenesis of GCA. Firstly, additional biopsies, if available, could be sequenced to improve the power of the study. Then, the transcriptional differences between biopsies from patients whose diagnosis was ultimately either positive or negative for GCA could be observed. This could offer insight into the cellular mechanisms underpinning aspects of GCA pathogenesis, such as the cellular composition and phenotypic switching contributing to intimal hyperplasia. Transitional changes in cellular phenotype could be interrogated using the 'scVelo' toolkit for RNA velocity analysis, which could also enable the identification of putative genes driving any changes.

6.1.2. The mechanism of LMGC formation

Different studies have identified disparate mechanisms of LMGC formation, providing evidence for either cell to cell fusion or modified cell division with incomplete cytokinesis. The early consensus that LMGCs form exclusively by the fusion of myeloid precursors was largely a result of investigations into the involvement of cell fusion mediating factors. The protein DC-STAMP was shown to be necessary for the process, and other factors including CD40, ADAM9, ICAM1 and β 1-integrin were thought to be involved^{159, 168, 215, 234, 282}. A later study using more advanced imaging techniques such as live confocal unveiled unanticipated intricacy by demonstrating LMGC formation by incomplete cell division⁹⁹, a mechanism which

had previously been identified in a number of more well characterised multinucleated cell types but never LMGCs^{91, 100, 218}.

DNA damage signalling is implicated in LMGC formation by modified cell division. Cultured LMGCs differentiated from murine macrophage precursors using BLP as inflammatory stimulated have increased γ H2AX, an indication of DDR activation⁹⁹. Similarly, human M.tuberculosis infected tissue LMGCs expressed γ H2AX⁹⁹. DNA-damage induced polyploidy may occur through different pathways involving either the suppression of the Cdk1/CycB protein complex²⁴¹, or by the formation of chromatin bridges following chromosome fusion events²⁴⁶. The mechanism by which chronic inflammation leads to DNA damage is unclear. In the literature, inflammation has been shown to induce DNA damage by the increased production of reactive oxygen and nitrogen species (RONS)²⁸³.

Here, live cell confocal imaging showed clear cell fusion events between mononucleated, binucleated and multinucleated cells leading to the development of large LMGCs, as well as numerous abnormal cytokinesis events resulting in binucleation, suggesting that the process may be a combination of both mechanisms. In support of the hypothesis that DNA-damage induced cytokinesis failure plays a role in LMGC formation, large chromatin bridges connecting pairs of nuclei were observed in both cultured and tissue LMGCs, and IFN γ was shown to induce DNA double strand breaks in these cells. Increased transcriptional expression of genes relating to the DDR were found in cultured LMGCs, and increased levels of the DNA double strand break marker 53BP1 were shown in primary monocyte cultures grown in the presence of IFN γ . Chromatin bridges were observed between pairs of nuclei within both *in vitro* and tissue LMGCs, suggesting DNA damage may promote polyploidy by causing chromosome fusion events. Telomeric DNA damage typically lead to chromosome fusion events severe enough to result in chromatin bridge formation, but the localisation of 53BP1 expression within cultured monocytes was not found in this study. To clarify this, further experimentation could be performed to investigate whether DNA double strand breaks are localised to telomeres by co-staining LMGC cultures with a telomere marker, such as fluorescent polyamides, and a DNA damage marker, such as 53BP1.

Further experimentation is required to clarify the mechanism by which persistent inflammatory stimulation leads to DNA damage, though the data shown in figure 27 suggests

a ROS-independent mechanism. This could be further explored with the use of alternative ROS-scavenging agents, and a measurement of ROS levels in culture in order to confirm the scavenging actions of mitoTEMPO would help to draw more meaningful conclusions. It is unclear whether LMGCs are an inadvertent product of the inflammatory environments in which they are found, or whether their formation is a more aimed process to elicit enhanced functionality in the immune response. Given that DNA damage induced by inflammation is an aberrant cell programme contributing to pathologies including carcinogenesis, it is surprising that here, it appears to be more purposeful²⁸³. RNA sequencing data generated in this thesis supports the unlikely hypothesis that LMGC formation is indeed purposeful. Many factors upregulated by LMGCs were anti-apoptotic genes; they appear to escape the cell death programmes which high levels of DNA damage would conventionally elicit, allowing them to persist and effectuate, as yet unclear, functional adaptations. Future experiments could explore the anti-apoptotic properties of LMGCs, by using annexin v staining to measure the number of apoptotic cells in LMGC cultures, compared with cultures of other comparator cells and mononucleated cells of the same culture, when subjected to culture under varying degrees of cellular stress. Stress could be induced by various means, perhaps starvation or hypoxia.

6.1.3. The functional adaptations of LMGCs

In well characterised polyploid cell types, polyploidy offers novel functional adaptations which are often beneficial to the organism. Osteoclasts, for example, gain the capacity to secrete collagenase and degrade bone following the fusion of their myeloid precursors²⁵⁴. It is unclear whether this is the case for LMGCs; their functional adaptations are poorly understood. Some evidence suggests they have a detrimental effect in GCA by causing ROS-mediated arterial damage, which correlates with evidence that they possess an enhanced capacity for the production of ROS^{58, 228, 253}. LMGCs are implicated in the secretion of a number of additional factors which are thought to play a role in the pathogenesis of GCA, including VEGF, PDGF and MMP9 which may contribute to novel vasa vasorum formation, VSMC hyperproliferation and breakdown of the elastic lamina respectively²²⁰⁻²²². These indications that LMGCs possess an increased secretory phenotype, coupled with the genomic abnormalities and DNA damage involved in their formation may be indicative of SASP. Telomere shortening is linked with the induction of senescence and telomeric damage, which

as discussed in 4.1.2 can lead to chromatin bridge formation, may also promote premature senescence regardless of telomere length²⁶². The fragmentation of chromatin bridges can also cause premature senescence through the detection of cytoplasmic chromatin fragments by cGAS and subsequent activation of the STING pathway.

In support of findings in the literature, the data presented in this project show that *in vitro* LMGCs possess enhanced capacity for ROS production. They also demonstrate the heightened expression of senescence marker p21 and increased expression of genes relating to endocytosis and secretion, supporting the hypothesis that they enter premature senescence and exhibit SASP. With the exception of increased ROS production, the constituents of the LMGC secretome were not identified. TNF α , IL-1 β , and IL-6, cytokines elevated in GCA and which correlate with the intensity of systemic inflammation were not produced in higher quantities by *in vitro* LMGCs²⁷⁸. This finding may have been affected by the fact that the cells used had been in culture for sufficient time for LMGCs to form, and while a 48-hour rest period was allowed before LPS stimulation, they may have been exhausted and unable to produce cytokines to their maximal capacity. While both CellROX, and MitoSOX dyes indicated increased capacity for ROS production upon stimulation with TBHP and antimycin-A respectively, CellROX was more reliable. MitoSOX staining with antimycin-A stimulation was successful once, and in all subsequent attempts to repeat the experiment, cultured cells found the antimycin-A treatment to be hypertoxic. This may be another consequence of donor variability in terms of the cellular capacity to cope with the additional stresses of antimycin-A incubation, given that all other variables were consistent.

The lab-time lost during the COVID-19 pandemic resulted in a number of experiments included in this thesis without repeated measures. This had an impact on section 5.4 in which the phagocytic properties of LMGCs were explored. As a result, the conclusions drawn are done so with the caveat of needing substantiation with additional experiments. Phagocytosis is a key effector function of tissue macrophages, which are specialised for the endocytosis and degradation of foreign particles or debris. FBGCs have also been shown to have enhanced complement uptake, giving them improved phagocytic capability²⁰¹. It is unclear whether LMGCs are specialised in this way, or even maintain the phagocytic properties of the macrophages from which they originate. The data shown in 5.4 indicates that LMGCs exhibit a similar rate of endocytosis as mononucleated cells from the same cultures, and primary

monocytes differentiated into macrophages by being cultured with GM-CSF alone, but that endocytoses particles are trafficked to a specific intracellular area in the centre of the cell. This may be the area observed by SEM in cultured LMGCs (Figure 34), a walled off zone of damaged or partially degraded organelles. Further investigations are required to determine the functionality of this area, and whether it is a specialisation to enhance the process of phagocytosis in defence against infection. A possible experiment to perform as a next step could be a pHrodo assay. pHrodo is a dye which becomes fluorescent in response to changes in pH, so indicates the degree of active phagocytosis.

6.1.4. COVID-19 mitigation statement

This project was impacted by the COVID-19 pandemic. Due to the national lockdown and the closure of the university, I was unable to access the laboratory for a period of approximately 9 months. Because of this a number of planned experiments, repeats of those for which the n number was 1 in particular, were unable to be completed. I lacked the interaction with other researchers and colleagues which is ordinarily crucial to develop deeper understanding of underlying science and stimulate ideas and discussion about research.

6.2. Future work

The work carried out in this thesis has generated a number of additional questions that warrant further investigation.

The data produced by the single cell RNA sequencing of cultured LMGCs identified numerous upregulated genes and gene modules of interest that, due to time constraints, were not explored further in this project. The gene TM4SF1 was amongst the most significantly upregulated genes in LMGCs, a protein expressed highly by pancreatic cancer cell lines which is thought to promote metastasis by mediating invadopodia formation²⁸⁴. Invadopodia are structures found on the surface of cells which are specialised for the breakdown of ECM, and are observed protruding from the plasma membrane of metastatic cancer cells, whereby they promote both ECM breakdown and directional movement^{285, 286}. Following proteomic validation of increased TM4SF1 expression by cultured LMGCs by western blot or flow cytometry, an investigation into their capacity to breakdown ECM could be performed. Previously it has been shown that a FITC gelatin degradation assay can be used to measure

this, showing changes in gelatin breakdown following transcriptional perturbation of TM4SF1²⁸⁴.

Another highly upregulated gene was SLAMF7, a cell surface protein which plays a role in activation of natural killer cell cytotoxicity²⁸⁷. Analysis of temporal artery cell populations in section 3.3.3 demonstrated an increase in the number of NK cells in patients with confirmed GCA versus patients without, albeit this was not sufficient to reach statistical significance due to a lack of statistical power. The relationship between LMGCs and NKs could be explored, by experimentally assessing the ability of LMGCs to activate NKs in co-culture systems.

The link between DNA damage and failed cytokinesis, which was recently implicated in the formation of LMGCs from murine macrophages and supported by this project, warrants further investigation. As discussed in 4.1.2, chromatin bridges arise as a result of catastrophic telomeric damage. To cement the role of DNA damage in the formation of LMGCs due to cytokinesis failure, experiments could be performed to investigate whether IFN γ induced DNA damage is localised to telomeres. Investigations into the molecular pathways involved in DNA damage-induced cell cycle arrest could provide insight into this process. IFN γ signals largely through signal transducer and activator of transcription 1 (STAT1), so to clarify the role that IFN γ plays in the induction of DNA damage a STAT1 inhibitor could be used in culture²⁸⁸. If LMGCs form to the same extent in the presence of a STAT1 modulating drug such as pravastatin²⁸⁹, then it may be true that DNA damage occurs through an independent mechanism. A reduction in multinucleation rate would confirm the importance of IFN γ signalling, though would not necessarily further implicate DNA damage as cell fusion machinery would also be affected. The role of chromatin bridges in polyploidy could be further explored by culturing monocytes with an additional p38 inhibitor. The p38 family of kinases are activated in response to cellular stresses, and are effectors of numerous processes such as autophagy and apoptosis, as well as playing a role in the G2/M cell cycle checkpoint. Deficiency of p38 has been shown to increase chromatin bridge formation²⁹⁰; By blocking their actions chromatin bridge formation may be supplemented and the effect of this on multinucleation rate could be measured. Depending on the capacity of monocyte-like cell lines to form LMGCs, knockdown/knockout studies could be performed for both p38 kinases and STAT1, to support any tissue culture investigations.

Repeated live cell imaging experiments at varying stages of LMGC differentiation may clarify the extent to which cell fusion and incomplete cell division contribute. For example, as chromatin bridges were observed exclusively between pairs of nuclei, it may be the case that only mononucleated cells undergo modified cell division and subsequent fusion of binucleated cells results in larger LMGCs. By capturing time-lapse footage of LMGC cultures at earlier time points one may hypothesise that a greater number of modified cell division events would be observed, followed by a higher proportion of cell fusion events at later stages as larger LMGCs enter premature senescence and are no longer actively cycling.

Electron microscopy was used to analyse the morphology of nuclei within LMGCs, but with more time additional morphological analysis could have been performed. Previously it was shown that within MGCs of tubulo-interstitial nephritis, mitochondrial volume densities were comparable to blood monocytes, however, the mitochondrion shape was significantly different with evidence for mitochondrial elongation in MGCs⁸⁷. Mitochondrial elongation acts as a mechanism to rescue partially damaged mitochondria from removal by autophagy, promoting fusion with healthy mitochondria with typical short-ellipsoidal morphology to become longer structures. The process occurs in response to cellular stresses such as starvation, which induce autophagy. The possibility that LMGC polyploidy occurs in response to inflammatory cytokine-induced cellular stress as a mechanism to preserve ATP production by pooling mitochondrial resources and promoting mitochondrial elongation could be investigated.

As described in chapter 5, electron microscopy revealed a large 'walled off' section of what appeared to be damaged or partially degraded organelles in the centre of cultured LMGCs. One hypothesis is that endocytosed materials, and intracellular debris are trafficked to this zone to be degraded. This could lead to an investigation into the properties of this zone, with a particular focus on the capacity for active degradation within this zone compared with mononuclear phagocytes.

Chapter 7. Materials and Methodology

7.1. Materials

7.1.1. Antibodies

The antibodies used during this thesis for both flow cytometry and immunofluorescence are outlined in table 5.

Target protein	Fluorophore	Supplier	Clone
p21	Unconjugated	Cell Signaling	12D1
53BP1	Unconjugated	Novus Bio	E-10
IL-6	PE	Biolegend	MQ2-13A5
IL-1 β	FITC	Biolegend	H1b-98
TNF α	AF647	Biolegend	MAb11
CD14	BUV737	BD	M5E2
CD9	APC	BD	M-L13
TM4SF1	PE	Miltenyi	REA851
SLAMF7	PerCP Cy5.5	Biolegend	162.1
Anti-Rb 2 ^o	AF647	Abcam	Ab150075

Table 5. Antibodies used for this research.

7.1.2. Tissue culture materials

The reagents used for tissue culture during this thesis are outlined in table 6:

Item	Supplier	Catalogue number / reference
DMEM	Life Technologies	#41965-039
FCS	Life Technologies	#10270-106
Glass coverslips 13mm	VWR INTERNATIONAL	#631-0150
Culture plates	CORNING	#3894
Culture flasks	Greiner	#690160
GM-CSF	Biologend	#572904
M-CSF	Biologend	#574804
IFN γ	Biologend	#570204
CELLview imaging dishes	Greiner bio-one	#627871
Glass coverslips 24x60mm	CORNING	#2975-246
RF10	Sigma	#R0883
α MEM	Life technologies	#22561-021
RANKL	STEMCELL technologies	#78214
IL-3	Biologend	#578002
IL-4	Biologend	#574002
Pam3CSK4	InvivoGen	#tlrl-pms

Table 6. Tissue culture materials used for this research.

7.1.3. Other materials

The reagents and materials used for all experimentation other than tissue culture are outlined in table 7. This includes all reagents for the isolation of monocytes from peripheral blood, flow cytometry and microscopy preparation, intracellular cytokine staining, cell counting, cell washing and harvesting, preparation for single cell sequencing, tissue digestion and 10X loading.

Item	Supplier	Catalogue number / reference
Lymphoprep solution	STEMCELL Technologies	#07851
CD14 microbeads	Miltenyi Biotec	#130-050-201
Phosphate buffered saline	Sigma	#D8537
Lipopolysaccharide	Sigma	#L2654
Brefeldin A	Sigma	#B7651
DAPI	Sigma	#D9542
DRAQ5	Biolegend	#424101
EDTA	Sigma	#E7889
MACS COLUMNS	Miltenyi Biotec	#130-042-401
HBSS	LONZA BioWhittaker	#BE10-543F
TRYPsin-EDTA	Sigma	#59418C
Accutase	Sigma	#A6964
Trypan blue	Sigma	#T8154

SiR DNA	Spirochrome	#SC007
Glycine	Sigma	#50046
BSA	Sigma	#A4503
Tween20	Sigma	#P1379
TritonX20	Sigma	#T9284
Giemsa stain	Sigma	#G5637
FITC DEXTRAN	Sigma	#FD10S
Edu Kit	Thermofisher	#C10337
Vectashield + DAPI	VECTOR laboratories	#H-1200
Glass coverslips 24x60mm	CORNING	#2975-246
DPX mountain medium	Sigma	#06522
DNA isolation kit	QIAGEN	#80204
FIX/PERM kit	BD	#554714
MitoSOX	Invitrogen	#M36008
CellROX	Life technologies	#C10414
MitoTEMPO	Sigma	#SML0737
Collagenase XI	Sigma	#C7657
Collagenase I	Sigma	#SCR103
Collagenase IV	WORTHINGTON	#LS004186
Hyaluronidase	Fox Pharma	n/a
DNase I	Sigma	#11284932001
MgCl2	Sigma	#M8266

10um filters	Pluriselect	#43-50010-01
20um filters	Sysmex	#04-004-2325
Leupeptin	Sigma	#L2884
Ammonium chloride	Sigma	#254134
B-mercaptoethanol	Sigma	#M3148
Buffer TCL	QIAGEN	#1031576
96 well PCR plates	Eppendorf	#0030129512
Superfrost slides	VWR INTERNATIONAL	#631-0108
Cytoslides	Thermofisher	#5991056
Methanol	Sigma	#322415
Ethanol	Sigma	#443611
Cell strainers	Fisher Scientific	#352360
96 well plates	QIAGEN	#19581
RNA-SPRI beads	Beckman Coulter	#A63987
RT primer	IDT	n/a
dNTP mix	Thermofisher	#R0192
RDil	Takara	#2313B
Maxima buffer	Thermofisher	#EP0751
Betaine	Sigma	#B0300
TSO	Qiagen	n/a
RNAse inhibitor	Takara	#2313B
Maxima RnaseH-minus RT	Thermofisher	#EP0751

ISPCR Primer	IDT	n/a
KAPA HiFi Hot Start Ready Mix	Roche	#7958935001
AMPure beads	Beckman Coulter	#A63881
Qubit reagent	Thermofisher	#Q32854

Table 7. All other materials used for this research.

7.2. Methodology

7.2.1. Tissue culture

All cell culture was performed in class II microbiological safety cabinets. Sterile technique was observed throughout.

7.2.1.1. Primary monocyte acquisition

The primary monocytes used in this study were acquired from healthy blood donors. Healthy donor blood was obtained most frequently through the 'Lime Survey' blood donation system, arranged by the immunity and inflammation theme within the Faculty of Medical Sciences at Newcastle University. Through this ethical approval, healthy donors volunteered to donate, with fully informed consent. Phlebotomy was performed by trained individuals. Blood samples received ranged in volume from 10ml – 100ml, and were drawn directly into EDTA-coated tubes to prevent coagulation. Blood samples were diluted 1:1 with HBSS (LONZA) + 2.5mM EDTA (SIGMA) before proceeding. Blood samples were always processed on the same day they were taken.

Alternatively, leukocyte apheresis cones were used. These were prepared by the Newcastle-Upon-Tyne Donor Centre of the NHS Blood and Transplant Service (NHSBT) by using centrifugation to separate peripheral blood into layers of platelets, plasma, leukocytes and erythrocytes. Many of these cells were subsequently used for clinical purposes or returned to the donor, and any remaining leukocytes were procured for research. Leukocyte cones were diluted 1:4 with HBSS + 2.5mM EDTA before continuing. Leukocyte cones were always used on the same day they were procured.

7.2.1.2. PBMC isolation from healthy donor blood

Density gradient centrifugation was used to isolate peripheral blood mononuclear cells; Between 10mL and 20mL of diluted blood was gently pipetted onto 15mL of lymphoprep solution (STEMCELL), and centrifuged at a speed of 900RPM, for 30 minutes at room temperature with acceleration and deceleration at minimum values. Centrifugation resulted in separation into three distinct layers, a Pasteur pipette was used to extract the cell at the plasma:Lymphoprep interface containing PBMCs into a new tube. This was made up to 50mL with 4°C HBSS containing 1% FCS (Life Technologies), and centrifuged at a speed of 600RPM for 8 minutes at 4°C. The supernatant was aspirated and the pellet resuspended in HBSS containing 1% FCS. The tube was twice more centrifuged, supernatant aspirated and pellet resuspended in HBSS containing 1% FCS, this time at 300RPM for 8 minutes at 4°C. 5µL of the resultant cell suspension was mixed with 5µL 0.4% trypan blue solution (SIGMA), and this mixture was applied to a haemocytometer (Fisher Scientific) to perform cell counting.

7.2.1.3. Cell counting

Cell suspensions were combined with 0.4% trypan blue solution at a 1:1 dilution, and 10µL of this mixture was pipetted under a coverslip placed on a glass haemocytometer. Cells within a 4x4 grid were counted, those in contact with the uppermost and leftmost sides of the squares were not included. Cells coloured blue due to trypan blue uptake were excluded from the count. This was repeated three times, and the mean of these multiplied by 2 to account for the dilution with trypan blue, and then by 10,000 to account for the difference in volume between the cell suspension and the volume within the counting grid to achieve the final cell count.

7.2.1.4. Monocyte isolation from PBMCs

Isolated PBMCs, now counted, were centrifuged at a speed of 400RPM for 8 minutes at 4°C and the pellet resuspended in MACS buffer, comprising PBS (SIGMA) with 1% FCS (Life technologies) and 0.5% EDTA (SIGMA), to which CD14 microbeads (Miltenyi Biotec) were added. Volumes of each were determined by PBMC cell count; 80µL of MACS buffer and 10µL of CD14 microbeads were used for every 10 million PBMCs. This was mixed by gentle pipetting and incubated at 4°C for 20 minutes. The mixture was then made up to 50mL with MACS buffer, and centrifuged at 400RPM for 8 minutes at 4°C. During this time, a MACS LS column (Miltenyi Biotec) was attached to a magnetic stand (Miltenyi Biotec) and 3mL MACS buffer

was pipetted through the column to lubricate it. Once centrifuged, the PBMC pellet was resuspended in 500 μ L MACS buffer then pipetted into the MACS LS column attached to the magnetic stand. Once dripped through, 3mL MACS buffer was added to the column and again allowed to drip through which was then repeated two more times. Finally, the LS column was removed from the magnetic stand, and 5mL MACS buffer was forcefully pipetted through the column, into a collection tube. This final flow through contained purified monocytes, which were counted as described in 7.2.1.3.

7.2.1.5. Generation of macrophages and multinucleated giant cells

Purified monocytes in suspension were centrifuged at 400RPM, and resuspended in culture medium. Different media were used throughout the study; RPMI (SIGMA), α MEM (Life Technologies) and DMEM (Life Technologies) were used, all containing 10% FCS (Life Technologies). DMEM was ultimately determined to be most effective for LMGC generation (Described in 2.4.2.). Cells were resuspended at a concentration of 5×10^5 cells per 1mL media. This cell suspension was pipetted into flat-bottom culture plates (CORNING), either 96 well, 48 well or 24 well depending on the requirements of the experiment. Cytokines and growth factors were added to wells to induce multinucleation according to the experiment. GM-CSF (BioLegend), M-CSF (Biolegend), RANK-L (STEMCELL), IFN γ (Biolegend), IL-4 (Biolegend), IL-3 (Biolegend) and Pam3CSK4 (InvivoGen) were added in various combinations and concentrations, described throughout chapter 2. Ultimately the combination of 50ng/mL GM-CSF and 200ng/mL IFN γ was deemed most effective for the production of LMGCs and was more frequently used in subsequent chapters unless otherwise stated. Plates were incubated in a 37 $^{\circ}$ C, 5% CO $_2$ incubator for between 5-10 days. Time varied due to donor dependent differences in the rate of LMGC development, which was assessed daily by visual inspection using standard light microscopy (Amscope, 40X-2000X Trinocular Biological Compound Microscope).

7.1.2.6. Cell culture maintenance

All cultures were grown in incubators maintained at 37 $^{\circ}$ C, with a 5% CO $_2$ environment. Incubators were shared between numerous lab users and regular checks and maintenance performed by the core technical staff of the immunity and inflammation theme. Monocytes were typically seeded into plastic, flat-bottomed 6 well, 24 well, 48 well or 96 well plates (CORNING), although for live cell imaging experiments, glass-bottomed plates (CELLview)

were used. All cultures were refreshed roughly every 72 hours, by gently aspirating 45% of the volume, and replacing this with 50% volume of fresh media containing the same concentrations of FCS, and cytokines. Fresh media was warmed in a 37°C water-bath for a minimum of 20 minutes before use. More media was added than removed to account for minor reduction of volume over time due to evaporation.

7.2.2. Flow cytometry

Flow cytometers used in this study were the FACSymphony, and LSRFortessa X-20, and FACS was performed using the FACS Aria Fusion cell sorter (All BD Biosciences). Data was analysed using FlowJo v8.0 (Treestar) and FACSDiva 6.1.3 (BD Biosciences).

7.2.2.1. Using flow cytometry and FACS to assess ploidy

LMGCs were cultured as described in 7.2.1.5. Cells were dissociated from plastic flat-bottomed wells by incubation with accutase for 5 minutes at 37°C followed by gentle pipetting. Cells were then washed twice with flow buffer, and resuspended in flow buffer containing 0.1% DRAQ5 to label nuclei in individual 5mL capacity round bottom test tubes (Fisher Scientific). Tubes were stained for a minimum of 10 minutes, and analysed without further washing steps. The preparation procedure was performed with ice-cold buffer, and test tubes were kept on ice during staining and data acquisition.

The ploidy of cell suspensions was analysed using the FACSymphony flow cytometer, illuminating samples with a 637nm excitation laser and detecting DRAQ5 signal using a 780/60 bandpass filter. A minimum of 10,000 events were captured for every sample. Cells were sorted based on ploidy by running DRAQ5 stained cell suspensions on the FACS Aria Fusion cell sorter, illuminating samples with a 640nm excitation laser and detecting with a 780/60 bandpass filter. Between 10,000 and 2,000,000 events were processed and sorted. FACS-enriched LMGC populations were subsequently used for cytopspins and giemsa staining, electron microscopy and for the generation of scRNAseq data, described in sections 7.2.3, 7.2.4, and 7.2.8.1 respectively.

7.2.2.2. ImageStream

LMGCs were cultured as described in 7.2.1.5. Once fully grown, CellROX GREEN reagent (Thermofisher) was added to the culture medium at a concentration of 1µM and incubated for 30 minutes at 37°C, before being harvested with accutase as described in 7.2.2.1, before

being incubated in flow buffer containing 0.1% DRAQ5 in order to label cell nuclei. Cells were then incubated for a minimum of 10 minutes before Imaging flow cytometry was performed. Samples were analysed by Dr. David Jamieson using the ImageStream X Mark II system, and images generated using Amnis AI Image analysis software version 6.3.

7.2.2.3. Intracellular cytokine staining

LMGCs were cultured as described in 7.2.1.5, and given a 2-day rest period in which cells were incubated with 10ng/mL GM-CSF only, 1µg/mL LPS (SIGMA) was added to LMGC cultures and incubated at 37°C for 1 hour, at which time 10µg/mL BFA (Sigma) was added. The cells were incubated for a further 5 hours at 37°C. An unstimulated control was established by excluding LPS. Following this incubation, cells were harvested by Accutase incubation as previously described. Cell suspensions were fixed and permeabilised using the BD fixation and permeabilization kit according to the manufacturer's protocol (BD Cytofix/Cytoperm); cells were washed with PBS and resuspended in 50µL fixation/permeabilization solution and incubated on ice for 20 minutes. Cells were then washed twice with permeabilization buffer. Cell suspensions were then stained with fluorophore conjugated flow cytometry antibodies against TNF α (AF647), IL-6 (PE) and IL-1 β (FITC), by adding antibodies at 1:100 dilution to cells suspended in permeabilization buffer. Cells were then washed once with permeabilization buffer and resuspended again in permeabilization buffer + 0.1% DAPI. After a short incubation at room temperature the samples were analysed using the Fortessa X20 flow cytometer. 635nm, 561nm, 488nm and 355nm lasers were used and 670/30, 582/15, 530/30, 450/50 bandpass filters were used to excite and detect AF647, PE, FITC fluorophores and DAPI respectively.

7.2.3. Generation of cytopins and giemsa staining

Cell suspensions were prepared for cytopins by washing with PBS containing 1% BSA. Between 100 and 10,000 cells were cytopun at 800 RPM for 10 minutes (Shandon Cytospin 3, Thermofisher) onto superfrost cytoslides (VWR). Slides were air-dried before pipetting sufficient methanol onto slides to fully cover the cells, and incubating them for 10 minutes at -20°C. Again, slides were air-dried. Giemsa solution (SIGMA) was prepared for staining by diluting it 1:20 with dH₂O. A hydrophobic pen was used to create a barrier on the slides around

the cells. Giemsa staining solution was applied to cells to cover them completely, and they were incubated for 20 minutes at room temperature. Slides were then thoroughly rinsed with room temperature dH₂O and air-dried. DPX mountant (SIGMA) was applied to the slides, and 60x24mm glass coverslips (CORNING) were applied with gentle pressure. The Zeiss Axiomager was used to image samples by standard brightfield. 20x and 63x objective magnifications were used with air and oil immersion respectively. Images were analysed using Fiji for ImageJ version 1.8.0.

7.2.4. Electron microscopy

In vitro LMGCs were generated as described in 7.2.1.5 for electron microscopy analysis. Once grown, the media of LMGC cultures was aspirated, and cells were gently washed with PBS. Accutase solution (STEMPRO) was then added to wells to be incubated for 5 minutes at 37°C. Gently pipetting was then used to fully dislodge cells from the wells and they were transferred to a 15mL tube. Centrifugation at 500RPM for 5 minutes at 4°C was then used to pellet the cells, which were subsequently resuspended in PBS and centrifuged again using the same settings. The resultant pellet was resuspended in 500µL FACS buffer, comprising PBS containing 2% FCS and 0.5% EDTA, and transferred to a FACS tube. To this, 0.5µL DRAQ5 (Thermofisher) was added and the tube immediately taken to be FACS sorted using the BD Aria Fusion cell sorter. The process of cell sorting to achieve purified populations of LMGCs is described in section 7.2.2.1, although in this instance cells were sorted directly into 1.5mL capacity Eppendorf tubes containing 1mL glutaraldehyde (SIGMA), rather than standard collection tubes. These Eppendorf tubes were delivered to the electron microscopy facility within the Faculty of Medical Sciences, Newcastle University where they were processed and imaged using SEM by the technical team; Dr K. White, T. Davey and R. Laws.

The acquisition of temporal artery tissue is described in section 7.2.9.3. A Small section of temporal artery from a patient with suspected and later confirmed GCA was cut using a scalpel, to be roughly 1mm³ in volume. This was placed into a 1.5mL Eppendorf containing 1mL glutaraldehyde, which was subsequently made up to a full volume of 1.5mL with glutaraldehyde. As before, this was delivered to the technical electron microscopy staff where it was processed and imaged by SEM.

Pre-processing and segmentation of electron microscopy images was performed using the software 'Microscopy Image Browser' (MIB), downloaded from (mib.helsinki.fi). Images were first contrast-adjusted and normalised to ensure consistent brightness/contrast levels between slices. Following this, the slices were aligned to account for any shifts in orientation while images were being taken. Segmentation of nuclei was performed with a combination of the '2D watershed' tool, and the manual brush tool within MIB. Once manually segmented for each slice, nuclei were compiled into three dimensional objects using the 'Models with Matlab isosurfaces' function within MIB, and visualised in Matlab volume viewer.

7.2.5. Immunocytochemistry

Plates for immunocytochemistry were prepared in advance of monocyte isolation. Circular glass coverslips (CORNING) were sterilised by submerging in 70% ethanol, and then rinsed thoroughly with sterile PBS before being carefully placed into the bottom of the wells of a 24 well flat-bottomed tissue culture plate (CORNING). These were then air dried for a minimum of 3 hours to ensure complete evaporation of any residual ethanol. Monocytes were seeded as described in 7.2.4. on top of the sterilised coverslips.

Once cultures were well developed and multinucleated giant cells were apparent, culture medium was aspirated and cells were washed 3 times with room temperature PBS. Depending on the optimal strategy for the given primary antibody, cells were now fixed with either 100% methanol (SIGMA), or a formaldehyde-based fixative (BD Biosciences). 500 μ L of fixative was added to the wells, and incubated for 20 minutes at -20°C in the case of methanol, or 20 minutes at room temperature for the formaldehyde-based fixative. Fixative was then aspirated and wells washed 3 times with PBS. Following this, a blocking solution was added to the wells comprising PBS with 0.1% Tween20, 22.4mg/mL glycine, 10mg/mL BSA, 5mg/mL milk powder and 0.01% Triton X (All SIGMA). The cells were incubated for 1 hour at room temperature with gentle agitation on a benchtop rocker. Following this, wells were washed once with PBS. Antibody solution was prepared, PBS with 0.5% BSA, and 50 μ L of this solution containing primary antibody at different concentrations, depending on the optimal staining concentration for each antibody, were pipetted onto parafilm (SIGMA) as droplets. A single droplet contained no antibody to be used as a secondary only control. Once these droplets were prepared, coverslips were removed carefully from the wells using forceps, and placed cell-side-down on the parafilm droplets. They were incubated at room temperature for 1

hour, covered from light in a moist environment. Coverslips were then removed from the parafilm with forceps, washed with PBS, and placed cell-side-down on secondary antibody solution droplets, prepared as before. Again, coverslips were incubated for 1 hour at room temperature covered from light in a moist environment. Following this, coverslips were removed and washed with PBS, and placed down on more droplets of PBS containing 50ng/mL DAPI (SIGMA). They were incubated for 20 minutes at room temperature. Microscope slides (VWR International) were labelled and 10 μ L drops of Vectashield mountant (VectaLabs) were pipetted onto the slides. Coverslips were washed with PBS for a final time, and placed cell-side-down onto the drops of Vectashield atop the microscopy slides. Any excess Vectashield was dried and coverslips were sealed with nail varnish. Slides were air dried for a minimum of three hours before being imaged using the AxioImager fluorescence microscope, or the Leica SP8 confocal microscope, with 20x, 40x, 63x, or 100x objective magnification. Image acquisition was performed with ZEN blue version 3.3, or LAS X version 4.13. For standard and confocal fluorescence imaging, 647nm, 488nm, 405nm argon lasers, and a 405nm diode laser were used for sample excitation.

7.2.6. Live cell confocal imaging

Primary monocytes were cultured in DMEM+10% FCS with 50ng/mL GM-CSF with or without 200ng/mL IFN γ . The cells were seeded directly into the quadrants of a 35/10mm glass bottom cell culture dish (CELLview). After 7 days in culture, 250nM SiR DNA (SiR-Hoeschst, Spirochrome) was added to all wells, and incubated for 1 hour before being taken to the bioimaging facility at FMS. With the guidance and assistance of Dr Mark Levasseur and Dr Alex Laude, samples were imaged using the Nikon A1R confocal microscope with 40X oil and 20X air objective lens magnification. NIS Elements AR software version 5.21.03 was used for imaging. A single fluorescence channel was used to detect SiR DNA, with absorption and emission values of approximately 652 and 674 respectively, allowing the visualisation of nuclei. Brightfield was imaged simultaneously to allow visualisation of gross cell structures. Eight fields of view were imaged per condition, and 8 focal planes imaged for each field to ensure full cells were captured. Each imaged field was repeatedly imaged every 5 minutes, for a total of 17 hours.

Nikon Elements viewer software version 4.11.0 was used to compile, analyse and export time lapse data as video clips in MP4 format. Video clips were annotated using Sony Vegas movie studio 15 and Adobe Illustrator version 22.1.

7.2.7. Measuring capacity for the production of reactive oxygen species

7.2.7.1. MitoSOX staining

LMGCs were cultured as described in 7.2.1.5. Once fully grown, cells were incubated with 5 μ M MitoSOX red reagent (Thermofisher) for 30 minutes at 37°C to allow dye uptake. Cells were then gently washed and harvested using Accutase solution, before being pipetted into FACS tubes containing FACS buffer and 5 μ M DRAQ5. Prior to measurement by flow cytometry, antimycin A was added to cell suspensions at a range of concentrations (0, 1 μ M, 5 μ M, 10 μ M and 20 μ M) in order to stimulate maximal ROS production.

7.2.7.2. CellROX staining

LMGCs were cultured as described in 7.2.1.5. Once fully grown, cells were incubated with 400 μ M tert-butyl hydroperoxide (TBHP) (Thermofisher) in culture medium for 30 minutes at 37°C, to stimulate ROS production. Following this, CellROX green reagent was added at a final concentration of 1 μ M, and cells were incubated for a further 30 minutes at 37°C. TBHP and CellROX concentrations were taken from the supplier's guidelines. For Imaging flow cytometry, cells were harvested with Accutase solution and stained with DRAQ5 as described in 7.2.2.2. For fluorescence microscopy, cells were fixed with a formaldehyde-based fixative solution, washed thoroughly and stained with DAPI at 1 μ g/mL to stain nuclei.

7.2.8. FITC DEXTRAN uptake microscopy

LMGCs were cultured as described in 7.2.1.5, on round glass coverslips. 2mg/mL FITC Dextran was added to culture medium and incubated for 30 minutes at 37°C or 4°C (internal control). Cells were then co-stained with SiR DNA for 1 hour at 37°C, washed with PBS and fixed with formalin solution (SIGMA) for 10 minutes at room temperature, before being mounted onto superfrost microscopy slides with vectashield and analysed on the AxioImager upright fluorescence microscope (Zeiss) with 63x oil immersion objective magnification. Images were analysed using Fiji for ImageJ version 1.8.0.

7.2.9. Single cell RNA sequencing

7.2.9.1. In vitro LMGC culture preparation for scRNAseq

Primary monocytes were cultured in three different conditions. First, in DMEM+10%FCS containing 50ng/mL GM-CSF, Second, in DMEM+10%FCS containing 50ng/mL GM-CSF and 200ng/mL IFN γ , and third, in α MEM+10%FCS containing 20ng/mL M-CSF and 100ng/mL RANKL. Cultured cells were removed from the plates by Accutase incubation, as previously described. Cell suspensions were then transferred to 50mL falcon tubes, and made up to 50mL with FACS buffer before being washed twice with FACS buffer. After this, the supernatant was aspirated and the pellet was resuspended in 500 μ L FACS buffer containing 0.1% DRAQ5. Samples were kept on ice and taken to the flow cytometry core facility to flow sort single cells into pre-prepared 96 well plates (QIAGEN) containing 10 μ L buffer TCL (QIAGEN) with 1% β -mercaptoethanol (SIGMA) per well. Five populations of cells were sorted using DRAQ5 as a measure of ploidy, outlined in figure 9. Per plate, a single row (12 wells) of GM-CSF treated macrophages, and a single row of osteoclasts were sorted, as well as two rows of mononucleated GM-CSF, IFN γ treated macrophages, one row of binucleated GM-CSF, IFN γ treated macrophages and three rows of multinucleated GM-CSF, IFN γ treated macrophages. FACS sorting was performed by technical staff of the FCCF. Once sorted, plates were briefly centrifuged at 300RPM for 30 seconds to ensure cells were at the bottom of the wells, in the lysis buffer mixture, and then stored immediately at -80°C to prevent degradation.

7.2.9.2. cDNA Library generation for smart-seq2

cDNA library generation was performed by Emily Stephenson and Justin Engelbert according to the SmartSeq2 protocol²⁹¹. Master mixes were prepared, the first containing 1 μ L each of RT primer (10 μ M), dNTP mix (10mM), RDil (10% RNase-inhib, final of 4 U/ μ L), and water per sample; The second containing 2 μ L each of Maxima Buffer, and Betaine (5M), 0.9 μ L MgCL2 (100mM), 1 μ L TSO (10 μ M), 0.25 μ L RNase Inhibitor (40U/ μ L), Maxima RnaseH-minus RT (200U/ μ L), and 0.75 μ L water per sample. 180 μ L RNA-SPRI beads were aliquoted into 12-well strip tubes (Thermofisher). Cell plates prepared as described in section 7.2.9.1 were thawed on ice and centrifuged at 100g for 1 minute. 20 μ L RNA-SPRI beads were added to each well and gently mixed before being incubated at room temperature for 10 minutes, and moved onto a magnet for a further 5 minutes. Supernatant was then removed from the beads, which

were washed with 100 μ L 80% EtOH three times. Beads were then left to dry for 5 minutes. 57 μ L of master mix 1 was aliquoted into 8-well strip tubes (Thermofisher). RNA was eluted in 4 μ L of mix, and beads were slowly removed from the magnet. The plate was then put into a thermocycler to run at 72 $^{\circ}$ C for 3 minutes. Following this, the plate was immediately placed on ice. Enzyme was now added to master mix 2, of which 67 μ L was aliquoted into 12-well strip tubes. 7 μ L of this mix was added to each well of the plate, and mixed before being centrifuged at 100g briefly. The plate was then put into the thermocycler and run on 'RT mod' setting: incubated at 50 $^{\circ}$ C for 90 minutes, 85 $^{\circ}$ C for 5 minutes, and 4 $^{\circ}$ C until ready for the next step.

PCR Preamplification was then performed. A third master mix was prepared containing 0.5 μ L ISPCR primer (10 μ M), 12.5 μ L KAPA HiFi Hot Start Ready Mix, and 1 μ L water per sample. 132 μ L of this was aliquoted into 12 well strip tubes and 14 μ L added to each well of the plate before being mixed. This was centrifuged at 100g briefly and put into the thermocycler to run at 98 $^{\circ}$ C for 3 minutes, then 22 cycles of 98 $^{\circ}$ C for 15 seconds, 67 $^{\circ}$ C for 20 seconds, and 72 $^{\circ}$ C for 6 minutes, followed by a single cycle of 72 $^{\circ}$ C for 5 minutes and 4 $^{\circ}$ C until ready for the next stage.

DNA SPRI Clean-up, and quantification/quality control were then performed. 180 μ L of AMPure beads (Beckman Coulter) were aliquoted into a 12 well strip tube, and 20 μ L of this added to each well of the plate. This was incubated at room temperature for 5 minutes and moved onto a magnet for 6 minutes. The supernatant was then removed and beads washed twice with 70% EtOH. Beads were then air dried before 15 μ L of TE (Thermofisher) was added to elute material with a 1-minute incubation. The elute was transferred to a new plate and this procedure was repeated once more. cDNA was quantified by added 2 μ L of sample to 198 μ L Qubit working solution (Thermofisher), and reading fluorescence with a plate reader with a standard for comparison.

275 μ L TD and 137.5 μ L ATM were added to an Eppendorf, and 50 μ L aliquoted into strip tubes. 3.75 μ L of this mix was added to each well of a new 96 well plate, and 1.25 μ L of each sample added following by thorough mixing and centrifugation at 3000RPM for 3 minutes. The plate was then put into the thermocycler and run at 55 $^{\circ}$ C for 10 minutes, and then placed on ice. 1.25 μ L of NT was added to each well and the plate centrifuged again at 3000RPM for 3

minutes, then incubated at room temperature for 10 minutes. 3.75µL of NPM was then added to each well, followed by 2.5µL of indexes. This was mixed well and centrifuged again at 3000RPM for 3 minutes, before being placed into the thermocycler and run for 1 cycle at 72°C for 3 minutes, 1 cycle at 95°C for 30 seconds, 12 cycles of 95°C for 10 seconds, 55°C for 30 seconds, and 72°C for 60 seconds, then 1 cycle at 72°C for 5 minutes and 4°C until ready for the next stage.

Samples were then pooled, with 2.5µL of each added to one 1.5ml tube and the total volume measured. AMPure beads were added to the material at a ratio of 0.9:1 and mixed well, then incubated for 5 minutes at room temperature, then a further 5 minutes on a magnet. The supernatant was removed and beads washed twice with 80% EtOH. Beads were dried for 10 minutes and 100µL TE was added for a 5-minute incubation at room temperature. The samples were then run on Bioanalyser 3x, and quantified using Qubit.

7.2.9.3. Temporal artery processing

Temporal artery biopsies were kindly donated for this research by patients with suspected GCA. Fully informed consent was obtained by Dr Gary Reynolds. Clinical details of biopsies included in the analysis are outlined in table 8.

Sample	Clinical Diagnosis	Age	Sex	Days on steroids	CRP at presentation
1	Positive	84	F	12	109
2	Positive	65	M	8	20
3	Negative	67	M	12	60
4	Negative	78	M	8	5

Table 8. Clinical metadata for temporal artery biopsies used.

Upon receipt of samples, a scalpel was used to dissect the blood vessels longitudinally, and half was used by clinical pathology to perform medical diagnostics. The other half was

digested as outlined in figure 15, by first being transferred to a sterile plastic petri dish (SIGMA) and manually minced with scalpels until chopped into a fine paste. This was then transferred to a universal tube containing 2mL DMEM + 10% FCS + 2.5mM MgCl₂ (SIGMA). This media was used to the rinse scalpels and the dish to maximise yield. A cocktail of enzymes was added to the digestion tube: Hyaluronidase (60µL/mL, Fox Pharma), Collagenase type I (32µL/mL, Sigma), Collagenase type XI (6µL/mL, Sigma) and DNase I (3µL/mL, Sigma). The tube was then placed in a pre-heated 37°C water bath and incubated for 50 minutes, inverting the tube to mix every 10 minutes. Following this incubation, the mixture was pipetted through a 100µm strainer (Fisher Scientific) into a new tube, rinsing the digestion tube with FACS buffer and pipetting this through the strainer as well. The strained mixture was then centrifuged at 500RPM for 5 minutes at 4°C, the supernatant was aspirated and the pellet resuspended in 5mL 1X RBC lysis buffer (SIGMA) and incubated at room temperature for 10 minutes. After this, the tube was topped up to 50mL with FACS buffer, and centrifuged again at 500RPM for 5 minutes at 4°C. This time the supernatant was aspirated and the pellet resuspended in as small a volume as possible – typically the residual volume in the tube following aspiration. 5µL of the resuspended cell suspension was taken and mixed with 5µL trypan blue, and the cells were counted as described in 7.2.1.3. While this is often a large proportion of the cells it is necessary to ensure an accurate count, which is crucial for effective 10X loading. Once an accurate count was reached the remaining cells were made up to a solution with a concentration of 1000 cells per µL, using FACS buffer, ready for loading onto the 10X genomics controller.

7.2.9.4. 10x library generation

Cells isolated from tissue and matched blood were manually loaded onto individual channels of a chromium chip, and encapsulated onto a chromium controller (Both 10x Genomics). cDNA libraries were generated using a chromium single cell V(D)K reagent kit, according to the manufacturers protocol (<https://support.10xgenomics.com/single-cell-vdj/library-prep>). Library generation was performed by Emily Stephenson and Justin Engelbert, and all reagents were supplied by 10x Genomics unless otherwise stated. In brief, cells were first partitioned into nanoliter-scale gel beads (GEMs), and then lysed. Oligonucleotides containing an Illumina R1 sequence, a 16 nt 10x Barcode, a 10 nt unique molecular identifying (UMI) and 13 nt template switch oligo (TSO) were mixed with the cell lysate and combined with a master mix

of poly(dT) primers and reagents for reverse transcription. This process generates barcoded first-strand cDNA, which is then purified from leftover reagents using silane magnetic beads before being amplified via PCR.

7.2.8.5. Computational analysis

Computational analysis of scRNAseq data was performed on an Apple MacBook Pro with MacOS High Sierra Version 10.13.6, using the Seurat platform in R (<https://satijalab.org/>). First, deconvoluted raw FASTQ files were aligned to the reference genome (GRCh38.p13) and quantified using the pseudoalignment tool Kallisto. Pathway analysis was performed using CytoScape (<https://cytoscape.org/>), a platform allowing the visualisation of protein networks using the gene ontology (GO) resource.

Testing for differential expression was performed using the 'Findallmarkers' function in the Seurat package. This function utilizes a Wilcoxon-rank sum test to test for significant differences in expression for each individual gene between experimental groups (population clusters). This test is non-parametric, so does not assume a normal distribution. This is a quantitative way to determine the genes which are differentially expressed in one group, for example the *in vitro* LMGC group identified by unbiased clustering, compared with all other groups. This way, for each group, a list of genes is generated giving insight into the transcriptional characteristics of that group.

7.2.10. General methodology

The work carried out in this thesis was performed with Good Laboratory Practice by individuals adhering to the Newcastle University FMS safety policies. Full training was received by qualified staff for use of the equipment within Bioimaging and Flow Cytometry core facilities.

Statistical analysis was performed with Prism software version 8.3.1 (GraphPad Software). Non-parametric tests, namely Mann-Whitney U and Kruskal Wallance tests, were used to determine the significance of differences between groups with a relatively low number of values or non-normal distributions in which 2 groups, or more than 2 groups were being compared respectively.

Parametric tests were performed on data which was normally distributed and contained a relatively large number of samples. One-way ANOVA was used with the addition of Tukey's

post-hoc test, in order to determine significance of the differences between 3 or more groups in which the sample sizes are equal, and a Welch's t-test used to determine the significance of the difference between 2 groups.

References

1. Crowson, C.S. Contemporary Prevalence Estimates for Giant Cell Arteritis and Polymyalgia Rheumatica, 2015. *Semin Arthritis Rheum* **47**, 253-256 (2017).
2. Baig, I.F., Pascoe, A.R., Kini, A. & Lee, A.G. Giant cell arteritis: early diagnosis is key. *Eye Brain* **11**, 1-12 (2019).
3. Lie, J.T. Aortic and extracranial large vessel giant cell arteritis: a review of 72 cases with histopathologic documentation. *Semin Arthritis Rheum* **24**, 422-431 (1995).
4. Gonzalez-Gay, M.A. *et al.* Visual manifestations of giant cell arteritis. Trends and clinical spectrum in 161 patients. *Medicine (Baltimore)* **79**, 283-292 (2000).
5. Amiri, N., De Vera, M., Choi, H.K., Sayre, E.C. & Avina-Zubieta, J.A. Increased risk of cardiovascular disease in giant cell arteritis: a general population-based study. *Rheumatology (Oxford)* **55**, 33-40 (2016).
6. Gonzalez-Gay, M.A. *et al.* Epidemiology of giant cell arteritis and polymyalgia rheumatica. *Arthritis Rheum* **61**, 1454-1461 (2009).
7. Nuenninghoff, D.M., Hunder, G.G., Christianson, T.J., McClelland, R.L. & Matteson, E.L. Incidence and predictors of large-artery complication (aortic aneurysm, aortic dissection, and/or large-artery stenosis) in patients with giant cell arteritis: a population-based study over 50 years. *Arthritis Rheum* **48**, 3522-3531 (2003).
8. Schmidt, W.A., Kraft, H.E., Vorpahl, K., Volker, L. & Gromnica-Ihle, E.J. Color duplex ultrasonography in the diagnosis of temporal arteritis. *N Engl J Med* **337**, 1336-1342 (1997).
9. Rubenstein, E., Maldini, C., Gonzalez-Chiappe, S., Chevret, S. & Mahr, A. Sensitivity of temporal artery biopsy in the diagnosis of giant cell arteritis: a systematic literature review and meta-analysis. *Rheumatology (Oxford)* **59**, 1011-1020 (2020).
10. Maleszewski, J.J. *et al.* Clinical and pathological evolution of giant cell arteritis: a prospective study of follow-up temporal artery biopsies in 40 treated patients. *Mod Pathol* **30**, 788-796 (2017).
11. van der Velden, V.H. Glucocorticoids: mechanisms of action and anti-inflammatory potential in asthma. *Mediators Inflamm* **7**, 229-237 (1998).
12. Ciccarone, F. *et al.* Age-dependent expression of DNMT1 and DNMT3B in PBMCs from a large European population enrolled in the MARK-AGE study. *Aging Cell* **15**, 755-765 (2016).
13. Petursdottir, V., Johansson, H., Nordborg, E. & Nordborg, C. The epidemiology of biopsy-positive giant cell arteritis: special reference to cyclic fluctuations. *Rheumatology (Oxford)* **38**, 1208-1212 (1999).
14. De Smit, E. *et al.* Geo-epidemiology of temporal artery biopsy-positive giant cell arteritis in Australia and New Zealand: is there a seasonal influence? *RMD Open* **3**, e000531 (2017).
15. Kizza, K. *et al.* Giant cell arteritis incidence: analysis by season and year in mid-Atlantic United States. *Clin Exp Ophthalmol* **41**, 577-581 (2013).

16. Powers, J.F., Bedri, S., Hussein, S., Salomon, R.N. & Tischler, A.S. High prevalence of herpes simplex virus DNA in temporal arteritis biopsy specimens. *Am J Clin Pathol* **123**, 261-264 (2005).
17. Duhaut, P., Bosshard, S. & Dumontet, C. Giant cell arteritis and polymyalgia rheumatica: role of viral infections. *Clin Exp Rheumatol* **18**, S22-23 (2000).
18. Wagner, A.D. *et al.* Detection of Chlamydia pneumoniae in giant cell vasculitis and correlation with the topographic arrangement of tissue-infiltrating dendritic cells. *Arthritis Rheum* **43**, 1543-1551 (2000).
19. Dababneh, A. *et al.* Giant cell arteritis and polymyalgia rheumatica can be differentiated by distinct patterns of HLA class II association. *J Rheumatol* **25**, 2140-2145 (1998).
20. Jacobsen, S. *et al.* Mannose-binding lectin variant alleles and HLA-DR4 alleles are associated with giant cell arteritis. *J Rheumatol* **29**, 2148-2153 (2002).
21. Mackie, S.L. *et al.* Association of HLA-DRB1 amino acid residues with giant cell arteritis: genetic association study, meta-analysis and geo-epidemiological investigation. *Arthritis Res Ther* **17**, 195 (2015).
22. Combe, B., Sany, J., Le Quellec, A., Clot, J. & Eliaou, J.F. Distribution of HLA-DRB1 alleles of patients with polymyalgia rheumatica and giant cell arteritis in a Mediterranean population. *J Rheumatol* **25**, 94-98 (1998).
23. Weyand, C.M., Hicok, K.C., Hunder, G.G. & Goronzy, J.J. The HLA-DRB1 locus as a genetic component in giant cell arteritis. Mapping of a disease-linked sequence motif to the antigen binding site of the HLA-DR molecule. *J Clin Invest* **90**, 2355-2361 (1992).
24. Gonzalez-Gay, M.A. Genetic epidemiology. Giant cell arteritis and polymyalgia rheumatica. *Arthritis Res* **3**, 154-157 (2001).
25. Boiardi, L. *et al.* Interleukin-10 promoter polymorphisms in giant cell arteritis. *Arthritis Rheum* **54**, 4011-4017 (2006).
26. Enjuanes, A. *et al.* Association of NOS2 and potential effect of VEGF, IL6, CCL2 and IL1RN polymorphisms and haplotypes on susceptibility to GCA--a simultaneous study of 130 potentially functional SNPs in 14 candidate genes. *Rheumatology (Oxford)* **51**, 841-851 (2012).
27. Marquez, A. *et al.* A candidate gene approach identifies an IL33 genetic variant as a novel genetic risk factor for GCA. *PLoS One* **9**, e113476 (2014).
28. Mattey, D.L. *et al.* Association of giant cell arteritis and polymyalgia rheumatica with different tumor necrosis factor microsatellite polymorphisms. *Arthritis Rheum* **43**, 1749-1755 (2000).
29. Gonzalez-Gay, M.A. *et al.* Corticotropin releasing hormone promoter polymorphisms in giant cell arteritis and polymyalgia rheumatica. *Clin Exp Rheumatol* **20**, 133-138 (2002).
30. Rueda, B., Miranda-Filloy, J.A., Martin, J. & Gonzalez-Gay, M.A. Association of CD24 gene polymorphisms with susceptibility to biopsy-proven giant cell arteritis. *J Rheumatol* **35**, 850-854 (2008).
31. Amoli, M.M., Garcia-Porrúa, C., Llorca, J., Ollier, W.E. & Gonzalez-Gay, M.A. Endothelial nitric oxide synthase haplotype associations in biopsy-proven giant cell arteritis. *J Rheumatol* **30**, 2019-2022 (2003).
32. Salvarani, C. *et al.* Intercellular adhesion molecule 1 gene polymorphisms in polymyalgia rheumatica/giant cell arteritis: association with disease risk and severity. *J Rheumatol* **27**, 1215-1221 (2000).
33. Boiardi, L. *et al.* Vascular endothelial growth factor gene polymorphisms in giant cell arteritis. *J Rheumatol* **30**, 2160-2164 (2003).
34. Coit, P., De Lott, L.B., Nan, B., Elner, V.M. & Sawalha, A.H. DNA methylation analysis of the temporal artery microenvironment in giant cell arteritis. *Ann Rheum Dis* **75**, 1196-1202 (2016).

35. Weyand, C.M., Liao, Y.J. & Goronzy, J.J. The immunopathology of giant cell arteritis: diagnostic and therapeutic implications. *J Neuroophthalmol* **32**, 259-265 (2012).
36. Ma-Krupa, W. *et al.* Activation of arterial wall dendritic cells and breakdown of self-tolerance in giant cell arteritis. *J Exp Med* **199**, 173-183 (2004).
37. Weyand, C.M. *et al.* Vascular dendritic cells in giant cell arteritis. *Ann N Y Acad Sci* **1062**, 195-208 (2005).
38. Deng, J., Younge, B.R., Olshen, R.A., Goronzy, J.J. & Weyand, C.M. Th17 and Th1 T-cell responses in giant cell arteritis. *Circulation* **121**, 906-915 (2010).
39. Terrier, B. *et al.* Interleukin-21 modulates Th1 and Th17 responses in giant cell arteritis. *Arthritis Rheum* **64**, 2001-2011 (2012).
40. Kaiser, M., Younge, B., Bjornsson, J., Goronzy, J.J. & Weyand, C.M. Formation of new vasa vasorum in vasculitis. Production of angiogenic cytokines by multinucleated giant cells. *Am J Pathol* **155**, 765-774 (1999).
41. Audia, S. *et al.* Preferential splenic CD8(+) T-cell activation in rituximab-nonresponder patients with immune thrombocytopenia. *Blood* **122**, 2477-2486 (2013).
42. Carneiro, H., da Silva, J.A. & Souto-Carneiro, M.M. Potential roles for CD8(+) T cells in rheumatoid arthritis. *Autoimmun Rev* **12**, 401-409 (2013).
43. Iking-Konert, C. *et al.* T lymphocytes in patients with primary vasculitis: expansion of CD8+ T cells with the propensity to activate polymorphonuclear neutrophils. *Rheumatology (Oxford)* **47**, 609-616 (2008).
44. Boita, M. *et al.* The molecular and functional characterization of clonally expanded CD8+ TCR BV T cells in eosinophilic granulomatosis with polyangiitis (EGPA). *Clin Immunol* **152**, 152-163 (2014).
45. Samson, M. *et al.* Involvement and prognosis value of CD8(+) T cells in giant cell arteritis. *J Autoimmun* **72**, 73-83 (2016).
46. Watanabe, R. *et al.* Pro-inflammatory and anti-inflammatory T cells in giant cell arteritis. *Joint Bone Spine* **84**, 421-426 (2017).
47. De Smit, E. *et al.* Longitudinal expression profiling of CD4+ and CD8+ cells in patients with active to quiescent giant cell arteritis. *BMC Med Genomics* **11**, 61 (2018).
48. Weyand, C.M., Hicok, K.C., Hunder, G.G. & Goronzy, J.J. Tissue cytokine patterns in patients with polymyalgia rheumatica and giant cell arteritis. *Ann Intern Med* **121**, 484-491 (1994).
49. Weyand, C.M. *et al.* Distinct vascular lesions in giant cell arteritis share identical T cell clonotypes. *J Exp Med* **179**, 951-960 (1994).
50. Samson, M. *et al.* Th1 and Th17 lymphocytes expressing CD161 are implicated in giant cell arteritis and polymyalgia rheumatica pathogenesis. *Arthritis Rheum* **64**, 3788-3798 (2012).
51. Macchioni, P. *et al.* Lymphocyte subpopulations analysis in peripheral blood in polymyalgia rheumatica/giant cell arteritis. *Br J Rheumatol* **32**, 666-670 (1993).
52. Elling, P., Olsson, A. & Elling, H. CD8+ T lymphocyte subset in giant cell arteritis and related disorders. *J Rheumatol* **17**, 225-227 (1990).
53. Dasgupta, B., Duke, O., Timms, A.M., Pitzalis, C. & Panayi, G.S. Selective depletion and activation of CD8+ lymphocytes from peripheral blood of patients with polymyalgia rheumatica and giant cell arteritis. *Ann Rheum Dis* **48**, 307-311 (1989).
54. Geest, K.v.d. Clues for a possible role of senescent T cells in giant cell arteritis pathogenesis. *Annals of the Rheumatic Diseases* **70** (2011).
55. van Sleen, Y. *et al.* Involvement of Monocyte Subsets in the Immunopathology of Giant Cell Arteritis. *Sci Rep* **7**, 6553 (2017).
56. Thomas, G., Tacke, R., Hedrick, C.C. & Hanna, R.N. Nonclassical patrolling monocyte function in the vasculature. *Arterioscler Thromb Vasc Biol* **35**, 1306-1316 (2015).
57. Ensan, S. *et al.* Self-renewing resident arterial macrophages arise from embryonic CX3CR1(+) precursors and circulating monocytes immediately after birth. *Nat Immunol* **17**, 159-168 (2016).

58. Rittner, H.L. *et al.* Tissue-destructive macrophages in giant cell arteritis. *Circ Res* **84**, 1050-1058 (1999).
59. Bauer, F. Illustrations of orchidaceous plants. *Ridegway, London* (1833-1838).
60. Brown, R. Observations on the organs and mode of fecundation in Orchideae and Asclepiadeae. *Trans Linn Soc Lond* **16**, 685-746 (1833).
61. Flemming, W. Zellsubstanz, Kern und Zelltheilung. *FCW Vogel, Leipzig* (1882).
62. Warner, J.R. The nucleolus and ribosome formation. *Curr Opin Cell Biol* **2**, 521-527 (1990).
63. Huang, S. & Spector, D.L. Intron-dependent recruitment of pre-mRNA splicing factors to sites of transcription. *J Cell Biol* **133**, 719-732 (1996).
64. Maul, G.G. Nuclear domain 10, the site of DNA virus transcription and replication. *Bioessays* **20**, 660-667 (1998).
65. Ruggero, D., Wang, Z.G. & Pandolfi, P.P. The puzzling multiple lives of PML and its role in the genesis of cancer. *Bioessays* **22**, 827-835 (2000).
66. Gall, J.G., Bellini, M., Wu, Z. & Murphy, C. Assembly of the nuclear transcription and processing machinery: Cajal bodies (coiled bodies) and transcriptosomes. *Mol Biol Cell* **10**, 4385-4402 (1999).
67. Gall, J.G. A role for Cajal bodies in assembly of the nuclear transcription machinery. *FEBS Lett* **498**, 164-167 (2001).
68. Boyle, S. *et al.* The spatial organization of human chromosomes within the nuclei of normal and emerin-mutant cells. *Hum Mol Genet* **10**, 211-219 (2001).
69. Kornberg, R.D. & Thomas, J.O. Chromatin structure; oligomers of the histones. *Science* **184**, 865-868 (1974).
70. Richmond, T.J., Finch, J.T., Rushton, B., Rhodes, D. & Klug, A. Structure of the nucleosome core particle at 7 Å resolution. *Nature* **311**, 532-537 (1984).
71. Kubai, D.F. Meiosis in *Sciara coprophila*: structure of the spindle and chromosome behavior during the first meiotic division. *J Cell Biol* **93**, 655-669 (1982).
72. Griffith, J.D. *et al.* Mammalian telomeres end in a large duplex loop. *Cell* **97**, 503-514 (1999).
73. Stansel, R.M., de Lange, T. & Griffith, J.D. T-loop assembly in vitro involves binding of TRF2 near the 3' telomeric overhang. *EMBO J* **20**, 5532-5540 (2001).
74. Blackburn, E.H. Telomere dynamics and genome instability in human cancer. *Cold Spring Harb Press, Plainview, NY* (1995).
75. Mable, B.K. Genpme duplication in amphibians and fish: an extended synthesis. *J. Zool* **284**, 151-182 (2011).
76. Otto, S.P. & Whitton, J. Polyploid incidence and evolution. *Annu Rev Genet* **34**, 401-437 (2000).
77. Soltis, D.E., Visger, C.J. & Soltis, P.S. The polyploidy revolution then...and now: Stebbins revisited. *Am J Bot* **101**, 1057-1078 (2014).
78. Matsumoto, T., Wakefield, L., Tarlow, B.D. & Grompe, M. In Vivo Lineage Tracing of Polyploid Hepatocytes Reveals Extensive Proliferation during Liver Regeneration. *Cell Stem Cell* **26**, 34-47 e33 (2020).
79. Gentric, G., Celton-Morizur, S. & Desdouets, C. Polyploidy and liver proliferation. *Clin Res Hepatol Gastroenterol* **36**, 29-34 (2012).
80. Gupta, S. Hepatic polyploidy and liver growth control. *Semin Cancer Biol* **10**, 161-171 (2000).
81. Losick, V.P. Wound-Induced Polyploidy Is Required for Tissue Repair. *Adv Wound Care (New Rochelle)* **5**, 271-278 (2016).
82. Losick, V.P., Fox, D.T. & Spradling, A.C. Polyploidization and cell fusion contribute to wound healing in the adult *Drosophila* epithelium. *Curr Biol* **23**, 2224-2232 (2013).
83. Orr-Weaver, T.L. When bigger is better: the role of polyploidy in organogenesis. *Trends Genet* **31**, 307-315 (2015).
84. Zhurinsky, J. *et al.* A coordinated global control over cellular transcription. *Curr Biol* **20**, 2010-2015 (2010).

85. Mittal, K. *et al.* Multinucleated polyploidy drives resistance to Docetaxel chemotherapy in prostate cancer. *Br J Cancer* **116**, 1186-1194 (2017).
86. Yao, C.H. *et al.* Mitochondrial fusion supports increased oxidative phosphorylation during cell proliferation. *Elife* **8** (2019).
87. Baum, H.P. & Thoenes, W. Differentiation of granuloma cells (epithelioid cells and multinucleated giant cells): a morphometric analysis. Investigations using the model of experimental autoimmune (anti-TBM) tubulo-interstitial nephritis. *Virchows Arch B Cell Pathol Incl Mol Pathol* **50**, 181-192 (1985).
88. Sutton, J.S. & Weiss, L. Transformation of monocytes in tissue culture into macrophages, epithelioid cells, and multinucleated giant cells. An electron microscope study. *J Cell Biol* **28**, 303-332 (1966).
89. Unhavaithaya, Y. & Orr-Weaver, T.L. Polyploidization of glia in neural development links tissue growth to blood-brain barrier integrity. *Genes Dev* **26**, 31-36 (2012).
90. Barlow, P.W. & Sherman, M.I. The biochemistry of differentiation of mouse trophoblast: studies on polyploidy. *J Embryol Exp Morphol* **27**, 447-465 (1972).
91. Zybina, T.G. & Zybina, E.V. Cell reproduction and genome multiplication in the proliferative and invasive trophoblast cell populations of mammalian placenta. *Cell Biol Int* **29**, 1071-1083 (2005).
92. Zanet, J. *et al.* A mitosis block links active cell cycle with human epidermal differentiation and results in endoreplication. *PLoS One* **5**, e15701 (2010).
93. Laiho, M. & Latonen, L. Cell cycle control, DNA damage checkpoints and cancer. *Ann Med* **35**, 391-397 (2003).
94. Sudakin, V., Chan, G.K. & Yen, T.J. Checkpoint inhibition of the APC/C in HeLa cells is mediated by a complex of BUBR1, BUB3, CDC20, and MAD2. *J Cell Biol* **154**, 925-936 (2001).
95. Collin, P., Nashchekina, O., Walker, R. & Pines, J. The spindle assembly checkpoint works like a rheostat rather than a toggle switch. *Nat Cell Biol* **15**, 1378-1385 (2013).
96. Carmena, M. Cytokinesis: the final stop for the chromosomal passengers. *Biochem Soc Trans* **36**, 367-370 (2008).
97. Steigemann, P. *et al.* Aurora B-mediated abscission checkpoint protects against tetraploidization. *Cell* **136**, 473-484 (2009).
98. Holt, D.J. & Grainger, D.W. Multinucleated giant cells from fibroblast cultures. *Biomaterials* **32**, 3977-3987 (2011).
99. Herrtwich, L. *et al.* DNA Damage Signaling Instructs Polyploid Macrophage Fate in Granulomas. *Cell* **167**, 1264-1280 e1218 (2016).
100. Margall-Ducos, G., Celton-Morizur, S., Couton, D., Bregerie, O. & Desdouets, C. Liver tetraploidization is controlled by a new process of incomplete cytokinesis. *J Cell Sci* **120**, 3633-3639 (2007).
101. Rappaport, R. Establishment of the mechanism of cytokinesis in animal cells. *Int Rev Cytol* **105**, 245-281 (1986).
102. Danowski, B.A. Fibroblast contractility and actin organization are stimulated by microtubule inhibitors. *J Cell Sci* **93 (Pt 2)**, 255-266 (1989).
103. Bringmann, H. & Hyman, A.A. A cytokinesis furrow is positioned by two consecutive signals. *Nature* **436**, 731-734 (2005).
104. Kamijo, K. *et al.* Dissecting the role of Rho-mediated signaling in contractile ring formation. *Mol Biol Cell* **17**, 43-55 (2006).
105. Yonemura, S., Hirao-Minakuchi, K. & Nishimura, Y. Rho localization in cells and tissues. *Exp Cell Res* **295**, 300-314 (2004).
106. Bement, W.M., Benink, H.A. & von Dassow, G. A microtubule-dependent zone of active RhoA during cleavage plane specification. *J Cell Biol* **170**, 91-101 (2005).

107. Mishima, M., Kaitna, S. & Glotzer, M. Central spindle assembly and cytokinesis require a kinesin-like protein/RhoGAP complex with microtubule bundling activity. *Dev Cell* **2**, 41-54 (2002).
108. Saito, S. *et al.* Deregulation and mislocalization of the cytokinesis regulator ECT2 activate the Rho signaling pathways leading to malignant transformation. *J Biol Chem* **279**, 7169-7179 (2004).
109. Yuce, O., Piekny, A. & Glotzer, M. An ECT2-centralspindlin complex regulates the localization and function of RhoA. *J Cell Biol* **170**, 571-582 (2005).
110. Guidotti, J.E. *et al.* Liver cell polyploidization: a pivotal role for binuclear hepatocytes. *J Biol Chem* **278**, 19095-19101 (2003).
111. Kaplan, K.B. *et al.* A role for the Adenomatous Polyposis Coli protein in chromosome segregation. *Nat Cell Biol* **3**, 429-432 (2001).
112. Green, R.A. & Kaplan, K.B. Chromosome instability in colorectal tumor cells is associated with defects in microtubule plus-end attachments caused by a dominant mutation in APC. *J Cell Biol* **163**, 949-961 (2003).
113. Wagner, E. & Glotzer, M. Local RhoA activation induces cytokinetic furrows independent of spindle position and cell cycle stage. *J Cell Biol* **213**, 641-649 (2016).
114. Alberts, A.S. Identification of a carboxyl-terminal diaphanous-related formin homology protein autoregulatory domain. *J Biol Chem* **276**, 2824-2830 (2001).
115. Tominaga, T. *et al.* Diaphanous-related formins bridge Rho GTPase and Src tyrosine kinase signaling. *Mol Cell* **5**, 13-25 (2000).
116. Watanabe, N. *et al.* p140mDia, a mammalian homolog of Drosophila diaphanous, is a target protein for Rho small GTPase and is a ligand for profilin. *EMBO J* **16**, 3044-3056 (1997).
117. Straight, A.F. *et al.* Dissecting temporal and spatial control of cytokinesis with a myosin II Inhibitor. *Science* **299**, 1743-1747 (2003).
118. Straight, A.F., Field, C.M. & Mitchison, T.J. Anillin binds nonmuscle myosin II and regulates the contractile ring. *Mol Biol Cell* **16**, 193-201 (2005).
119. Field, C.M. & Alberts, B.M. Anillin, a contractile ring protein that cycles from the nucleus to the cell cortex. *J Cell Biol* **131**, 165-178 (1995).
120. Engel, F.B., Schebesta, M. & Keating, M.T. Anillin localization defect in cardiomyocyte binucleation. *J Mol Cell Cardiol* **41**, 601-612 (2006).
121. Gonzalez, M.E. *et al.* High SEPT9_v1 expression in human breast cancer cells is associated with oncogenic phenotypes. *Cancer Res* **67**, 8554-8564 (2007).
122. Silio, V., Marques, M., Cortes, I., Zuluaga, S. & Carrera, A.C. A cascade involving p85, Cdc42 and septin 2 regulates cytokinesis. *Biochem Soc Trans* **35**, 222-224 (2007).
123. Mollinari, C. *et al.* PRC1 is a microtubule binding and bundling protein essential to maintain the mitotic spindle midzone. *J Cell Biol* **157**, 1175-1186 (2002).
124. Julian, M. *et al.* gamma-Tubulin participates in the formation of the midbody during cytokinesis in mammalian cells. *J Cell Sci* **105 (Pt 1)**, 145-156 (1993).
125. Mollinari, C. *et al.* Ablation of PRC1 by small interfering RNA demonstrates that cytokinetic abscission requires a central spindle bundle in mammalian cells, whereas completion of furrowing does not. *Mol Biol Cell* **16**, 1043-1055 (2005).
126. Skop, A.R., Liu, H., Yates, J., 3rd, Meyer, B.J. & Heald, R. Dissection of the mammalian midbody proteome reveals conserved cytokinesis mechanisms. *Science* **305**, 61-66 (2004).
127. Conner, S.D. & Wessel, G.M. Syntaxin is required for cell division. *Mol Biol Cell* **10**, 2735-2743 (1999).
128. Li, W.M., Webb, S.E., Lee, K.W. & Miller, A.L. Recruitment and SNARE-mediated fusion of vesicles in furrow membrane remodeling during cytokinesis in zebrafish embryos. *Exp Cell Res* **312**, 3260-3275 (2006).
129. Echard, A., Hickson, G.R., Foley, E. & O'Farrell, P.H. Terminal cytokinesis events uncovered after an RNAi screen. *Curr Biol* **14**, 1685-1693 (2004).

130. Low, S.H. *et al.* Syntaxin 2 and endobrevin are required for the terminal step of cytokinesis in mammalian cells. *Dev Cell* **4**, 753-759 (2003).
131. Dukes, J.D., Richardson, J.D., Simmons, R. & Whitley, P. A dominant-negative ESCRT-III protein perturbs cytokinesis and trafficking to lysosomes. *Biochem J* **411**, 233-239 (2008).
132. Fabbro, M. *et al.* Cdk1/Erk2- and Plk1-dependent phosphorylation of a centrosome protein, Cep55, is required for its recruitment to midbody and cytokinesis. *Dev Cell* **9**, 477-488 (2005).
133. Morita, E. *et al.* Human ESCRT and ALIX proteins interact with proteins of the midbody and function in cytokinesis. *EMBO J* **26**, 4215-4227 (2007).
134. Carlton, J.G. & Martin-Serrano, J. Parallels between cytokinesis and retroviral budding: a role for the ESCRT machinery. *Science* **316**, 1908-1912 (2007).
135. Fox, D.T. & Duronio, R.J. Endoreplication and polyploidy: insights into development and disease. *Development* **140**, 3-12 (2013).
136. Joubes, J. & Chevalier, C. Endoreduplication in higher plants. *Plant Mol Biol* **43**, 735-745 (2000).
137. Yin, L., Gater, S.T. & Karrer, K.M. A developmentally regulated gene, ASI2, is required for endocycling in the macronuclear anlagen of Tetrahymena. *Eukaryot Cell* **9**, 1343-1353 (2010).
138. Zielke, N., Edgar, B.A. & DePamphilis, M.L. Endoreplication. *Cold Spring Harb Perspect Biol* **5**, a012948 (2013).
139. Nowicka, A. *et al.* Dynamics of endoreduplication in developing barley seeds. *J Exp Bot* **72**, 268-282 (2021).
140. Larkins, B.A. *et al.* Investigating the hows and whys of DNA endoreduplication. *J Exp Bot* **52**, 183-192 (2001).
141. Rewers, M. & Sliwiska, E. Endoreduplication intensity as a marker of seed developmental stage in the Fabaceae. *Cytometry A* **81**, 1067-1075 (2012).
142. Nern, C. *et al.* Fusion of hematopoietic cells with Purkinje neurons does not lead to stable heterokaryon formation under noninvasive conditions. *J Neurosci* **29**, 3799-3807 (2009).
143. Kashofer, K., Siapati, E.K. & Bonnet, D. In vivo formation of unstable heterokaryons after liver damage and hematopoietic stem cell/progenitor transplantation. *Stem Cells* **24**, 1104-1112 (2006).
144. Helming, L. & Gordon, S. The molecular basis of macrophage fusion. *Immunobiology* **212**, 785-793 (2007).
145. Shen, Z. *et al.* The role played by cell-substrate interactions in the pathogenesis of osteoclast-mediated peri-implant osteolysis. *Arthritis Res Ther* **8**, R70 (2006).
146. Kukita, T. *et al.* RANKL-induced DC-STAMP is essential for osteoclastogenesis. *J Exp Med* **200**, 941-946 (2004).
147. Byrd, T.F. Multinucleated giant cell formation induced by IFN-gamma/IL-3 is associated with restriction of virulent Mycobacterium tuberculosis cell to cell invasion in human monocyte monolayers. *Cell Immunol* **188**, 89-96 (1998).
148. Yagi, M. *et al.* Induction of DC-STAMP by alternative activation and downstream signaling mechanisms. *J Bone Miner Res* **22**, 992-1001 (2007).
149. Moreno, J.L., Mikhailenko, I., Tondravi, M.M. & Keegan, A.D. IL-4 promotes the formation of multinucleated giant cells from macrophage precursors by a STAT6-dependent, homotypic mechanism: contribution of E-cadherin. *J Leukoc Biol* **82**, 1542-1553 (2007).
150. Helming, L. *et al.* Essential role of DAP12 signaling in macrophage programming into a fusion-competent state. *Sci Signal* **1**, ra11 (2008).
151. Kyriakides, T.R. *et al.* The CC chemokine ligand, CCL2/MCP1, participates in macrophage fusion and foreign body giant cell formation. *Am J Pathol* **165**, 2157-2166 (2004).
152. Kim, M.S., Day, C.J. & Morrison, N.A. MCP-1 is induced by receptor activator of nuclear factor- κ B ligand, promotes human osteoclast fusion, and rescues granulocyte

- macrophage colony-stimulating factor suppression of osteoclast formation. *J Biol Chem* **280**, 16163-16169 (2005).
153. Miyamoto, K. *et al.* MCP-1 expressed by osteoclasts stimulates osteoclastogenesis in an autocrine/paracrine manner. *Biochem Biophys Res Commun* **383**, 373-377 (2009).
 154. Siddiqui, J.A. & Partridge, N.C. CCL2/Monocyte Chemoattractant Protein 1 and Parathyroid Hormone Action on Bone. *Front Endocrinol (Lausanne)* **8**, 49 (2017).
 155. Binder, N.B. *et al.* Estrogen-dependent and C-C chemokine receptor-2-dependent pathways determine osteoclast behavior in osteoporosis. *Nat Med* **15**, 417-424 (2009).
 156. Rhee, I., Davidson, D., Souza, C.M., Vacher, J. & Veillette, A. Macrophage fusion is controlled by the cytoplasmic protein tyrosine phosphatase PTP-PEST/PTPN12. *Mol Cell Biol* **33**, 2458-2469 (2013).
 157. Mbalaviele, G., Chen, H., Boyce, B.F., Mundy, G.R. & Yoneda, T. The role of cadherin in the generation of multinucleated osteoclasts from mononuclear precursors in murine marrow. *J Clin Invest* **95**, 2757-2765 (1995).
 158. Hynes, R.O. Integrins: bidirectional, allosteric signaling machines. *Cell* **110**, 673-687 (2002).
 159. Puissegur, M.P. *et al.* Mycobacterial lipomannan induces granuloma macrophage fusion via a TLR2-dependent, ADAM9- and beta1 integrin-mediated pathway. *J Immunol* **178**, 3161-3169 (2007).
 160. McNally, A.K. & Anderson, J.M. Beta1 and beta2 integrins mediate adhesion during macrophage fusion and multinucleated foreign body giant cell formation. *Am J Pathol* **160**, 621-630 (2002).
 161. Kim, S. *et al.* A critical function for the actin cytoskeleton in targeted exocytosis of prefusion vesicles during myoblast fusion. *Dev Cell* **12**, 571-586 (2007).
 162. Erickson, M.R., Galletta, B.J. & Abmayr, S.M. Drosophila myoblast city encodes a conserved protein that is essential for myoblast fusion, dorsal closure, and cytoskeletal organization. *J Cell Biol* **138**, 589-603 (1997).
 163. Richardson, B.E., Beckett, K., Nowak, S.J. & Baylies, M.K. SCAR/WAVE and Arp2/3 are crucial for cytoskeletal remodeling at the site of myoblast fusion. *Development* **134**, 4357-4367 (2007).
 164. Jay, S.M., Skokos, E., Laiwalla, F., Krady, M.M. & Kyriakides, T.R. Foreign body giant cell formation is preceded by lamellipodia formation and can be attenuated by inhibition of Rac1 activation. *Am J Pathol* **171**, 632-640 (2007).
 165. Rodriguez-Perez, F. *et al.* Ubiquitin-dependent remodeling of the actin cytoskeleton drives cell fusion. *Dev Cell* **56**, 588-601 e589 (2021).
 166. van den Eijnde, S.M. *et al.* Transient expression of phosphatidylserine at cell-cell contact areas is required for myotube formation. *J Cell Sci* **114**, 3631-3642 (2001).
 167. Helming, L., Winter, J. & Gordon, S. The scavenger receptor CD36 plays a role in cytokine-induced macrophage fusion. *J Cell Sci* **122**, 453-459 (2009).
 168. Fais, S. *et al.* Multinucleated giant cells generation induced by interferon-gamma. Changes in the expression and distribution of the intercellular adhesion molecule-1 during macrophages fusion and multinucleated giant cell formation. *Lab Invest* **71**, 737-744 (1994).
 169. DesJardin, L.E. *et al.* Mycobacterium tuberculosis-infected human macrophages exhibit enhanced cellular adhesion with increased expression of LFA-1 and ICAM-1 and reduced expression and/or function of complement receptors, FcγRII and the mannose receptor. *Microbiology (Reading)* **148**, 3161-3171 (2002).
 170. Tachibana, I. & Hemler, M.E. Role of transmembrane 4 superfamily (TM4SF) proteins CD9 and CD81 in muscle cell fusion and myotube maintenance. *J Cell Biol* **146**, 893-904 (1999).
 171. Le Naour, F., Rubinstein, E., Jasmin, C., Prenant, M. & Boucheix, C. Severely reduced female fertility in CD9-deficient mice. *Science* **287**, 319-321 (2000).

172. Miller, B.J., Georges-Labouesse, E., Primakoff, P. & Myles, D.G. Normal fertilization occurs with eggs lacking the integrin alpha6beta1 and is CD9-dependent. *J Cell Biol* **149**, 1289-1296 (2000).
173. Takeda, Y. *et al.* Tetraspanins CD9 and CD81 function to prevent the fusion of mononuclear phagocytes. *J Cell Biol* **161**, 945-956 (2003).
174. Weng, J., Kremontsov, D.N., Khurana, S., Roy, N.H. & Thali, M. Formation of syncytia is repressed by tetraspanins in human immunodeficiency virus type 1-producing cells. *J Virol* **83**, 7467-7474 (2009).
175. Hulme, R.S., Higginbottom, A., Palmer, J., Partridge, L.J. & Monk, P.N. Distinct regions of the large extracellular domain of tetraspanin CD9 are involved in the control of human multinucleated giant cell formation. *PLoS One* **9**, e116289 (2014).
176. Singethan, K. *et al.* CD9 clustering and formation of microvilli zippers between contacting cells regulates virus-induced cell fusion. *Traffic* **9**, 924-935 (2008).
177. Ishii, M. *et al.* RANKL-induced expression of tetraspanin CD9 in lipid raft membrane microdomain is essential for cell fusion during osteoclastogenesis. *J Bone Miner Res* **21**, 965-976 (2006).
178. Tippett, E., Cameron, P.U., Marsh, M. & Crowe, S.M. Characterization of tetraspanins CD9, CD53, CD63, and CD81 in monocytes and macrophages in HIV-1 infection. *J Leukoc Biol* **93**, 913-920 (2013).
179. MacLauchlan, S. *et al.* Macrophage fusion, giant cell formation, and the foreign body response require matrix metalloproteinase 9. *J Leukoc Biol* **85**, 617-626 (2009).
180. Han, X. *et al.* CD47, a ligand for the macrophage fusion receptor, participates in macrophage multinucleation. *J Biol Chem* **275**, 37984-37992 (2000).
181. Cui, W. *et al.* The intracellular domain of CD44 promotes the fusion of macrophages. *Blood* **107**, 796-805 (2006).
182. Bord, S., Horner, A., Hembry, R.M., Reynolds, J.J. & Compston, J.E. Production of collagenase by human osteoblasts and osteoclasts in vivo. *Bone* **19**, 35-40 (1996).
183. Cegielski, M., Izykowska, I., Podhorska-Okolow, M., Zabel, M. & Dziegiel, P. Development of foreign body giant cells in response to implantation of Spongostan as a scaffold for cartilage tissue engineering. *In Vivo* **22**, 203-206 (2008).
184. Villa, A., Guerrini, M.M., Cassani, B., Pangrazio, A. & Sobacchi, C. Infantile malignant, autosomal recessive osteopetrosis: the rich and the poor. *Calcif Tissue Int* **84**, 1-12 (2009).
185. Sobacchi, C. *et al.* Osteoclast-poor human osteopetrosis due to mutations in the gene encoding RANKL. *Nat Genet* **39**, 960-962 (2007).
186. Geurts, J. *et al.* Elevated marrow inflammatory cells and osteoclasts in subchondral osteosclerosis in human knee osteoarthritis. *J Orthop Res* **34**, 262-269 (2016).
187. Weir, E.C. *et al.* Macrophage colony-stimulating factor release and receptor expression in bone cells. *J Bone Miner Res* **8**, 1507-1518 (1993).
188. Ross, F.P. M-CSF, c-Fms, and signaling in osteoclasts and their precursors. *Ann N Y Acad Sci* **1068**, 110-116 (2006).
189. Wada, T., Nakashima, T., Hiroshi, N. & Penninger, J.M. RANKL-RANK signaling in osteoclastogenesis and bone disease. *Trends Mol Med* **12**, 17-25 (2006).
190. Boyde, A., Ali, N.N. & Jones, S.J. Resorption of dentine by isolated osteoclasts in vitro. *Br Dent J* **156**, 216-220 (1984).
191. Chambers, T.J., Revell, P.A., Fuller, K. & Athanasou, N.A. Resorption of bone by isolated rabbit osteoclasts. *J Cell Sci* **66**, 383-399 (1984).
192. Arnett, T.R. & Dempster, D.W. A comparative study of disaggregated chick and rat osteoclasts in vitro: effects of calcitonin and prostaglandins. *Endocrinology* **120**, 602-608 (1987).
193. Collin-Osdoby, P. & Osdoby, P. RANKL-mediated osteoclast formation from murine RAW 264.7 cells. *Methods Mol Biol* **816**, 187-202 (2012).

194. Grigoriadis, A.E. *et al.* Directed differentiation of hematopoietic precursors and functional osteoclasts from human ES and iPS cells. *Blood* **115**, 2769-2776 (2010).
195. Marino, S., Logan, J.G., Mellis, D. & Capulli, M. Generation and culture of osteoclasts. *Bonekey Rep* **3**, 570 (2014).
196. Lomaga, M.A. *et al.* TRAF6 deficiency results in osteopetrosis and defective interleukin-1, CD40, and LPS signaling. *Genes Dev* **13**, 1015-1024 (1999).
197. Mizukami, J. *et al.* Receptor activator of NF-kappaB ligand (RANKL) activates TAK1 mitogen-activated protein kinase kinase through a signaling complex containing RANK, TAB2, and TRAF6. *Mol Cell Biol* **22**, 992-1000 (2002).
198. Huang, H. *et al.* Osteoclast differentiation requires TAK1 and MKK6 for NFATc1 induction and NF-kappaB transactivation by RANKL. *Cell Death Differ* **13**, 1879-1891 (2006).
199. Takayanagi, H. The role of NFAT in osteoclast formation. *Ann N Y Acad Sci* **1116**, 227-237 (2007).
200. Rodriguez, G. & Arias, V. Giant cells lepromatous leprosy. Diffuse dermatitis with exuberant foreign body giant cells in treated lepromatous leprosy. *Biomedica* **39**, 26-31 (2019).
201. Milde, R. *et al.* Multinucleated Giant Cells Are Specialized for Complement-Mediated Phagocytosis and Large Target Destruction. *Cell Rep* **13**, 1937-1948 (2015).
202. Chambers, T.J. Studies on the phagocytic capacity of macrophage polykaryons. *J Pathol* **123**, 65-77 (1977).
203. Schlesinger, L., Musson, R.A. & Johnston, R.B., Jr. Functional and biochemical studies of multinucleated giant cells derived from the culture of human monocytes. *J Exp Med* **159**, 1289-1294 (1984).
204. Luttkhuizen, D.T., Harmsen, M.C. & Van Luyn, M.J. Cellular and molecular dynamics in the foreign body reaction. *Tissue Eng* **12**, 1955-1970 (2006).
205. Anderson, F.M. Biological Responses to Materials. *Annu Rev Mater Res.* **31**, 81-110 (2001).
206. Zhao, O.H., Anderson, J.M., Hiltner, A., Lodoen, G.A. & Payet, C.R. Theoretical analysis on cell size distribution and kinetics of foreign-body giant cell formation in vivo on polyurethane elastomers. *J Biomed Mater Res* **26**, 1019-1038 (1992).
207. McNally, A.K. & Anderson, J.M. Interleukin-4 induces foreign body giant cells from human monocytes/macrophages. Differential lymphokine regulation of macrophage fusion leads to morphological variants of multinucleated giant cells. *Am J Pathol* **147**, 1487-1499 (1995).
208. DeFife, K.M., Jenney, C.R., Colton, E. & Anderson, J.M. Cytoskeletal and adhesive structural polarizations accompany IL-13-induced human macrophage fusion. *J Histochem Cytochem* **47**, 65-74 (1999).
209. Okamoto, H., Mizuno, K. & Horio, T. Langhans-type and foreign-body-type multinucleated giant cells in cutaneous lesions of sarcoidosis. *Acta Derm Venereol* **83**, 171-174 (2003).
210. Enelow, R.I., Sullivan, G.W., Carper, H.T. & Mandell, G.L. Induction of multinucleated giant cell formation from in vitro culture of human monocytes with interleukin-3 and interferon-gamma: comparison with other stimulating factors. *Am J Respir Cell Mol Biol* **6**, 57-62 (1992).
211. Postlethwaite, A.E., Jackson, B.K., Beachey, E.H. & Kang, A.H. Formation of multinucleated giant cells from human monocyte precursors. Mediation by a soluble protein from antigen- and mitogen-stimulated lymphocytes. *J Exp Med* **155**, 168-178 (1982).
212. Most, J. *et al.* Formation of multinucleated giant cells in vitro is dependent on the stage of monocyte to macrophage maturation. *Blood* **89**, 662-671 (1997).
213. Champion, T.C. *et al.* Monocyte Subsets Have Distinct Patterns of Tetraspanin Expression and Different Capacities to Form Multinucleate Giant Cells. *Front Immunol* **9**, 1247 (2018).
214. Wang, H. *et al.* Cellular, Molecular, and Immunological Characteristics of Langhans Multinucleated Giant Cells Programmed by IL-15. *J Invest Dermatol* **140**, 1824-1836 e1827 (2020).
215. Yagi, M. *et al.* DC-STAMP is essential for cell-cell fusion in osteoclasts and foreign body giant cells. *J Exp Med* **202**, 345-351 (2005).

216. Thoenes, W., Sonntag, W., Heine, W.D. & Langer, K.H. Cell fusion as a mechanism for the formation of giant cells (Langhans' type). Autoradiographic findings in autoimmune tubulo-interstitial nephritis of the rat. *Virchows Arch B Cell Pathol Incl Mol Pathol* **41**, 45-50 (1982).
217. Langer, K.H. & Thoenes, W. Characterization of cells involved in the formation of granuloma. An ultrastructural study on macrophages, epithelioid cells, and giant cells in experimental tubulo-interstitial nephritis. *Virchows Arch B Cell Pathol Incl Mol Pathol* **36**, 177-194 (1981).
218. Lordier, L. *et al.* Megakaryocyte endomitosis is a failure of late cytokinesis related to defects in the contractile ring and Rho/Rock signaling. *Blood* **112**, 3164-3174 (2008).
219. Sher, N. *et al.* Fundamental differences in endoreplication in mammals and Drosophila revealed by analysis of endocycling and endomitotic cells. *Proc Natl Acad Sci U S A* **110**, 9368-9373 (2013).
220. Rodriguez-Pla, A. *et al.* Metalloproteinase-2 and -9 in giant cell arteritis: involvement in vascular remodeling. *Circulation* **112**, 264-269 (2005).
221. Kaiser, M., Weyand, C.M., Bjornsson, J. & Goronzy, J.J. Platelet-derived growth factor, intimal hyperplasia, and ischemic complications in giant cell arteritis. *Arthritis Rheum* **41**, 623-633 (1998).
222. Smets, P. *et al.* Vascular endothelial growth factor levels and rheumatic diseases of the elderly. *Arthritis Res Ther* **18**, 283 (2016).
223. Mariano, M. & Spector, W.G. The formation and properties of macrophage polykaryons (inflammatory giant cells). *J Pathol* **113**, 1-19 (1974).
224. van der Rhee, H.J., Hillebrands, W. & Daems, W.T. Are Langhans giant cells precursors of foreign-body giant cells? *Arch Dermatol Res* **263**, 13-21 (1978).
225. Murch, A.R., Grounds, M.D., Marshall, C.A. & Papadimitriou, J.M. Direct evidence that inflammatory multinucleate giant cells form by fusion. *J Pathol* **137**, 177-180 (1982).
226. Warfel, A.H. Macrophage fusion and multinucleated giant cell formation, surface morphology. *Exp Mol Pathol* **28**, 163-176 (1978).
227. Gasser, A. & Most, J. Generation of multinucleated giant cells in vitro by culture of human monocytes with Mycobacterium bovis BCG in combination with cytokine-containing supernatants. *Infect Immun* **67**, 395-402 (1999).
228. Lay, G. *et al.* Langhans giant cells from M. tuberculosis-induced human granulomas cannot mediate mycobacterial uptake. *J Pathol* **211**, 76-85 (2007).
229. Sakai, H. *et al.* The CD40-CD40L axis and IFN-gamma play critical roles in Langhans giant cell formation. *Int Immunol* **24**, 5-15 (2012).
230. Mezouar, S., Diarra, I., Roudier, J., Desnues, B. & Mege, J.L. Tumor Necrosis Factor-Alpha Antagonist Interferes With the Formation of Granulomatous Multinucleated Giant Cells: New Insights Into Mycobacterium tuberculosis Infection. *Front Immunol* **10**, 1947 (2019).
231. Fais, S. *et al.* Interferon expression in Crohn's disease patients: increased interferon-gamma and -alpha mRNA in the intestinal lamina propria mononuclear cells. *J Interferon Res* **14**, 235-238 (1994).
232. Rozenblatt-Rosen, O., Stubbington, M.J.T., Regev, A. & Teichmann, S.A. The Human Cell Atlas: from vision to reality. *Nature* **550**, 451-453 (2017).
233. Wang, L. *et al.* ROS-producing immature neutrophils in giant cell arteritis are linked to vascular pathologies. *JCI Insight* **5** (2020).
234. Levaot, N. *et al.* Osteoclast fusion is initiated by a small subset of RANKL-stimulated monocyte progenitors, which can fuse to RANKL-unstimulated progenitors. *Bone* **79**, 21-28 (2015).
235. Pampalona, J., Soler, D., Genesca, A. & Tusell, L. Telomere dysfunction and chromosome structure modulate the contribution of individual chromosomes in abnormal nuclear morphologies. *Mutat Res* **683**, 16-22 (2010).
236. Geddis, A.E. & Kaushansky, K. Endomitotic megakaryocytes form a midzone in anaphase but have a deficiency in cleavage furrow formation. *Cell Cycle* **5**, 538-545 (2006).

237. Lordier, L. *et al.* Presence of a defect in karyokinesis during megakaryocyte endomitosis. *Cell Cycle* **11**, 4385-4389 (2012).
238. Pandit, S.K., Westendorp, B. & de Bruin, A. Physiological significance of polyploidization in mammalian cells. *Trends Cell Biol* **23**, 556-566 (2013).
239. Mah, L.J., El-Osta, A. & Karagiannis, T.C. gammaH2AX: a sensitive molecular marker of DNA damage and repair. *Leukemia* **24**, 679-686 (2010).
240. Zeman, M.K. & Cimprich, K.A. Causes and consequences of replication stress. *Nat Cell Biol* **16**, 2-9 (2014).
241. Davoli, T., Denchi, E.L. & de Lange, T. Persistent telomere damage induces bypass of mitosis and tetraploidy. *Cell* **141**, 81-93 (2010).
242. Novak, B. & Tyson, J.J. Numerical analysis of a comprehensive model of M-phase control in *Xenopus* oocyte extracts and intact embryos. *J Cell Sci* **106 (Pt 4)**, 1153-1168 (1993).
243. Sfeir, A. & de Lange, T. Removal of shelterin reveals the telomere end-protection problem. *Science* **336**, 593-597 (2012).
244. Pampalona, J. *et al.* Chromosome Bridges Maintain Kinetochores-Microtubule Attachment throughout Mitosis and Rarely Break during Anaphase. *PLoS One* **11**, e0147420 (2016).
245. Maciejowski, J., Li, Y., Bosco, N., Campbell, P.J. & de Lange, T. Chromothripsis and Kataegis Induced by Telomere Crisis. *Cell* **163**, 1641-1654 (2015).
246. Stroik, S. & Hendrickson, E.A. Telomere fusions and translocations: a bridge too far? *Curr Opin Genet Dev* **60**, 85-91 (2020).
247. Umbreit, N.T. *et al.* Mechanisms generating cancer genome complexity from a single cell division error. *Science* **368** (2020).
248. Yang, H., Wang, H., Ren, J., Chen, Q. & Chen, Z.J. cGAS is essential for cellular senescence. *Proc Natl Acad Sci U S A* **114**, E4612-E4620 (2017).
249. Bai, J. *et al.* Actin reduction by MsrB2 is a key component of the cytokinetic abscission checkpoint and prevents tetraploidy. *Proc Natl Acad Sci U S A* **117**, 4169-4179 (2020).
250. Lukas, C. *et al.* 53BP1 nuclear bodies form around DNA lesions generated by mitotic transmission of chromosomes under replication stress. *Nat Cell Biol* **13**, 243-253 (2011).
251. Nazarewicz, R.R. *et al.* Does scavenging of mitochondrial superoxide attenuate cancer prosurvival signaling pathways? *Antioxid Redox Signal* **19**, 344-349 (2013).
252. Steinbeck, M.J., Appel, W.H., Jr., Verhoeven, A.J. & Karnovsky, M.J. NADPH-oxidase expression and in situ production of superoxide by osteoclasts actively resorbing bone. *J Cell Biol* **126**, 765-772 (1994).
253. Kreipe, H. *et al.* Multinucleated giant cells generated in vitro. Terminally differentiated macrophages with down-regulated c-fms expression. *Am J Pathol* **130**, 232-243 (1988).
254. Darden, A.G., Ries, W.L., Wolf, W.C., Rodriguiz, R.M. & Key, L.L., Jr. Osteoclastic superoxide production and bone resorption: stimulation and inhibition by modulators of NADPH oxidase. *J Bone Miner Res* **11**, 671-675 (1996).
255. Zhu, X.W., Price, N.M., Gilman, R.H., Recarvarren, S. & Friedland, J.S. Multinucleate giant cells release functionally unopposed matrix metalloproteinase-9 in vitro and in vivo. *J Infect Dis* **196**, 1076-1079 (2007).
256. d'Adda di Fagagna, F. *et al.* A DNA damage checkpoint response in telomere-initiated senescence. *Nature* **426**, 194-198 (2003).
257. Hayflick, L. & Moorhead, P.S. The serial cultivation of human diploid cell strains. *Exp Cell Res* **25**, 585-621 (1961).
258. Kirschner, K. *et al.* Phenotype specific analyses reveal distinct regulatory mechanism for chronically activated p53. *PLoS Genet* **11**, e1005053 (2015).
259. Yosef, R. *et al.* Directed elimination of senescent cells by inhibition of BCL-W and BCL-XL. *Nat Commun* **7**, 11190 (2016).
260. Hemann, M.T., Strong, M.A., Hao, L.Y. & Greider, C.W. The shortest telomere, not average telomere length, is critical for cell viability and chromosome stability. *Cell* **107**, 67-77 (2001).

261. Jackson, S.P. & Bartek, J. The DNA-damage response in human biology and disease. *Nature* **461**, 1071-1078 (2009).
262. Rossiello, F. *et al.* DNA damage response inhibition at dysfunctional telomeres by modulation of telomeric DNA damage response RNAs. *Nat Commun* **8**, 13980 (2017).
263. Gluck, S. *et al.* Innate immune sensing of cytosolic chromatin fragments through cGAS promotes senescence. *Nat Cell Biol* **19**, 1061-1070 (2017).
264. Kato, K., Omura, H., Ishitani, R. & Nureki, O. Cyclic GMP-AMP as an Endogenous Second Messenger in Innate Immune Signaling by Cytosolic DNA. *Annu Rev Biochem* **86**, 541-566 (2017).
265. Ishikawa, H., Ma, Z. & Barber, G.N. STING regulates intracellular DNA-mediated, type I interferon-dependent innate immunity. *Nature* **461**, 788-792 (2009).
266. Abe, T. & Barber, G.N. Cytosolic-DNA-mediated, STING-dependent proinflammatory gene induction necessitates canonical NF-kappaB activation through TBK1. *J Virol* **88**, 5328-5341 (2014).
267. Rodier, F. *et al.* Persistent DNA damage signalling triggers senescence-associated inflammatory cytokine secretion. *Nat Cell Biol* **11**, 973-979 (2009).
268. Garfinkel, S., Brown, S., Wessendorf, J.H. & Maciag, T. Post-transcriptional regulation of interleukin 1 alpha in various strains of young and senescent human umbilical vein endothelial cells. *Proc Natl Acad Sci U S A* **91**, 1559-1563 (1994).
269. Castro, P., Giri, D., Lamb, D. & Ittmann, M. Cellular senescence in the pathogenesis of benign prostatic hyperplasia. *Prostate* **55**, 30-38 (2003).
270. Bode-Boger, S.M., Scalera, F. & Martens-Lobenhoffer, J. Asymmetric dimethylarginine (ADMA) accelerates cell senescence. *Vasc Med* **10 Suppl 1**, S65-71 (2005).
271. Sarkar, D. *et al.* Human polynucleotide phosphorylase (hPNPaseold-35): a potential link between aging and inflammation. *Cancer Res* **64**, 7473-7478 (2004).
272. Coppe, J.P. *et al.* Senescence-associated secretory phenotypes reveal cell-nonautonomous functions of oncogenic RAS and the p53 tumor suppressor. *PLoS Biol* **6**, 2853-2868 (2008).
273. Coppe, J.P., Desprez, P.Y., Krtolica, A. & Campisi, J. The senescence-associated secretory phenotype: the dark side of tumor suppression. *Annu Rev Pathol* **5**, 99-118 (2010).
274. Liu, D. & Hornsby, P.J. Senescent human fibroblasts increase the early growth of xenograft tumors via matrix metalloproteinase secretion. *Cancer Res* **67**, 3117-3126 (2007).
275. Kim, K.H. *et al.* Expression of connective tissue growth factor, a biomarker in senescence of human diploid fibroblasts, is up-regulated by a transforming growth factor-beta-mediated signaling pathway. *Biochem Biophys Res Commun* **318**, 819-825 (2004).
276. Stein, G.H., Drullinger, L.F., Soulard, A. & Dulic, V. Differential roles for cyclin-dependent kinase inhibitors p21 and p16 in the mechanisms of senescence and differentiation in human fibroblasts. *Mol Cell Biol* **19**, 2109-2117 (1999).
277. Beausejour, C.M. *et al.* Reversal of human cellular senescence: roles of the p53 and p16 pathways. *EMBO J* **22**, 4212-4222 (2003).
278. Hernandez-Rodriguez, J. *et al.* Tissue production of pro-inflammatory cytokines (IL-1beta, TNFalpha and IL-6) correlates with the intensity of the systemic inflammatory response and with corticosteroid requirements in giant-cell arteritis. *Rheumatology (Oxford)* **43**, 294-301 (2004).
279. Boveris, A. & Cadenas, E. Mitochondrial production of superoxide anions and its relationship to the antimycin insensitive respiration. *FEBS Lett* **54**, 311-314 (1975).
280. Kaur, P., Kaur, G. & Bansal, M.P. Tertiary-butyl hydroperoxide induced oxidative stress and male reproductive activity in mice: role of transcription factor NF-kappaB and testicular antioxidant enzymes. *Reprod Toxicol* **22**, 479-484 (2006).
281. Nordborg, E., Bengtsson, B.A., Petursdottir, V. & Nordborg, C. Morphological aspects of giant cells in giant cell arteritis: an electron-microscopic and immunocytochemical study. *Clin Exp Rheumatol* **15**, 129-134 (1997).

282. Yagi, M., Miyamoto, T., Toyama, Y. & Suda, T. Role of DC-STAMP in cellular fusion of osteoclasts and macrophage giant cells. *J Bone Miner Metab* **24**, 355-358 (2006).
283. Kawanishi, S., Ohnishi, S., Ma, N., Hiraku, Y. & Murata, M. Crosstalk between DNA Damage and Inflammation in the Multiple Steps of Carcinogenesis. *Int J Mol Sci* **18** (2017).
284. Yang, J.C. *et al.* TM4SF1 Promotes Metastasis of Pancreatic Cancer via Regulating the Expression of DDR1. *Sci Rep* **7**, 45895 (2017).
285. Revach, O.Y. & Geiger, B. The interplay between the proteolytic, invasive, and adhesive domains of invadopodia and their roles in cancer invasion. *Cell Adh Migr* **8**, 215-225 (2014).
286. Chen, W.T. Proteolytic activity of specialized surface protrusions formed at rosette contact sites of transformed cells. *J Exp Zool* **251**, 167-185 (1989).
287. Kumaresan, P.R., Lai, W.C., Chuang, S.S., Bennett, M. & Mathew, P.A. CS1, a novel member of the CD2 family, is homophilic and regulates NK cell function. *Mol Immunol* **39**, 1-8 (2002).
288. Kim, H.S. *et al.* STAT1 deficiency redirects IFN signalling toward suppression of TLR response through a feedback activation of STAT3. *Sci Rep* **5**, 13414 (2015).
289. Zhou, X.X., Gao, P.J. & Sun, B.G. Pravastatin attenuates interferon-gamma action via modulation of STAT1 to prevent aortic atherosclerosis in apolipoprotein E-knockout mice. *Clin Exp Pharmacol Physiol* **36**, 373-379 (2009).
290. Kukkonen-Macchi, A. *et al.* Loss of p38gamma MAPK induces pleiotropic mitotic defects and massive cell death. *J Cell Sci* **124**, 216-227 (2011).
291. Picelli, S. *et al.* Full-length RNA-seq from single cells using Smart-seq2. *Nat Protoc* **9**, 171-181 (2014).
292. Weyand, CM *et al.* Correlation of the topographical arrangement and the functional pattern of tissue-infiltrating macrophages in giant cell arteritis. *J. Clin. Investig* **98**, 1642-1649 (1996).
293. Wagner, AD *et al.* Functional profile of tissue-infiltrating and circulating CD68+ cells in giant cell arteritis. Evidence for two components of the disease. *J. Clin. Investig.* **94**, 1134-1140. (1994).
294. Weinberger, T *et al.* Ontology of arterial macrophages defines their functions in homeostasis and inflammation. *Nat Comm.* **11**, 4549. (2020).

Appendix 1

In vitro LMGC cluster	Tissue macrophage cluster 0
GPC4	S100A8
MALAT1	S100A9
ITGA7	LYZ
METTL7B	TYROBP
IGFBP6	CTSS
CCL22	FCN1
OCSTAMP	LAPTM5
NEAT1	NEAT1
OTUD78	SPP1
SLC15A3	S100A12
TM4SF1	LST1
CRABP2	PLAUR
SLC38A1	IL1B
DHRS9	GPC4
RHOC	HPGD
CD52	CD52
TSPAN17	FCER1G
LPAR6	IER3
CA2	BCL2A1
B2M	SOD2
NCAM1	CSF3R
DUSP14	CD163
MDK	NDKBIA

NPR1	S100A4
CCL1	H3F3A
CYP19A1	TM4SF1
GPAT3	MNDA
PHLDA1	CXCL8
SLAMF7	EREG
CYP27B1	CDCP1
CHI3L2	DHR59
GIPR	B2M
AOC1	SAT1
MSRB1	CSTA
CDCP1	C5AR1
SPP1	SLC11A1
ATF3	TSPO
AC131944.1	KDM6B
HPGD	VSIR
ZBTB38	PTPRE
S100A9	SRGN
SLC6A12	FPR1
RGCC	TNFAIP3
C15orf48	TNFRSF1B
IL1RN	HCLS1
LRRC28	PPP1R15A
COX5B	FGR
AC025580.1	SLAMF7
SOD2	MCL1
ARHGEF1	SPI1

Supplementary table 1. Top 50 differentially expressed genes for in vitro LMGC cluster, and tissue macrophage cluster 0. Shared genes coloured red.